BERICHTE
aus dem Fachbereich Geowissenschaften
der Universität Bremen

No. 175

Schmidt, Andrea M.

MAGNETIC MINERAL FLUXES IN THE LATE QUATERNARY SOUTH ATLANTIC: IMPLICATIONS FOR THE PALEOENVIRONMENT

Berichte, Fachbereich Geowissenschaften, Universität Bremen, No. 175,
97 pages, Bremen 2001

ISSN 0931-0800

The "Berichte aus dem Fachbereich Geowissenschaften" are produced at irregular intervals by the Department of Geosciences, Bremen University.

They serve for the publication of experimental works, Ph.D.-theses and scientific contributions made by members of the department.

Reports can be ordered from:

Gisela Boelen

Sonderforschungsbereich 261

Universität Bremen

Postfach 330 440

D 28334 BREMEN

Phone: (49) 421 218-4124

Fax: (49) 421 218-3116

e-mail: boelen@uni-bremen.de

Citation:

Schmidt, A.M.

Magnetic Mineral Fluxes in the Late Quarternary South Atlantic: Implications for the Paleoenvironment.

Berichte, Fachbereich Geowissenschaften, Universität Bremen, No. 175, 97 pages, Bremen, 2001.

ISSN 0931-0800

Tag des Kolloquiums:

26.04.2000

Gutachter:

Prof. Dr. Ulrich Bleil

Prof. Dr. Heinz Miller

Prüfer:

Prof. Dr. Heiner Villinger

Prof. Dr. Reinhard X. Fischer

CONTENTS

Chapter 1 Introduction

1.1 Paleoenvironmental information of South Atlantic sedimentary magnetism

The mineral flux from eroding continental bedrock into deep sea sediments involves a variety of geological processes: physical or chemical weathering, erosion, eolian, fluvial or oceanic current transport, deposition, and early diagenesis. The identification of particle sources, transport pathways, and of pre- or post-depositional mineral alteration therefore provides important information about states, interactions, and climatic variations of the lithosphere, hydrosphere, and atmosphere. Marine sediments comprise the most continuous records of long-term environmental variability.

Magnetic mineral assemblages within sediments are suitable archives for (paleo-) environmental reconstruction, since their concentration, magnetic mineralogy, grain-size (more precisely: domain state), and magnetic stability (coercivity) are indicative of their genesis and the geological processes they have undergone. An overview of origins and pathways of magnetic minerals to the marine environment is shown in Chapter 4, Figure 1. Furthermore, magnetic characteristics can be quantified by physical bulk sample measurements, most of which require relatively little time.

Figure 1 of this chapter shows the transmission electron micrograph of a magnetic extract from a sediment surface sample from the Rio Grande Rise in the southwestern South

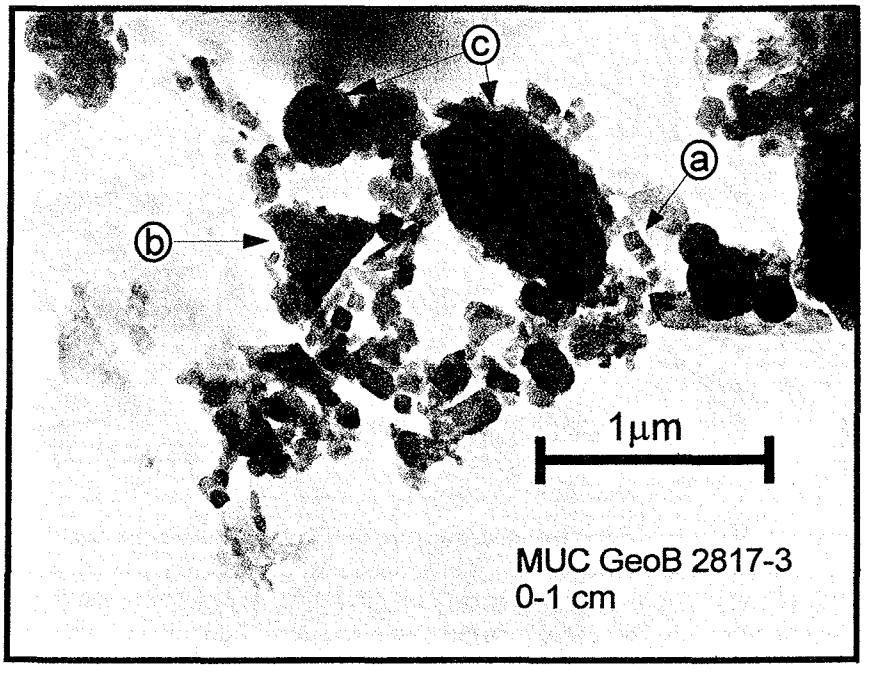

Figure 1. Transmission electron micrograph (TEM) of a magnetic extract from Multicorer (MUC) 2817-3 (Rio Grande Rise, 30°54,9'S, 38°04,3'W, WD: 2932 m) sediment surface sample (0-1 cm). The extract comprises magnetic particles of different grain-sizes and shapes. (a) Chain of SD magnetite crystals, most probably of biogenic origin. (b) Coarse (~0.5 μm) triangular shaped particle. Grains of this shape have also been observed by *von Dobeneck*, [1993], but could not be identified yet. (c) Rounded grain shapes are indicative of progressed weathering or a prolonged fluvial or eolian particle transport.

Atlantic. Fractions of distinct grain-sizes and particle shapes are discernable, indicating this sample to combine magnetic material of different origin.

The majority of sedimentary magneto-minerals is of terrigenous origin. In case of a relatively constant continental supply, their concentration primarily reflects variable dilution by non-magnetic calcareous ($CaCO_3$) or siliceous (SiO_2) microfossils and therefore represents an inverse indicator of productivity. If the terrigeneous influx is not constant, the concentration of the sedimentary magnetic mineral fractions reflect a more complex combination of dilution and supply which can be revealed by further rock magnetic investigations [*von Dobeneck and Schmieder*, 1999]. In areas of enhanced productivity, like nutrient-rich upwelling systems, another source of magnetic minerals, the biomineralization of perfectly crystallized magnetite by magnetotactic bacteria [*Petersen et al.*, 1986; *Petermann and Bleil*,

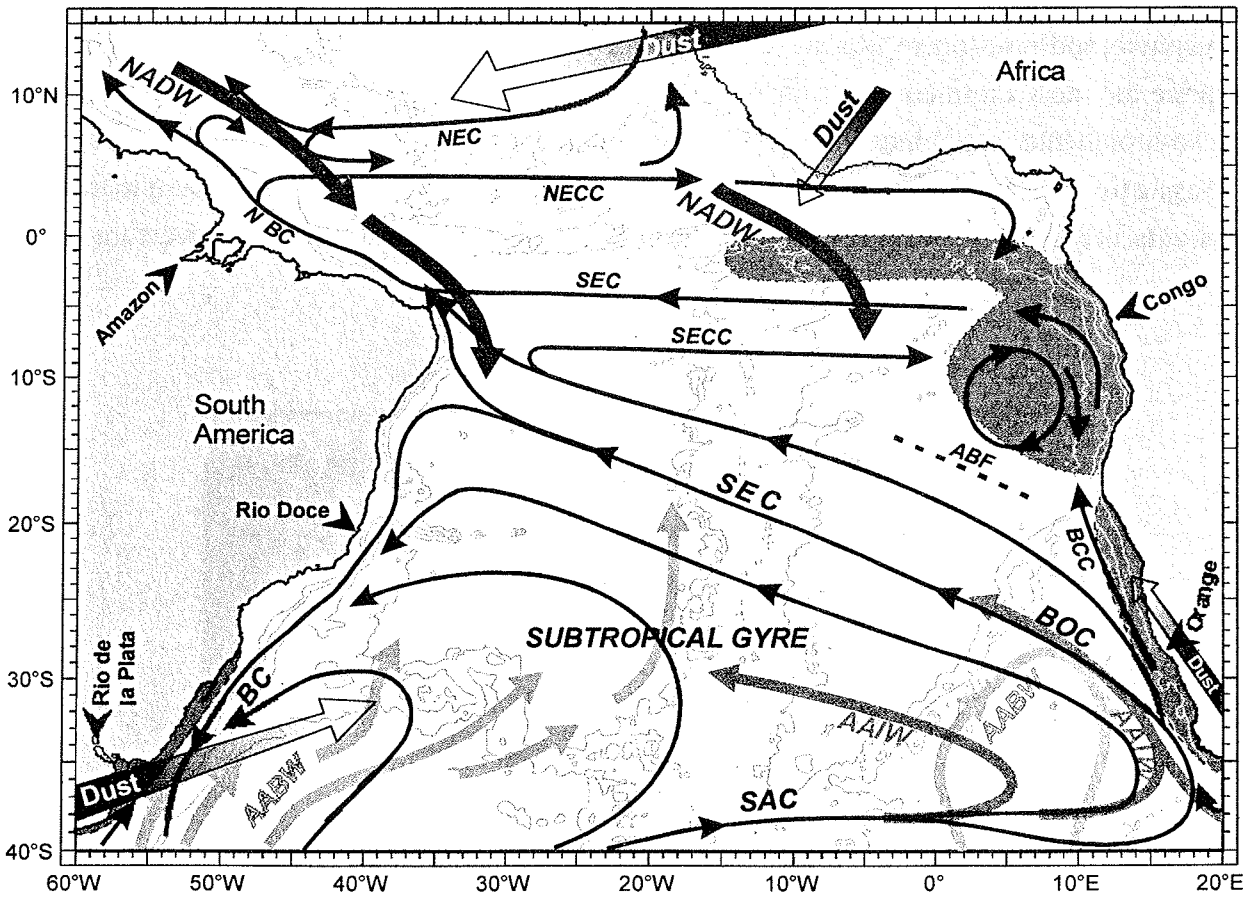

Figure 2. The working area. Surface currents (solid arrows) are the North Equatorial Current (NEC), North Equatorial Countercurrent (NECC), North Brazil Current (NBC), South Equatorial Current (SEC), South Equatorial Countercurrent (SECC), South Atlantic Current (SAC), Benguela Ocean Current (BOC), Benguela Coastal Current (BCC), and Brazil Current (BC). The Angola-Benguela Front (ABF) is indicated by a dashed line. Deep water currents (lightly shaded arrows) are the North Atlantic Deep Water (NADW), Antarctic Intermediate Water (AAIW), and Antarctic Bottom Water (AABW). Modified after *Shannon and Nelson* [1996], *Talley* [1996], *Peterson and Stramma* [1991], and *Reid*, [1996]. Transparent arrows denote main dust trajectories by midtropospheric zonal winds, NE and SW trades, and westerlies [*Glaccum and Prospero*, 1980; *Pye*, 1987]. Shaded areas denote high-productivity upwelling regions [*Schneider et al.*, 1996]. The Amazon and Congo Rivers are the major fluvial sources of continental detritus to the tropical South Atlantic and the Rio de La Plata, Rio Doce, and Orange Rivers are the major fluvial sources to the subtropical South Atlantic [*Milliman and Meade*, 1983].

1993], is of particular importance. If the terrigeneous influx is low in these areas, magnetofossils make up the major part of the magnetic fraction.

Among others, *Kobayashi and Nomura* [1974] and *Bloemendal et al.* [1992] published pioneer work illustrating the links between magnetic mineral properties and oceanic environment in the Pacific and North Atlantic Oceans and the Arabian Sea. The general concept of "environmental magnetism" has been advanced by *Thompson et al.* [1980], *Thompson and Oldfield* [1986], and *Maher and Thompson*, [1999]. Recent reviews were compiled by *Lund and Karlin* [1990], *King and Channell* [1991], *Oldfield* [1991a], and *Verosub and Roberts* [1995].

1.2 Environmental setting in the South Atlantic

The work presented here summarizes applications of environmental magnetic methods in the context of an interdisciplinary long-term paleoceanographic research project in the South Atlantic (SFB 261 "The South Atlantic in the Late Quaternary: reconstruction of material budget and current systems"). The South Atlantic represents a passage for the so-called "conveyor belt" [e.g., *Gordon*, 1986], the large-scale interhemispherical exchange of deep and surface water masses related to the production of North Atlantic Deep Water (NADW) at North Atlantic high latitudes [e.g., *Berger and Wefer*, 1996]. The oceanwide system of surface and deep currents plays an important role in the dislocation of terrigeneous material (Figure 2).

The tropical and subtropical South Atlantic includes provinces of significant terrigenous eolian and fluvial discharge. The major load of fluvial detritus to the South Atlantic is released by the rivers Amazon ($900 \cdot 10^6$ tons/yr), Rio de la Plata ($92 \cdot 10^6$ tons/yr), and Congo ($43 \cdot 10^6$ tons/yr) [*Lisitzin*, 1996]. Vast quantities of dust from the northwest African desert regions are transported in the Saharan Air Layer across the entire equatorial Atlantic [*Pye*, 1987], while in the subtropical South Atlantic westerly winds carry terrigeneous matter from the southern South American continent to the ocean. Large areas of high-productivity in the eastern parts of the South Atlantic are related to current induced provinces of oceanic upwelling as the Benguela [*Shannon and Nelson*, 1996] and the equatorial upwelling systems [*Schneider et al.*, 1996]. Fluvial nutrient supply considerably amplifies bioproductivity at the Congo continental margins.

1.3 Magnetic mineral fluxes in the South Atlantic

This cumulative thesis investigates South Atlantic magnetic mineral fluxes and their sedimentation areas as sensitive tracers of lateral particle transport. It combines a description of rock magnetic foundations, statistical methods and three thematically associated publications.

Chapter 2 presents evolution, concepts, and techniques of environmental magnetism, natural magnetic minerals, environmental magnetic parameters, and environmental processes.

Chapter 3 outlines the principles of the statistical distribution testing and cluster analytical techniques which are applied in the following studies.

The advantages of combining rock magnetic and statistical methods are illustrated in a case study within an introductory summary on environmental magnetic applications in paleoceanographic research (Chapter 4):

The magnetic view on the marine paleoenvironment: parameters, techniques and potentials of rock magnetic studies as a key to paleoclimatic and paleoceanographic changes

T. Frederichs, U. Bleil, K. Däumler, T. von Dobeneck, and A.M. Schmidt
In: G. Fischer and G. Wefer (eds.), *Use of Proxies in Paleoceanography: Examples from the South Atlantic*. Springer-Verlag Berlin Heidelberg, pp. 575-599, 1999.

As a regional study, its concern is to trace terrigeneous and biogeneous magnetic particle fluxes and to identify sedimentary provinces in the Holocene equatorial Atlantic with rock magnetic methods and multivariate classification techniques (probabilistic cluster analysis). A probabilistic c-means cluster analysis of relational (concentration independent, see case study 2) rock magnetic properties of equatorial Atlantic surface sediment samples allows to differentiate Holocene depositional environments. The resulting cluster structure reveals a distinct regionality suggesting an interpretation in terms of sedimentation provinces. The rock magnetic cluster characteristics delineate different input mechanisms of terrigenous material via fluvial transport by the Amazon and Congo Rivers at the South American and African continental margins as well as eolian transport from the Sahara and Sahel Zone into the central and eastern equatorial South Atlantic.

On the basis of this regional study, the second publication (Chapter 5) is a paleoceanographic research paper.

Magnetic characterization of Holocene sedimentation in the South Atlantic

A.M. Schmidt, T. von Dobeneck, and U. Bleil
Paleoceanography, 14, 4, pp. 465-481, 1999.

It extends the methodological and interpretative techniques of Chapter 4 to the entire Holocene tropical and subtropical South Atlantic (15°N to 40°S). A representative surface sample collection was investigated by rock magnetic methods to detect magnetic mineral distribution patterns and to identify their predominant Holocene climatic and oceanographic controls. Five concentration independent magnetic properties constitute the data basis for a probabilistic c-means cluster analysis of the sample collection. The definition of weighted standard deviations of the cluster characteristics allows to assess the extend of class overlap due to particular magnetic sediment properties. The resulting cluster structure establishes an oceanwide magnetic sediment classification scheme tracing the major terrigenous eolian and fluvial fluxes, authigenic biogenic magnetite accumulation in high-productivity areas, transport by ocean current systems, and effects of bottom water velocity on depositional regimes. As such, it forms an actualistic basis for further paleoceanographic research.

Monitoring Termination II from environmental magnetic records in South Atlantic sediments

A.M. Schmidt
Submitted to Paleoceanography

Particle source and transport changes during Termination II, the penultimate major deglaciation from oxygen isotope substage 6.2 to 5.5 at around 130 ka, is of special interest as it may represent a climatic analogue to Termination I, the deglaciation towards the present Holocene interglacial [e.g.,*Kellogg*, 1980].

Eight gravity cores forming an ocean-spanning West-East transect across the South Atlantic at about 30°S were rock magnetically analyzed for the age interval from 145 to 110 ka. Since this transect includes deposition areas sensitive for shifts in terrigeneous and biogenous influx and

deep ocean currents, it is a prime region to detect effects of glacial/interglacial climatic changes. Thermal demagnetization of representative samples from stages 6.2 and 5.5 identify magnetite and hematite as the predominant minerals controlling the rock magnetic records in this area. Significant regional trends in the magnetic sediment properties discern terrigeneous sediment sources and allow to distinguish eolian and fluvial influxes from the South American and African continents. The contrasts between average rock magnetic characteristics of stages 6.2 and 5.5 sedimentary deposits are small in comparison to these regional variations. Nevertheless, they reflect shifts in particle discharge and transport intensity during Termination II. Cores from the central part of the transect remarkably deviate in some rock magnetic properties. Modeling of the hysteresis curve shapes after *von Dobeneck* [1996] over the entire investigated age interval show that contributions of two distinct magnetic fractions in these cores control this outstanding magnetic signature. For the westernmost cores from the Santos Plateau continuous plots of the rock magnetic data reveal sharply restricted layers of reductive diagenesis indicating episodically enhanced C_{org} deposition.

CHAPTER 2 Roots and fundamentals of environmental magnetism

2.1 Milestones in the history of magnetism

Magnetism is a physical phenomenon which has fascinated mankind over several stages of civilization. The magnetic compass was one of the first technological achievements and pushed forward the expansion of trade and culture in the Chinese and Arabic world. Centuries later *Peregrinus* [1269] gave the first European description of a compass. An idea of the shape of the earth's magnetic field with its surrounding field lines was developed by *William Gilbert* [1600]. *Gauss* [1839] established a spherical harmonic analysis and postulated that the bulk of the magnetic field originated from the interior of the earth. About the same time the variability of the earth's field was observed. Early in the twentieth century, *Brunhes* [1906] and *David* [1904] found rocks that carried a magnetization reverse to the local geomagnetic field and were the first to prove that the geomagnetic field had switched and that rocks recorded the ancient field direction. *Matuyama* [1929] established this idea, when he encountered the latest prominent field reversal now more precisely dated at 780 ka.

While paleomagnetism is the science of the past variability of the earth's magnetic field, rock magnetism is concerned with the acquisition process of natural remanent magnetization. *Weiss* [1907] developed the basic idea of ferro-

Table 1 Specific susceptibilities of some dia- and paramagnetic minerals. From *Dunlop and Özdemir* [1997]

Mineral	Formula	Specific magnetic susceptibility [10^{-8} m^3/kg]
Diamagnetic		
Water	H_2O	-0.90
Sodium chloride	NaCl	-0.90*
Calcite	$CaCO_3$	-0.48
Orthoclase feldspar	$(KAlSi_3O_8)$	-0.58
Paramagnetic		
Pyrite	FeS_2	+30
Siderite	$FeCO_3$	+123
Ilmenite	$FeTiO_3$	+100 - 113
Orthopyroxenes	(Fe,Mg)SiO	+43 - 92
Fayalite	Fe_2SiO_4	+126
Olivine	$(Fe,Mg)_2SiO_4$	+36
Amphiboles		+16 - 94
Biotites		+67 - 98
Illite (clay)		+15
Montmorillonite (clay)		+14

* [*Thompson and Oldfield*, 1986]

magnetism and magnetic domains, regions within a crystal whose atomic magnetic moments align due to an internal molecular field, but whose mutually different bulk directions almost perfectly neutralize in the absence of an external magnetic field. He proposed that applied fields much less intense than the molecular fields can rotate domains or move the domain walls, the boundaries between the domains, generating an external net magnetic moment. On the basis of Weiss' molecular field description *Néel* [1948] explained the exchange coupling between magnetic sublattices in antiferromagnetic and ferrimagnetic materials.

First laboratory studies with the objective to reproduce and understand the mechanism by which rocks are magnetized in nature were carried out by *Koenigsberger* [1938], *Thellier* [1938] and *Nagata* [1943] with primary focus on thermoremanent magnetization of igneous rocks. Other important mechanisms by which a natural remanence can emerge is during crystallization (chemical remanent magnetization) or sedimentation (detrital remanent magnetization).

2.2 Fundamentals of magnetism

All substances can be magnetized, however there are extreme differences of how materials react to an external magnetic field.

Diamagnetism is a universal property of all matter. In a magnetic field H the electron with a charge e moving with the velocity v in its orbit experiences a Lorentz force $e\mu_0 v \times \mathbf{H}$ which causes the electron orbit to precess around **H**. After the Lenz' rule, the resulting Larmor precession of Z electrons (Z is the atomic number) produces a negative induced magnetic moment

$$\mu_{\text{dia}} = \frac{-Ze^2\frac{2}{3}\langle r^2\rangle}{(4m_e)\mu_0 \boldsymbol{H}}$$

with m_e the electron mass and $\langle r^2\rangle$ the mean square distance of the electrons to the atomic core. The diamagnetic susceptibility is then given by

$$\kappa_{dia} = \frac{M}{H} = \frac{n\mu_{dia}}{H} = \frac{-\mu_0 Z_e \cdot 2\langle r^2\rangle}{6m_e},$$

where n is the number of atoms per unit volume, μ_0 the absolute magnetic permeability constant. Most non-iron-bearing materials like water, quartz, calcite and feldspars are purely diamagnetic. For para- or ferromagnetic minerals the effect of diamagnetism is neglectible.

Paramagnetism is the alignment of permanent atomic moments in the direction of an external magnetic field ***H***. At ordinary temperatures the degree of alignment is very low, but sufficient to surpass diamagnetism. The torque that ***H*** exerts on each atomic moment μ is expressed in the potential magnetic field (or Zeeman) energy

$$E_m = -\mu\mu_0 \boldsymbol{H} = -\mu\mu_0 H\cos\phi$$

Thermal perturbations prevent the perfect alignment of all moments with ***H***. The paramagnetic magnetization can be written as

$$\boldsymbol{M}_{para}(H,T) = n\boldsymbol{\mu}L(\alpha) = n\boldsymbol{\mu}\cdot\left(\coth(\alpha) - \frac{1}{\alpha}\right)$$

and the paramagnetic susceptibility is given by the Curie-law

$$\kappa_{para} = \frac{M_{para}}{H} = \frac{n\mu_0\mu^2}{3kT} = \frac{C}{T}$$

with $L(\alpha)$: Langevin function, C: Curie constant, k: Boltzmann constant, and T: absolute temperature.

As an essential result, M_{para} and κ_{para} are positive and decrease with increasing temperature, M_{para} increases with intensifying external field. Table 1 gives specific susceptibi-

lities of common natural dia- and paramagnetic minerals.

For both diamagnetics and paramagnetics the magnetization is induced and disappears, when the external field is removed. At ordinary temperatures extremely large fields

$$\boldsymbol{B} = \mu_0 \cdot (\boldsymbol{H} + \boldsymbol{M}) \quad [\mathrm{T}]$$

on the order of 100 T are required to saturate paramagnetic minerals.

In contrast, ferromagnetics, ferrimagnetics, and antiferromagnetics retain a magnetically ordered state after the external field has been removed.

As predicted by *Landau and Lifshitz* [1935], the magnetostatic energy of a ferro-, ferri-, or antiferromagnetic particle is reduced by the existence of *magnetic domains*. In the interior of a crystal lamellar body domains show alternating opposed directions of magnetization. On the surface, wedge-shaped closure domains with magnetization direction nearly parallel to the surface provide flux closure paths between adjacent body domains. Between neighbouring domains narrow domain walls exist, in which the magnetization direction rotates through 180° or 90° (for magnetite: 70.5° and 109.5°, Figure 3).

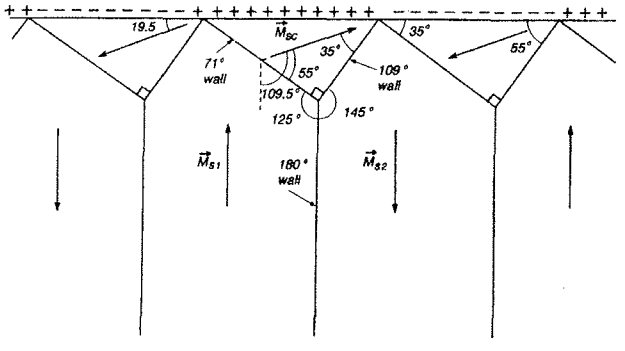

Figure 3. Typical multidomain structure of magnetite, with body domain magnetization vectors $\boldsymbol{M}_S$ along ⟨111⟩ easy axes and 71° and 109° Bloch walls separating closure and body domains. Where the closure domain magnetization vector $\boldsymbol{M}_{SC}$ cuts the crystal surface, magnetic surface charges result (+ and – signs) [*Dunlop and Özdemir*, 1997, after *Özdemir et al.*, 1995]

The critical grain-size d_0 below which a particle contains only one domain (single domain, SD) is reached, when the domain wall width approaches the particle size. For ideal magnetite particles, the number of domains increases with increasing grain-size from SD (0.03 μm < ∅ < 0.1 μm) [*Butler and Banerjee*, 1975; *Dunlop*, 1973] intermediate pseudo-single-domain (PSD) (0.1 μm < ∅ < ~5-10 μm) [*Parry*, 1965] to multidomain (MD) (∅ > ~5-10 μm).

The lower limit of the stable SD range is defined by the superparamagnetic (SP) threshold. The energy barrier ΔE for spontaneous magnetization reversals of a SD grain is dependent on crystalline, magnetoelastic and shape anisotropy, proportional to the particle volume. In small enough grains (< 0.03 μm for magnetite) ΔE is surpassed by thermal activation energy. Figure 4 illustrates domain state thresholds as a function of particle size and elongation.

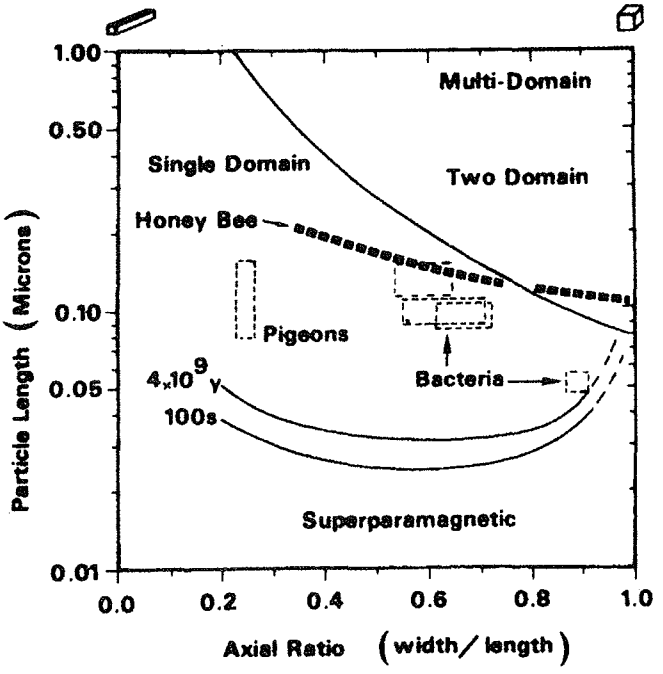

Figure 4. Theoretical critical single-domain size range for magnetite as a function of grain elongation. Values for different magnetosome particles serving as microbial biocompass or as field sensor for higher species are labelled from [*Dunlop and Özdemir*, 1997, after *Butler and Banerjee*, 1975].

Pure ferromagnetics do not occur as rock forming minerals, but only as solid metals like metallic iron or nickel. They require only very weak magnetic fields in the order of 10 mT to be saturated and retain a considerable remanent magnetization. These phenomena can be explained by definition of an internal molecular field [*Weiss*, 1907] which produces a spontaneous magnetization by alignment of the atomic moments. Within a domain, the molecular field is proportional to the mean magnetization of the domain

$\boldsymbol{H}_m = W \cdot \boldsymbol{M}$ with W: Weiss' constant

The origin of the molecular field is the exchange coupling between uncompensated electron spins of neighbouring ions within the crystal. In an external field $\boldsymbol{H}$ the effective field acting on every atomic moment is

$$\boldsymbol{H}_{eff} = \boldsymbol{H} + \boldsymbol{H}_m$$

For small applied fields the ferromagnetic susceptibility is given by

$$\kappa_{fer} = \frac{M_{fer}}{H} = \frac{n\mu_0\mu_{fer}^2}{3kT}\left(1 + \frac{H_m}{H}\right)$$

At the Curie temperature T_C, thermal agitation destroys the ordering of moments. Above this temperature, ferromagnetic minerals become paramagnetic which is expressed by the Curie-Weiss-law

$$\kappa_{para} = \frac{M}{H} = \frac{C}{T - T_C} \quad \text{for } T > T_C$$

The remanence carrying minerals in terrestrial rocks are specific iron oxides, hydroxides, and sulfides. Unlike in ferromagnetic metals, their iron atoms are not close enough for direct exchange interaction. Instead, indirect exchange interaction of 3d electrons occurs through overlap of their orbitals with 2p orbitals of intervening oxygen ions or 3p orbitals of sulphur ions. A pair of 2p (or 3p) electrons with opposite spins is involved in the negative exchange coupling. As a result, two magnetic sublattices A and B of oppositely directed spins and magnetic moments are established, while also weak negative AA and BB interactions between cations in the same sublattice occur. After *Néel* [1948] sublattices A and B have oppositely directed magnetizations $\boldsymbol{M}_A$ and $\boldsymbol{M}_B$ and every sublattice experiences its own molecular field

$$\boldsymbol{H}_A = -W_{AA}\boldsymbol{M}_A - W_{AB}\boldsymbol{M}_B,$$
$$\boldsymbol{H}_B = -W_{AB}\boldsymbol{M}_A - W_{BB}\boldsymbol{M}_B$$

In a *ferrimagnetic* mineral A and B sublattices contain different numbers and kinds of cations. Magnetite, maghemite and titanomagnetite are the most common ferrimagnetics . For magnetite the cationic distribution is $Fe^{3+}[Fe^{2+}Fe^{3+}]$, with octrahedral or B-site cations bracketed. The Fe^{3+} ions on the two sublattices balance and the net magnetic moment is due to Fe^{2+} ions on the B-sites. Nevertheless, the exchange interactions and magnetic properties depend on all cations. Below T_C, the spontaneous magnetization is given by the sum of the sublattice magnetizations $\boldsymbol{M}_A$ and $\boldsymbol{M}_B$.

For *antiferromagnetics* $\boldsymbol{M}_A = -\boldsymbol{M}_B$ at all temperatures, with no resulting net magnetization. The ordering temperature for antiferromagnets is called the Néel temperature T_N. With $C_A = C_B$

$$T_N = \left(\frac{C}{2}\right)W_{AB}$$

Although the sublattice magnetizations balance perfectly in the absence of an applied field, in the presence of $\boldsymbol{H}$ antiferromagnetic minerals acquire an induced magnetization. Below T_N, an external field applied perpendicular to the sublattice magnetizations deflects $\boldsymbol{M}_A$ and $\boldsymbol{M}_B$ slightly, resulting in a small magnetization component in the direction of $\boldsymbol{H}$. Due to magnetocrystalline anisotropy the deflection angle ϕ is small at any field. The perpendicular

susceptibility is given by

$$\kappa_{\perp} = \frac{2M\sin\phi}{H} = \frac{1}{W_{AB}} \quad \text{with } M_A = M_B = M.$$

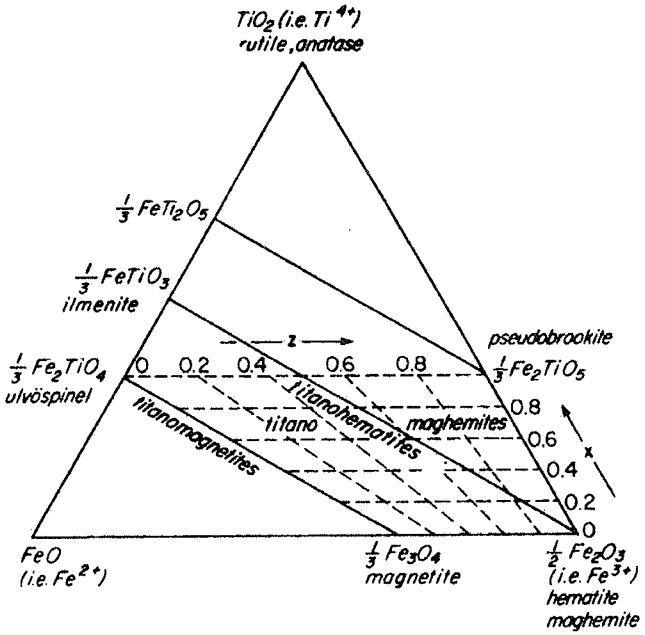

Figure 5. TiO_2-FeO-Fe_2O_3 ternary diagram, with titanomagnetite and titanohematite solid solution lines and the titanomaghemite field. z gives the oxidation parameter, x the titanium content. From *Dunlop and Özdemir*, [1997].

If the easy axes for M_A and M_B differ, the sublattice magnetizations are permanently slightly deflected, even if $H = 0$. This behavior is called spin-canting antiferromagnetism. Common natural antiferromagnetic minerals are hematite (α–Fe_2O_3), goethite (α–FeOOH). Specific susceptibilities of some ferro-, ferri-, and antiferromagnetic minerals are given in Table 2.

Table 2 Specific susceptibilities of some ferro-, ferri-, and antiferromagnetic minerals. from *Thompson and Oldfield* [1986]

Mineral	Formula	Specific magnetic susceptibility [10^{-8} m^3/kg]
Ferromagnetic		
Iron	Fe	$2 \cdot 10^7$
Ferrimagnetic		
Magnetite	Fe_3O_4	$5 \cdot 10^4$
Maghemite	γ-Fe_2O_3	$4 \cdot 10^4$
Pyrrhotite	Fe_7S_8	$\sim 5 \cdot 10^3$
Antiferromagnetic		
Hematite	α-Fe_2O_3	60
Goethite	α-FeOOH	70

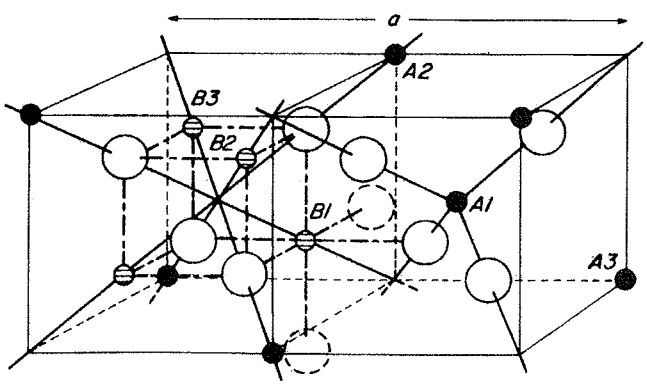

Figure 6. ¼ of a unit cell of magnetite. Cations in tetrahedral (A-site) and octahedral (B-site) coordination are represented by solid and hatched circles, O^{2-} ions by large open circles, a denotes the lattice parameter. From *Dunlop and Özdemir*, [1997].

2.3 Natural magnetic minerals

The processes by which natural magnetic particles are generated and to which they have been subjected afterwards play a central role in the control of their magnetic properties. Mineralogy primarily reflects the composition of the source material.

Iron titanium oxides are the most common natural magnetic minerals. They exist as a solid solution series within a ternary diagram illustrated in Figure 5. Crystallographically, two main groups of iron titanium oxides are important, the spinel and the corundum group (Table 3).

Spinel group

Magnetite (Fe_3O_4) is the most common ferrimagnetic mineral. Fe^{3+} ions occupy the 8

Table 3 Crystallographic structures of iron oxides

Group	*Spinel*		*Corundum*	
Unit cell	Cubic face centered 32 oxygen ions nearly cubic close packed, cations occupy 16 octahedral and 8 tetrahedral sites within the oxygen framework (Figure 6)		Rhombohedral hematite: Fe^{3+} ions occupy all cation layers (Figure 9) ilmenite: Fe^{2+} and Ti^{4+} layers alternate	
Mineral	magnetite titanomagnetite maghemite titanomaghemite	Fe_3O_4 $(0 \leq x \leq 1)$ $Ti_xFe_{3-x}O_4$ γ-Fe_2O_3 $Fe_{(1+x)R}Ti_{xR}\square_{3(1-R)}O_4$ $(0<x<1, 0<z<1, R=8/(8+z(1+x)))$	hematite titanohematite ilmenite	α-Fe_2O_3 $Ti_xFe_{2-x}O_3$ $(0 \leq x \leq 1)$ $FeTiO_3$

tetrahedral sites of its inverse spinel structure and one half of the 16 octahedral sites, Fe^{2+} ions are situated on the other half (Figure 6). Its saturation magnetization is the strongest of all natural magnetic minerals. At room temperature it amounts to $M_s \approx 480$ kAm^{-1}, its Curie temperature T_C is 580 °C. Lithogenic magnetite, often containing titanium, chromium, manganese and magnesium compounds, occurs as primary or secondary mineral in most all magmatic and metamorphic rocks as well as in terrigeneous and marine sediments. The titanium contents of iron oxides in basic magmatites like basalts or gabbro is generally higher than in acidic ones. By high temperature oxidation (> 600 °C) commonly occuring during subaerial cooling, primary titanomagnetites are altered to intergrown near-magnetite and near-ilmenite exsolution lamellae. Magnetite grain-size of igneous rocks is critically dependent on cooling velocity. Consequently generally coarser crystals generate within slowly cooling plutonic rocks than in volcanics. Within metamorphites, large crystals of almost pure magnetite are found, not incorporating titanium ions until highest metamorphic grades, i.e. in the granulite facies. Another important source of pure magnetite is the biomineralization of perfectly crystallized single domain magnetosomes by magnetotactic bacteria [*Petersen et al.*, 1986] which occur in soils [e.g., *Fassbinder et al.*, 1990; *Oldfield*, 1991b], in lake [e.g., *Moskowitz et al.*, 1988; *Petersen et al.*, 1989; *Snowball*, 1994; *Vali and Kirschvink*, 1991] and marine sediments, where they provide the main

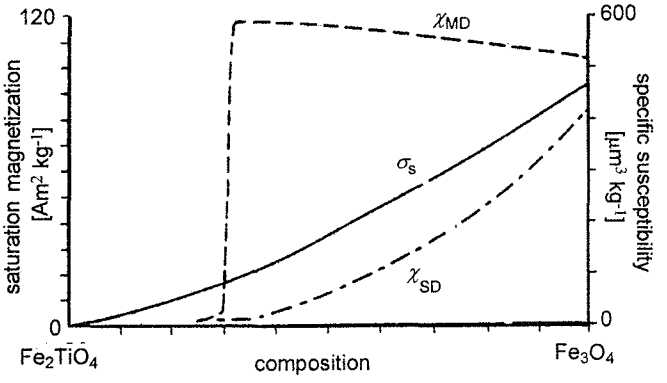

Figure 7. Saturation magnetization (σ_s) and susceptibility of multidomain (χ_{MD}) and single domain (χ_{SD}) titanomagnetite grains as function of composition [*Thompson and Oldfield*, 1986].

remanence carrying fraction especially in regions with minor terrigeneous influx and elevated productivity like the Benguela upwelling system off southwest Africa [*Petermann and Bleil*, 1993].

Titanomagnetites ($Ti_xFe_{3-x}O_4$, $0 \leq x \leq 1$) have the same inverse spinel structure as magnetite. Above 600 °C they exist as complete solid

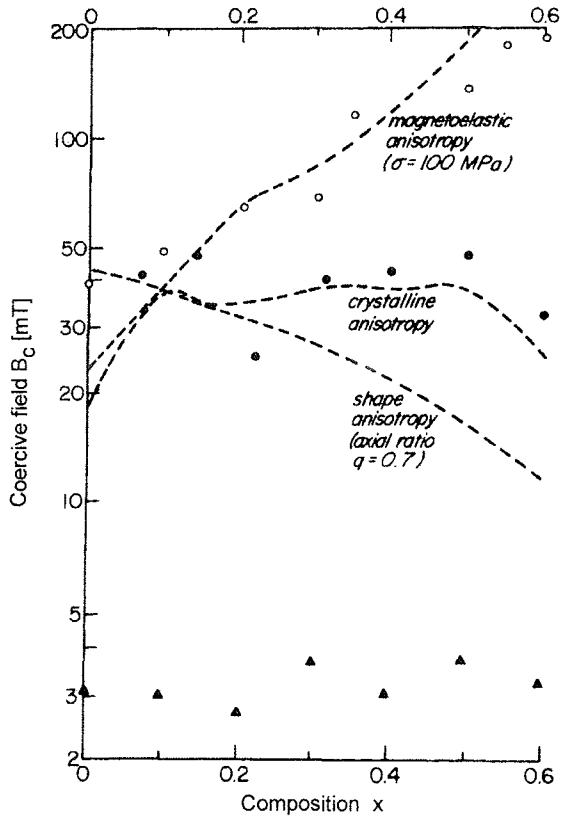

Figure 8. Measured coercive field B_C for titanomagnetites as a function of titanium content x. Open circles: single-domain grains (~0.1 μm), solid circles: ~1.5 μm grains, triangles: large (>150 μm) multidomain grains. Dashed curves represent theoretical critical fields resulting from pure magnetoelastic, magnetocrystalline, and shape anisotropy in single domain grains [*Dunlop and Özdemir*, 1997, after *Day et al.*, 1977].

solution series between magnetite (Fe_3O_4) and ulvöspinel (Fe_2TiO_4) which is paramagnetic at room temperature. In ulvöspinel Ti^{4+} ions occupy half of the octahedral sites which are filled by Fe^{3+} in magnetite, Fe^{2+} ions taking up all remaining cation sites. The most common titanomagnetite is the so called TM60, with a titanium content of 60% (x = 0.6). It occurs as primary iron oxide in submarine basalts, often containing Al and Mg as impurities. TM60 is preserved by rapid quenching from high temperatures without unmixing into two phases. Oxidation of titanomagnetite during initial cooling at mid-ocean ridges is also prevented by the excess of sulphur over oxygen once the oxides and silicates have crystallized. Rapid cooling is similarly the cause of fine grain-sizes within oceanic basalts.

Rock magnetic properties of titanomagnetites are a function of titanium content and oxidation state. Their Curie temperature falls with increasing titanium content. TM60 has a Curie temperature of $T_C \approx 150$ °C. Al and Mg impurities lower T_C as well, while low temperature oxidation (termed maghemitization) raises T_C. As the exchange interactions between neighbouring atoms decrease with increasing Ti content, the saturation magnetization decreases (M_s = 125 kAm^{-1} for TM60 at room temperature), as does the susceptibility for SD titanomagnetite grains. For MD titanomagnetites the susceptibility changes little with composition [*Thompson and Oldfield*, 1986] (Figure 7). Coercivity (reverse field necessary to get an in-field magnetization of zero) increases with rising x. SD titanomagnetites with high x may have coercivities of 100 mT or more due to crystalline or magnetoelastic anisotropies [*Day et al.*, 1977] (Figure 8). In oceanic basalts, however, single-domain TM60 grains tend to be maghemized and consequently show lower coercivities. MD titanomagnetites largely resist oxidation, but typically have coercivities < 20 mT [*Day et al.*, 1977].

Maghemite (γ-Fe_2O_3) has the same chemical formula as hematite, but the inverse spinel structure of magnetite. Its structural formula can be written as $Fe^{3+}\left[Fe^{3+}_{5/3\ 1/3}\right]O^{2-}_4$, where octahedral sites are bracketed and □ stands for a lattice vacancy, ordered on a tetragonal superlattice. Maghemite is the ultimate low-temperature oxidation product of magnetite and is common in both subaerial and submarine environments. Above 400 °C it converts to hematite. The saturation magnetization of maghemite at room

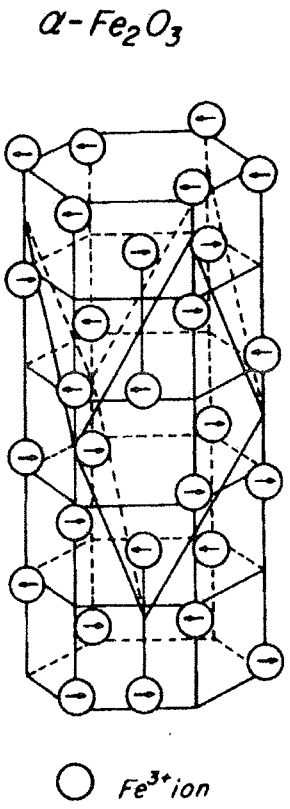

Figure 9. Rhombohedral structure of hematite (α-Fe_2O_3). Fe^{3+} ions occupy all cation layers. The sublattices are magnetized in antiparallel directions (antiferromagnetism). Between T_{Morin} and T_N, spin canting results in a net magnetic moment perpendicular to the sublattice planes. From *Dunlop and Özdemir*, [1997].

temperature is $M_s = 380$ kAm^{-1} and its Curie temperature $T_C \approx 645$ °C [*Özdemir and Banerjee*, 1984]. Its coercivity and susceptibility are comparable to magnetite.

Titanomaghemites are partially oxidized titanomagnetites. After *O'Reilly* [1984] the structural formula of a titanomaghemite can be written as

$$Fe^{3+}_{[2-2x+z(1+x)]R}Fe^{2+}_{(1+x)(1-z)R}Ti^{4+}_{xR}\square_{3(1-R)}O^{2-}_4$$

with $R = \frac{8}{8+z(1+x)}$, x the Ti content and z the oxidation parameter. During the low-temperature oxidation of titanomagnetite the cubic face centered oxygen lattice is preserved and the Fe^{2+} ions migrate to the crystal surface. In this course, the crystal surface oxidizes more quickly than the interior resulting in a strong gradient in cation deficiency and oxidation parameter z. Hence partially oxidized titanomagnetites are not homogeneous in their magnetic properties. M_s and Fe/Ti ratio decrease, T_C increases with progressing oxidation. The unit cell edge reduces, leading to shrinking and following cracking of the oxidized particle surface. With increasing temperature, titanomaghemites invert irreversibly to intergrows of Ti-rich rhombohedral (near ilmenite) and Ti-poor spinel (near magnetite) phases. Maghemitization of primary titanomagnetites and inversion of the titanomaghemites occurs in the upper oceanic crust.

Corundum group

Hematite (α-Fe_2O_3) is rhombohedral in structure (Figure 9). Between the Morin transition, a discontinuity of magnetic properties at around -15 °C [*Liebermann and Banerjee*, 1971], and the Néel temperature $T_N = 675$ °C, the sublattice magnetizations are canted slightly out of antiparallelism, a behavior which is called *spin-canting antiferromagnetism* or *parasitic ferromagnetism*. The resulting magnetic moment lies in the basal plane perpendicular to the sublattice magnetizations. Below T_{Morin}, the sublattice moments are pinned along the c-axis with no resulting spin-canting. Saturation magnetization $M_s > 2.5$ kAm-1 and susceptibility $k > 125 \cdot 10^{-6}$ SI [*Thompson and Oldfield*, 1986] of hematite are low in comparison to magnetite values. The coercivities vary from > 1 mT in large MD hematite grains to several hundreds of mT in single-domain hematite. Hematite forms as the end product of prolonged oxidation of magnetite at ordinary temperatures. It is also generated by high-temperature oxidation of titanomagnetite during initial cooling from the melt

or as inversion product of maghemite or titanomaghemite during reheating. Important secondary processes to form hematite are the dehydration of weathering products like goethite (α-FeOOH) and precipitation of ultra-fine-grained hematite from iron-rich solutions within the pore space of clastic sediments, giving the red beds their distinctive color.

Titanohematites or *hemoilmenites* ($Fe^{2+}_{y}Fe^{3+}_{2-2y}Ti^{4+}_{y}O^{2-}_{3}$ $0 \le y \le 1$) have compositions that lie between the end-members hematite and ilmenite. Solid solution is complete only at high temperatures. Within the corundum structure of titanohematites the oxygen ions form a hexagonal close packed lattice and Fe and Ti cations occupy two-thirds of the interstices. For $0 \le y \le 0.5$, Ti^{4+} and Fe^{2+} ions are equally distributed among all c-planes and the titanohematites of this composition are, like hematite, antiferromagnetic with a weak parasitic ferromagnetism. For $0.5 \le y < 1$, titanohematite is ferrimagnetic as a result of an ordered cation distribution with Ti^{4+} and Fe^{2+} ions occupying alternate planes. Since for $0.5 \le y \le 0.7$, T_C is between 200 and 20 °C and for $y > 0.7$, T_C is below room temperature, ilmenite-near titanohematites are paramagnetic at room temperature. Titanohematites are found in volcanites, granites, metamorphites and in some sediments.

Goethite (α-FeOOH) is the most important iron oxihydroxide. It forms as weathering product and is common in soils and sediments. Goethite is antiferromagnetic and has a Néel temperature of 120 °C. It shows a parasitic ferromagnetism with T_C coinciding with T_N [*Özdemir and Dunlop*, 1996]. Ferromagnetism seems to result from a defect moment, perhaps due to unbalanced numbers of spins in the usually very fine goethite crystals [*Dunlop and Özdemir*, 1997]. Its weak M_s between 0.01 and 5 kAm^{-1} combines with very high coercivities of often many hundreds of mT, even higher than those of fine-grained hematite. At intermediate temperatures (≈ 350 °C) goethite dehydrates and converts to hematite or maghemite [*Dunlop*, 1990].

Iron Sulfides.

Greigite (Fe_3S_4), formerly thought to be a rare mineral, commonly occurs in sediments formed under anoxic conditions [*Roberts*, 1995] and can also be biomineralized by magnetotactic bacteria [*Mann et al.*, 1990]. Greigite is ferrimagnetic and has the same inverse spinel structure as magnetite. Its M_s amounts to only 1/4 that of magnetite [*Hoffmann*, 1992]. T_C is around 330 °C [*Dunlop and Özdemir*, 1997] which may rather reflect the Néel and Curie temperatures of pyrrhotite ($Fe_{1-x}S$) to which it converts together with pyrite (FeS) above 320 °C [*Skinner et al.*, 1964].

Pyrrhotite ($Fe_{1-x}S$) is a common mineral in igneous, metamorphic and sedimentary rocks. Natural pyrrhotite is a mixture of the monoclinic ferrimagnetic Fe_7S_8 and hexagonal antiferromagnetic phases as Fe_9S_{10} and $Fe_{11}S_{12}$. Like maghemite, monoclinic pyrrhotite owes its ferrimagnetism to cation deficiency and vacancy ordering. The grain-size dependence of pyrrhotite magnetic properties have been studied in detail by *Clark* [1984] and *Dekkers* [1988b; 1989]. Within the hexagonal symmetry, Fe and S ions are confined to alternate c-planes. Alternate Fe planes form the two magnetic sublattices. In Fe_7S_8 vacancies are preferentially located on one of the sublattices, distorting the hexagonal structure to a monoclinic one and causing a ferrimagnetic

moment. Its Curie point is 320 °C. During weathering pyrrhotite converts to magnetite or hematite and pyrite.

Detailed tabular summaries containing magnetic properties of numerous minerals can be found in *Bleil and Petersen* [1982]

2.4 Environmental Magnetic Parameters

Mineralogy, domain structure, morphology, crystal stress, chemical impurities, and grain interactions critically control the magnetic properties of common natural magnetic minerals which can be revealed by rock magnetic methods. Chapter 4 gives a review of common environmental magnetic techniques. Especially for magnetic particle assemblies in continental sedimentary deposits, as for example loess [*Banerjee et al.*, 1993; *Heller and Liu*, 1984; *Liu et al.*, 1992; *Maher and Thompson*, 1991], and in marine sediments [*Robinson*, 1986; *deMenocal et al.*, 1988; *Doh et al.*, 1988; *Bloemendal et al.*, 1992; *Oldfield*, 1994; *Urbat et al.*, 1999] magnetic properties can serve as powerful paleoclimatic proxies reflecting sedimentation milieus in the deposition areas as well as geologic and climatic conditions in the source regions and means and pathways of particle transport. Magnetic properties of soils illustrate weathering processes and lake sediments yield important clues on catchment and transport conditions. The eminent potential of *Environmental Magnetism* has been extensively outlined in a textbook by *Thompson and Oldfield* [1986].

Concentration dependent parameters

Theoretically, saturation magnetization M_s is the only domain state (grain-size) independent measure to quantify the concentration of the magnetic mineral fraction. Its precise experimental determination may require extraordinarily high magnetic fields, generally not available in geoscience laboratories. The most commonly used easily measured concentrational parameter therefore is magnetic susceptibility κ, for magnetite fairly grain-size independent over a wide grain-size range from 0.1 to 10000 μm [*Heider et al.*, 1995]. Where magnetite is present, it most always dominates the susceptibility signal, since other ferri- or antiferromagnetic minerals as well as paramagnetic matrix constituents have much lower specific susceptibilities. For $k < 10^{-4}$ SI para- and/or diamagnetism must be considered, however.

This non-ferromagnetic susceptibility κ_{nf} is determined from the slope of the outer branch of the high field hysteresis curve (Chapter 4, Figure 2a).

Ultra-fine SP particles are unable to carry a remanence. Due to relaxation effects, their susceptibility shows a dependence on the frequency of the alternating field measurement. The loss between susceptibility measurements at a lower (κ) and a typically one magnitude higher frequency (κ_{hf}) provides an estimate of the relative SP content

$$\kappa_{fd\%} = 100 \cdot \frac{(\kappa - \kappa_{hf})}{\kappa}$$

Concentrations of specific grain-size fractions are selectively reflected by remanence based parameters summarized in Chapter 4 (Example 2, Table 1). The saturation remanence M_{rs} (M_{sir}) depends on the amount of all remanence carriers in a sample. It is defined as the remanence remaining after magnetization of the sample up to saturation. As fine SD and intermediate PSD particles carry a higher remanence than coarse MD grains, M_{rs} is biased by the magnetic grain-

size distribution in a sample.

While fields of about 0.3 Tesla (T) are sufficient to saturate ferrimagnetic minerals, antiferromagnetica require several Tesla to reach M_{rs}. This fact is used to quantify the concentration of antiferromagnetic minerals by the *hard isothermal remanent magnetization*:

$$M_{hir} = 0.5\ (M_{sir}+M_{-0.3T})$$

[*Stoner et al.*, 1996] with $M_{-0.3T}$ the remanence remaining after magnetization of the sample to saturation and subsequently to a reverse field of 0.3 T.

As the anhysteretic magnetization M_{ar} is most pronounced in the SD/PSD range [*Banerjee et al.*, 1981; *King et al.*, 1982], it provides a measure of the fine-grained fraction.

Mineralogy dependent parameters

The ratio of the non-ferromagnetic susceptibility to the total susceptibility κ_{nf}/κ_{tot} (κ_{tot} defined as the hysteresis loop gradient at B = 0) estimates the contribution of paramagnetic (e.g., terrigenous or diagenetic iron compounds) and diamagnetic (e.g., calcite, quartz, opal) matrix constituents to susceptibility differentiating distinct depositional regimes.

The *S* ratio [*Stober and Thompson*, 1979] compares concentrations of high-coercive (e.g., hematite and goethite) to low-coercive (e.g., (titano-)magnetite) fractions.

$$S_{-0.3T} = 0.5 \cdot \left(1 + \frac{M_{-0.3T}}{M_{sir}}\right)$$

as defined by [*Bloemendal et al.*, 1992] relates the back field magnetization $M_{-0.3T}$ to the saturation remanence M_{sir} and non-linearly varies from 0 to 1 (Chapter 4, Figure 4a). Because of much lower specific magnetizations, a reliable assessment of relative antiferromagnetic mineral concentrations is only achieved if their fraction exceeds about 80 % [*Bloemendal et al.*, 1992]. Furthermore, the distinct grain-size dependence of magnetite M_{sir} limits a quantitative interpretation of the $S_{-0.3T}$ parameter in terms of mineral proportions.

Coercivity parameters

The bulk magnetic stability (coercivity) of a sample is given by the inverse coercive field B_c necessary to reduce the net in-field remanent magnetization after saturation to zero. B_c is particularly sensitive to grain-size and magnetomineralogy. As B_c is measured in an external field, it is affected by induced magnetizations of superparamagnetic and non-ferromagnetic compounds.

A further increased inverse field which leaves a zero remanent magnetization after its removal defines the coercivity of remanence B_{cr} quantifying exclusively the coercivity of the remanence carrying particles.

Incremental triaxial alternating field (AF) demagnetization of isothermal (M_{ir}) and anhysteretic (M_{ar}) magnetizations yields coercivity spectra characterized by the median destructive fields necessary to randomize half of the initial magnetizations. The selectivity of $B_{½}(M_{ir})$ and $B_{½}(M_{ar})$ for mineralogy and grain-size is equivalent to that of M_{ir} and M_{ar}.

Grain-size parameters

The standard hysteresis parameters saturation magnetization M_s, saturation remanence M_{rs}, coercive field B_c, and coercivity of remanence B_{cr} compose the ratios M_{rs}/M_s and B_{cr}/B_c sensitive for the predominant (titano-)magnetite domain state or grain-size [*Wasilewski*, 1973]. With decreasing grain-size M_{rs}/M_s varies from 0.01 for coarse MD particles to 0.5 for ideal, non-interacting SD particles, B_{cr}/B_c between about 10 and 1. *Day et al.* [1977] combined both parameters in a diagram (Chapter 4, Figure 5).

Table 4 Maximum coercivities and blocking temperatures of current ferromagnetic minerals. The star (*) marks disintegration temperatures. From [*Frederichs*, 1995b].

Mineral	*Formula*	$B_{cr,max}$	$T_{B,max}$	*Source*
Magnetite	Fe_3O_4	0.3	575	O'Reilly (1994)
Maghemite	γ-Fe_2O_3	0.3	$\approx$ 350 *	O'Reilly (1994)
Titanomagnetite	$Ti_xFe_{3-x}O_4$ $0 \leq x \leq 1$			
	x = 0.3	0.2	350	O'Reilly (1994)
	x = 0.6	0.1	150	O'Reilly (1994)
Hematite	α-Fe_2O_3	1.5 - 5	675	O'Reilly (1994), Lowrie and Heller (1982)
Goethite	α-FeOOH	> 5	80 - 120	Hedley (1971), Heller (1978), Rochette and Fillion (1989)
Greigite	Fe_3S_4	?	200 - 350*	Snowball (1991)
Pyrrhotite	FeS_{1+x} $0 < x < 0.13$	0.5 - 1	325	Clark (1984), Dekkers (1988)

Since M_{ar} shows a more pronounced grain-size dependence than M_{ir}, the ratio M_{ar}/M_{ir} assesses fine-particle variations in the magnetite grain-size distribution [*Maher*, 1988; *Heider et al.*, 1995].

In addition to these isothermal magnetic methods, a variety of *thermomagnetic measurements* may be employed. Most of them are not very suitable for marine sediments, because of their low magnetic mineral concentrations. One exception, applied in Chapter 6, is a determination of the blocking temperature T_B which enables to distinguish magnetic minerals of similar coercivity on the basis of their mineralogy [*Lowrie and Heller*, 1982]. Maximum blocking temperatures of natural magnetic minerals are given in Table 4. A remanent magnetization imparted along three orthogonal axes of the sample at successively smaller fields allows the investigation of different coercivity ranges during one thermal demagnetization procedure [*Lowrie et al.*, 1980].

Further detailed reviews of isothermal and temperature dependent magnetomineralogic and –granulometric methods are given by *Thompson and Oldfield* [1986], *King and Channell* [1991] and *Dunlop and Özdemir* [1997]

2.5 Magnetic particle fluxes and environmental processes

Between source and deposition the sediment material undergoes various modifications. During physical weathering, erosion and transport sorting mechanisms affect both the magnetic and non-magnetic fractions. As a consequence, the magnetic properties of sediments may considerably differ from those of the original rocks. Grain-sizes, generally fining with increasing distance from the source, can therefore serve as tracers of the transport means and pathways.

Magnetic mineral concentration in sedimentary deposits is controlled by their accumulation in the deposition area and the dilution by non-magnetic components such as biogenic calcite or silica.

In oligotrophic marine regions with a relatively invariant terrigeneous particle supply, their dilution effect can provide direct information about carbonate accumulation. This has convincingly been demonstrated by *Schmieder* [1999], who established a detailed age model on the basis of orbitally tuned susceptibility signals of a core transect across the oligotrophic South Atlantic.

With knowledge of the sedimentation rate and the dry bulk density of the sediment, concentration dependent parameters allow to assess the accumulation rates of different magnetic sediment compounds. As shown in Chapter 6, magnetite accumulation can be determined from the ferromagnetic susceptibility κ_{fer}, hematite accumulation from the hard isothermal remanence M_{hir}, and the accumulation of paramagnetic material can be estimated from the paramagnetic susceptibility κ_{para}. Evaluation of these concentration independent accumulation rates is indicative of the intensity of different magnetic material influxes and allows to discriminate variable inputs from distinct particle sources.

High coercive minerals such as hematite or goethite are typical products of weathering under semiarid to humid conditions. Elevated contents of these minerals relative to the (titano-)magnetite fraction therefore hint at specific climatic conditions in the source region. Since hematite is ubiquitous and amounts to over 50% in most all South Atlantic sediments [*Schmidt et al.*, 1999] (Chapter 5), its relative scarcity indicates an additional, often biogenic supply of magnetite to the sediment.

The biomineralization of stable SD magnetite by magnetotactic bacteria living in the uppermost centimeters of the sedimentary column [*Petermann and Bleil*, 1993] is a sensible indicator of enhanced primary productivity.

Apart from mineralogy and grain-size, the quality of crystallization imparts information about the source material. Rapidly cooled particles of eruptive volcanic origin commonly comprise high crystal stresses which increase the coercivity [*Hodych*, 1982]. Similarly, an influence on coercivity and domain structure is observed in titanium-rich titanomagnetite at high cation deficiency [*Appel*, 1987].

Numerous investigations have shown [*Karlin*, 1990; *Karlin and Levi*, 1983; *Leslie et al.*, 1990a; *Leslie et al.*, 1990b; *Tarduno*, 1994; *Tarduno*, 1995; *Tarduno and Wilkison*, 1996] that reductive diagenesis may greatly modify magnetic mineral inventories in sediments by dissolution of primary iron oxides and authigenic formation of magnetic iron sulfides such as greigite. Suitable first order indicators of diagenesis are a reduced relative content and coarsening of magnetite since dissolution preferentially affects fine grain-sizes of ferrimagnetics.

CHAPTER 3. Statistics and multivariate data analysis

3.1 Distribution analyses

Geostatistics are based on the premise that information about a phenomenon can be deduced from the analysis of a small number of samples from a vastly larger set of potential observations. In the absence of an adequate definition of their nature, geologic populations may often fail rigorous tests of statistical hypotheses. For instance, distribution and trend analyses are very useful in geoscientific data interpretation. In Chapter 5 the "Komolgorov-Smirnov test" and the more stringent "chi-square test" [*Davis*, 1986]

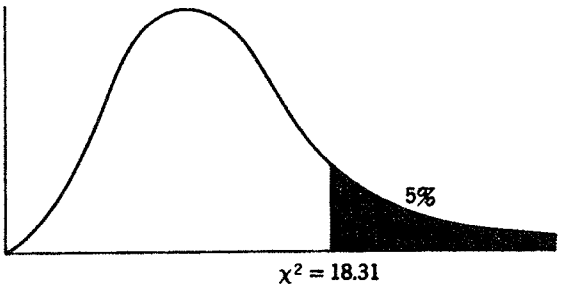

Figure 10. Typical χ^2 distribution. The shaded region which contains 5% of the area under the curve, corresponding to a critical value of $\chi^2_{crit} = 18.31$ [*Davis*, 1986].

are applied to evaluate all magnetic data sets for normal or lognormal distributions. Both tests compare the frequency distribution of a sample to a hypothetical distribution.

The "*chi-square test*" is based on the χ^2 distribution (Figure 10). If a sample is taken from a normal population having a mean μ and standard deviation σ, each observation within the sample v can be standardized to

$$z = \frac{v - \mu}{\sigma}$$

having a zero mean and standard deviation of one. If all possible samples of a given size are drawn from a normal distribution, the squared sums of z form a χ^2 distribution. A *goodness of fit* test reveals how well the distribution of sample values conforms with a hypothetical normal or log-normal distribution. For this purpose, the hypothesized distribution is divided into a number of segments. The probability that an observation falls into one of the segments is equal to the area under the particular curve section. From these probabilities the number of observations that would be expected within each section is calculated. For each segment, the expected frequency of occurence can then be compared to the frequency of observations. The test statistic is calculated by

$$\chi^2 = \sum_{j=1}^{k} \frac{(O_j - E_j)^2}{E_j}$$

where k is the number of segments, O_j the number of observations within interval j, and E_j the number of expected observations. For a specified level of significance and degrees of freedom, which are dependent on the chosen number of segments, a critical value χ^2_{crit} is defined [*Davis*, 1986, Table 2.18]. If $\chi^2 < \chi^2_{crit}$, the hypothesized distribution can be accepted.

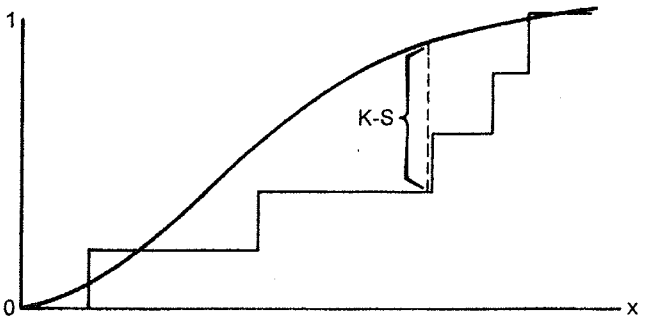

Figure 11. Komolgorov-Smirnov procedure testing the goodness-of-fit of a sample distribution (staircase curve) to the hypothetical model of the population (bold line). Both are plotted in cumulative form from 0 to 1. The maximum difference gives the test statistic, K-S [*Davis*, 1986].

An alternative, more commonly used and less stringent *goodness of fit* test is the "*Komolgorov-Smirnov*" test. For this method no grouping of observations into arbitrary categories is necessary. Figure 11 illustrates the Komolgorov-Smirnov procedure. Both the sample in standardized normal form and the hypothetical population are plottet together in cumulative form, each scaled so their cumulative sums 1. The largest difference between the two curves is the Komolgorov-Smirnov statistic, K-S. The Komolgorov-Smirnov test is generally used, when the hypothetical model can be completely specified from information other than that contained in the sample itself. *Lillefors* [1967] introduced criteria permitting to test the fit of a sample to a normal distribution with an unspecified mean and variance. Critical values for a sample size up to $n = 40$ are available in a tabular form [e.g., *Davis, 1986*, Table 2.26]. For $n > 40$ approximate values can be calculated for specified values of significance. For a significance level of $\alpha = 0.05$ as in Chapter 5, the critical value is

$$\text{K-S}_{\text{crit}} = \frac{1.36}{\sqrt{n}}$$

3.2 Cluster analyses

In the reconstruction of environmental processes the expansion from single parameter analytical and interpretative techniques to multivariate studies is of rising interest, as it advances the untangling of complex interrelations and superimposing influences and the specification of regional or temporal peculiarities. One major concern is the empirical classification of frequently large multiparametric data collections. Cluster analytical techniques are used in numerous disciplines of science like numerical taxonomy, medicine, and psychology as an effective tool for the multivariate classification of objects into more or less homogeneous groups, providing the quantification of their relationships. A multiparameter data set **X** is represented as the scatter of sample specific data points $\mathbf{x} \in \mathbf{X}$ in an n-dimensional vector space spanned by n parameters. The Euclidian distance between any two samples $\mathbf{x}, \mathbf{y} \in \mathbf{X}$

$$D(\mathbf{x},\mathbf{y}) = \sqrt{\sum_{i=1}^{n}(x_i - y_i)^2}$$

can be used to quantify their multiparameteric similarity. All cluster analytic methods require parameter standardization to provide an equal weighting of all sample properties. In its standard normal form, the parameter set has zero mean and unity standard deviation.

Clustering algorithms can be assigned to two general types, deterministic clustering and probabilistic clustering. Deterministic methods firmly ascribe a sample to only one cluster, whereas probabilistic clustering attributes every sample to every cluster with a certain probability. Deterministic clustering techniques can be hierarchical or partitioning.

Deterministic clustering techniques

Hierarchical clustering starts with the joining of the most similar observations, then successively connecting objects of higher dissimilarities. The first step of this iterative process is the calculation of an $l \times l$ matrix of the similarities between all pairs of l observations. After having merged the most similar pairs, the matrix is recalculated by averaging the similarities that the combined objects have with the remaining set of observations. This procedure is repeated until the similarity matrix is reduced to 2×2. The results are graphically presented in

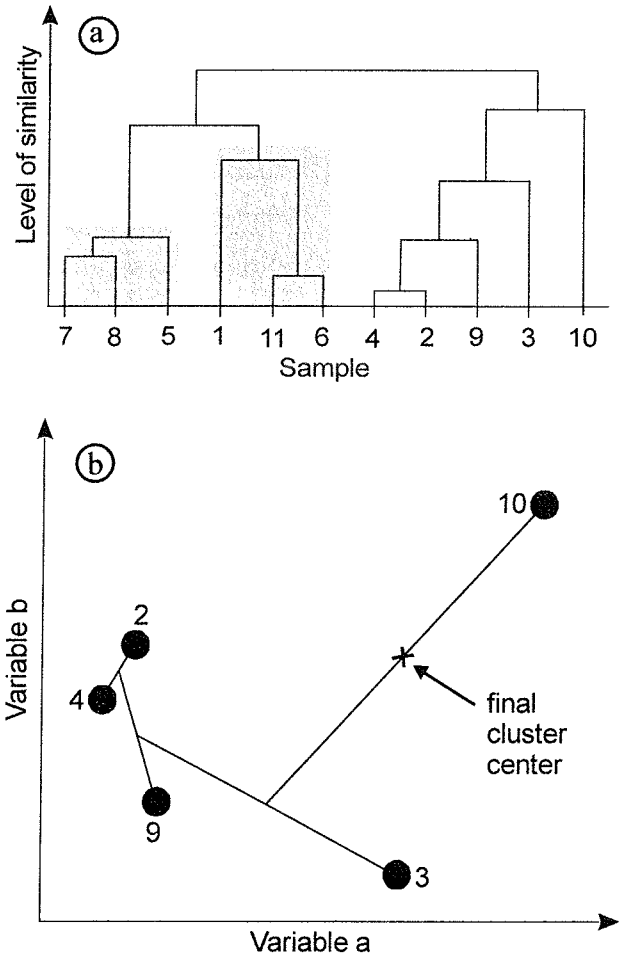

Figure 12. a. Example of dendrogram representing results of a hierarchical cluster analysis of 11 samples and two variables. Two major clusters are discernable (lightly gray shaded), one of which splits into two subclusters (darkly gray shaded). **b.** Illustration of cluster center displacement during hierarchical clustering procedure. The final center of the cluster which contains samples 4, 2, 9, 3, and 10 is strongly biased towards sample 10 which joins the cluster at least.

a dendrogram, depicting the levels of similarity at which the observations are merged (Figure 12a). As a result, for each level of similarity more or less homogeneous groups or clusters of samples are found. The characteristic of a cluster is given by the arithmetic mean of the respective sample properties. One disadvantage of this method is demonstrated in figure 12b. During the hierarchical procedure, the arithmetic mean of a cluster is calculated by averaging the means of several clusters or by joining sample by sample to a cluster. In the latter case the properties of individual samples are unevenly weighted, leading to a distortion of the joint cluster mean.

Partitioning clustering methods principally find accumulations of observations within the *n*-dimensional parameter space and group them into clusters. In contrast to hierarcical methods, the cluster characteristic is represented here by the mean of all contributing sample properties (Figure 13a). The most commonly used partitioning clustering technique is the *k-means* method. The idea of this procedure is the calculation of cluster means, or cluster centers, such that the squared sum of deviations within the clusters is minimized. This involves a minimization of the squared Euclidian distances between each sample x_j and cluster center c_k

$$\sum_k \sum_j d_{j,k}^2 \rightarrow \min$$

As a first step in the iterative *k-means* procedure, the number of clusters and starting values for the cluster centers have to be predefined. This starting partition can be defined by various techniques [*Bacher*, 1994]. Next, the samples are now attributed to the cluster centers which are nearest in the parameter space. After assignment of all samples to clusters, the cluster centers are recalculated as arithmetic means of all contributing sample properties i

$$c_{ki} = \frac{\sum_j x_{ij}}{n_k}$$

where n_k denotes the number of samples within cluster k. This procedure is repeated iteratively until the algorithm converges to a final cluster structure with minimal internal heterogeneity.

Probabilistic clustering techniques

Probabilistic clustering procedures are based on a generalization of the *k-means* cluster analysis. Different from deterministic methods,

probabilistic clustering assigns an object or sample to every cluster with a certain probability or membership function (Figure 13b). This concept of „fuzzyness" [*Zadeh*, 1965] takes into account that in nature groupings are unlikely to be characterized by sharp boundaries. The classification and characterization of partly overlapping sedimentation areas presented in Chapters 5 and 6 demonstrate this concept. Fuzzy cluster analysis FCM [*Bezdek*, 1973; *Bezdek*, 1981; *Bezdek and Dunn*, 1975] establishes fuzzy partitions on the basis of multivariate similarity. Prime interest is not in a strict assignment, but in the quantification of resemblances amongst samples and clusters.

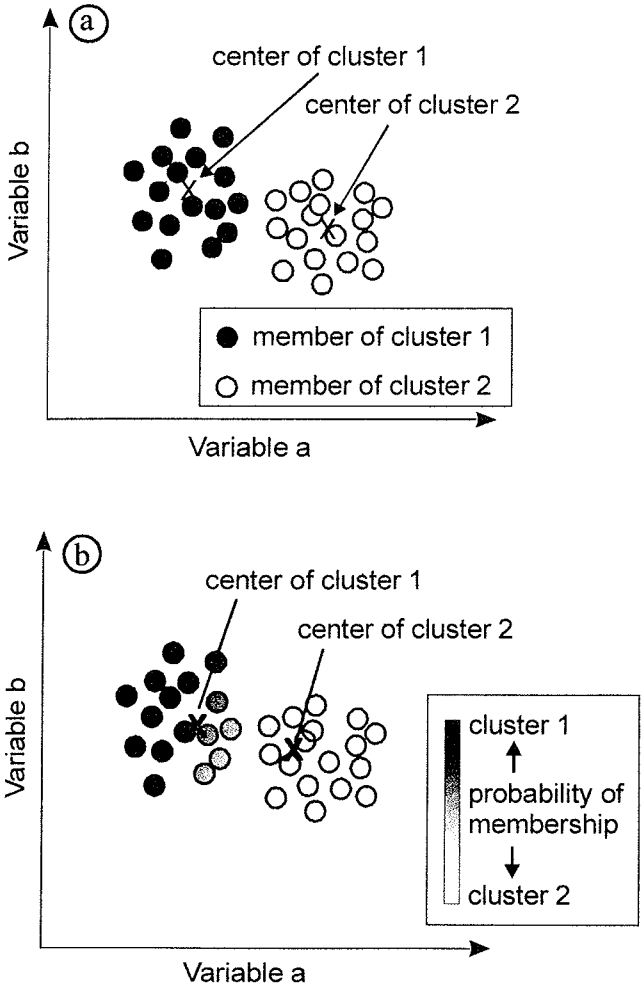

Figure 13. a. Principle of partitioning clustering method illustrated for a sample collection and two variables. Every sample is strictly assigned to only one cluster. The cluster centers are calculated as means of all equally weighted cluster members. **b.** Probabilistic clustering of the same sample assemblage as in a. Every sample is related to each cluster with a certain probability of membership, represented by gray shading levels. Black indicates 100% probability of membership to cluster 1, white 100% probability of membership to cluster 2. The gray shaded samples correspond to an intermediate state, partially being assigned to both clusters. The cluster centers are calculated as weighted arithmetic means of all cluster members, the probability of membership acting as weight factor. Note that the cluster centers differ from the partitioning clustering results.

The FCM algorithm [*Bezdek*, 1981] includes a measure of the degree of fuzzyness defined by an exponent q which quantifies the extent of membership sharing between the clusters. The cluster structure converges for $q \approx 1$ towards the partitioning k-means clustering result as described above. $q = +\infty$ indicates total fuzzyness and memberships of all samples to all clusters are equal. Frequently used q values range between 1.5 and 3 [*Urbat et al.*, 1999]. For the applications presented in Chapters 5 and 6 q = 2 has been chosen to give the best results.

If the appropriate cluster number is m, a fuzzy cluster structure is defined in which the affinity of each sample $\mathbf{x} \in \mathbf{X}$ to every individual cluster k (k = 1...m) is quantified by its membership function $p_k(\mathbf{x})$ which is a continuous function between zero (no similarity) and one (identical). All memperships of one sample sum up to unity:

$$\sum_{k=1}^{m} p_k(\mathbf{x}) = 1 \qquad 0 \le p_k(\mathbf{x}) \le 1$$

The membership of sample j to cluster k is given by

$$p_{jk} = \frac{\left(d_{jk}^2\right)^{\frac{1}{q-1}}}{\sum_{k=1}^{m}\left(d_{jk}^2\right)^{\frac{1}{q-1}}}$$

with d_{jk} the Eucledian distance of sample j to the cluster center of k. The cluster centers c_k are determined as weighted arithmetic means and

represent the characteristic properties of every cluster k. For each variable i and cluster k, the mean is calculated with the squared membership $p_k(\mathbf{x})$ acting as weight factor:

$$\bar{x}_{ik} = \frac{\sum_{\mathbf{x}\in\mathbf{X}} p_k^q(\mathbf{x}) \cdot x_i}{\sum_{\mathbf{x}\in\mathbf{X}} p_k^q(\mathbf{x})}$$

In Chapter 5 a weighted standard deviation for each cluster k and variable i is calculated:

$$s_{ik} = \sqrt{\frac{\sum_{\mathbf{x}\in\mathbf{X}} p_k^q(\mathbf{x}) \cdot (x_i - \bar{x}_i)^2}{\sum_{\mathbf{x}\in\mathbf{X}} p_k^q(\mathbf{x})}}$$

In selecting the number of clusters m, validity indicators such as partition coefficient F and partition entropy H [*Bezdek*, 1981] must be taken into account:

$$F = \sum_{j=1}^{n}\sum_{k=1}^{m} \frac{p_{jk}^2}{n} \qquad 1/m \le F \le 1$$

$$H = -\sum_{j=1}^{n}\sum_{k=1}^{m} \frac{p_{jk} \cdot \log(p_{jk})}{n} \qquad 0 \le H \le \log(m)$$

Theoreticaly, the best solution maximizes F and minimizes H. For a decision which number of clusters is the most appropriate to match the respective data structure also all available background knowledge about the data set should be considered.

This chapter should not be concluded without mentioning the danger hidden in the uncritical application of statistical methods. If the underlying data basis does not contain valid and diversified information, statistical analyses are nothing but GIGO: "Garbage In, Garbage Out".

The Magnetic View on the Marine Paleoenvironment: Parameters, Techniques and Potentials of Rock Magnetic Studies as a Key to Paleoclimatic and Paleoceanographic Changes

T. Frederichs*, U. Bleil, K. Däumler, T. von Dobeneck and A.M. Schmidt

Fachbereich Geowissenschaften, Universität Bremen, Postfach 33 04 40, D-28334 Bremen, Germany
**corresponding author (e-mail): thofred@geomarin.uni-bremen.de*

Abstract: The eminent potential of *Environmental Magnetism* analytical techniques to delineate depositional regimes and climatic changes in the marine realm is reviewed and illustrated with results of three individual studies of sediment series from the South Atlantic Ocean. Rock magnetic properties related to the mineralogy, concentration, domain state and hence grain-size of the magnetic mineral assemblage are explained on grounds of physical principles and discussed as proxy parameters for terrigenous particle fluxes, bioproductivity and diagenetic redox conditions. With cluster analysis of rock magnetic parameters determined for a large collection of surface samples, the regional characteristics of recent depositional environments in the equatorial South Atlantic are established. Notably, the different input mechanisms of terrigenous material via fluvial transport by the Amazon and Congo Rivers at the African and South American continental margins are as clearly identified as the eolian transport from the Sahara and Sahel Zone into the central and eastern equatorial South Atlantic. Based on a detailed susceptibility log and measurements of various laboratory remanences, high-coercive hematite components and different magnetite grain-size fractions could quantitatively be discriminated in a late Quaternary sediment sequence from the central equatorial Atlantic. The data sets allow to assess variations in eolian influx from the Saharan dust plume and several redox events during the last 400 kyr can be recognized. While biogenic magnetite is generally of minor importance in pelagic deposits, it may completely dominate the sediment magnetic properties in high productive areas. An intense primary biologic productivity in surface waters of the Benguela upwelling center supplies a high flux of organic matter to the sea floor at the continental slope off Namibia and causes reducing conditions in the sediment column. Resulting strong diagenetic effects on the biomagnetic mineral component are traced in detail by high-resolution rock magnetic analyses and transmission electron micrographs.

Introduction

Magnetic mineral inventories of marine sediments reflect source materials, transport mechanisms and diagenetic phenomena. Due to the particular physical properties of magnetic particles, their mineralogy, concentration and grain-size can be directly determined from rapid bulk sample measurements. Through space and time these records describe varying paleoceanographic conditions related to changes in lithosphere, hydrosphere and atmosphere (Fig. 1).

Following a suggestion by Thompson et al. (1980), this type of investigation, a relatively new expansion of geophysics, is called *Environmental Magnetism*. It was also the title of a milestone textbook by Thompson and Oldfield (1986) which provided a comprehensive summary of the broad range of relevant rock magnetic methods to study marine, limnic and fluvial sediments, soils and atmospheric dust. More recent reviews were compiled by Lund and Karlin (1990), Oldfield (1991), King and

From FISCHER G, WEFER G (eds), 1999, *Use of Proxies in Paleoceanography: Examples from the South Atlantic.* Springer-Verlag Berlin Heidelberg, pp 575-599

576 Frederichs et al.

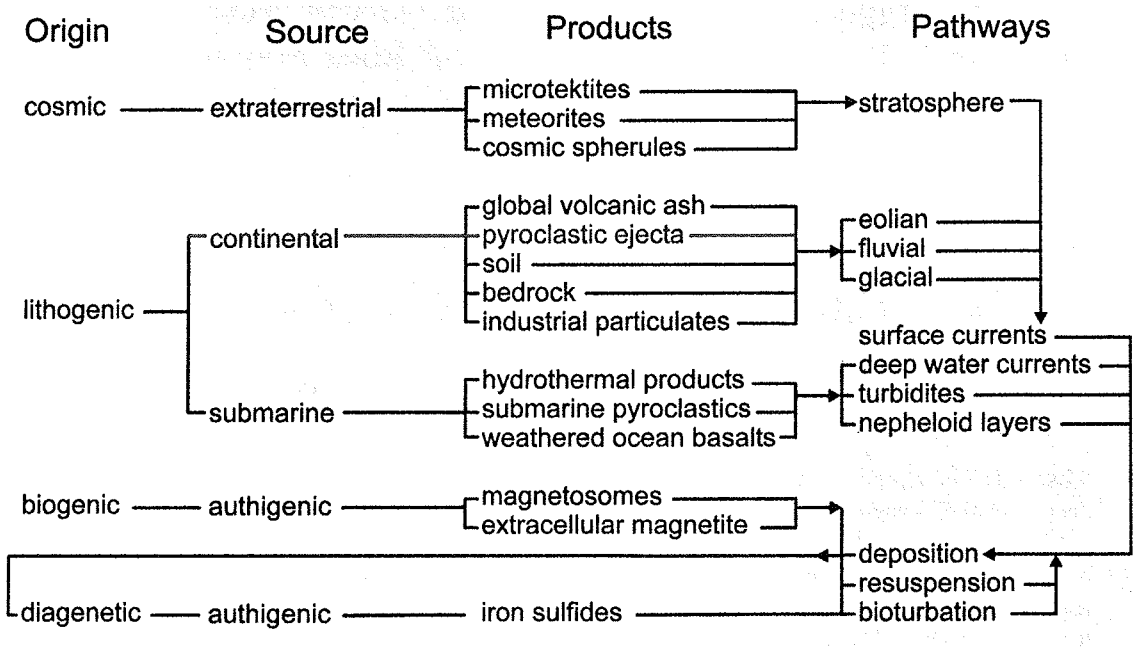

Fig. 1. Roots and tracks of magnetic minerals to the marine environment (modified from Thompson and Oldfield 1986).

Channell (1991) and Verosub and Roberts (1995). Among other topics, they address various successful applications of environmental magnetism techniques in paleoceanography:

- identification of source areas and pathways of eolian, fluvial and glaciogenic terrigenous components in deep-sea sediments;
- characterization of depositional regimes and their variability on the basis of authigenic magnetic minerals formed by biomineralization, abiotic precipitation and diagenetic processes;
- analysis of sediment fabric to reconstruct past bottom current intensities and directions;
- regional stratigraphic correlations and orbitally tuned chronostratigraphies of sediment series based on high-resolution records of rock magnetic parameters (see also von Dobeneck and Schmieder this volume).

The following publications paved the way for rock magnetism to marine sediments. Kent (1982) and Robinson (1986) found convincing correlations of oxygen isotope and calcium carbonate variations with the magnetic susceptibility signal which they explained as cyclic dilution and enrichment of the magnetic mineral component by climatically driven changes in carbonate accumulation. Bloemendal et al. (1988) used rock magnetic parameter core logs as a direct proxy for oxygen isotope records. Mead et al. (1986) applied spectral analysis to magnetic susceptibility data sets to illustrate their relation to orbitally driven periodicities. DeMenocal et al. (1988) found variations in bottom current activity documented in rock magnetic properties of marine sedimentary deposits. Sager and Hall (1990) described the magnetic signature of turbidity currents. Doh et al. (1988) identified the eolian contribution to central North Pacific deep-sea sediments. Bloemendal et al. (1992) related rock magnetic parameters to sediment sources, lithology and diagenetic processes. Stoner et al. (1996) compared the magnetic characteristics of detrital horizons from the deep Labrador Sea to North Atlantic Heinrich layers.

Mineral Magnetism

Magnetic, i.e., remanence carrying minerals amount to only a very small fraction (typically << 1%) of marine sediments. All other constituents are *diamagnetic* (e.g., biogenic carbonate and

silica, water) or *paramagnetic* (e.g., Fe-rich silicates including clays). Dia- and paramagnetic minerals acquire a weak induced magnetization in magnetic fields, but they cannot carry a remanent magnetization, i.e., a permanent magnetization in zero field. They are discerned by their susceptibility which is negative for diamagnetic and positive for paramagnetic minerals.

Natural magnetic minerals are classified as *ferrimagnetic* ((titano-)magnetite, maghemite, pyrrhotite, greigite) or *antiferromagnetic* (hematite, goethite). Ferrimagnets exhibit much higher but less stable magnetizations as compared to antiferromagnets.

The basic physical principles of ferromagnets (e.g., iron) also apply to ferrimagnets and antiferromagnets (e.g., Chikazumi 1997). To emphasize their fundamentally different origin, diamagnetic and paramagnetic contributions to the magnetic properties of sediments are referred to as non-ferromagnetic. (Note that there are no natural ferromagnetic minerals).

The phenomenon of permanent magnetism is associated to the existence of *magnetic domains* with uniformly oriented atomic magnetic moments. As a function of grain-size, the number of domains within a magnetic particle increases from one to several hundreds. *Single-domain* (SD) and *multi-domain* (MD) particles differ considerably in their magnetic characteristics. MD grains with a few domains (<10) have similar properties as SD particles and are categorized as *pseudo-single-domain* (PSD) particles. The magnetization of ultra-fine particles below a certain threshold size is unstable due to thermal activation. Because of their high susceptibility and, on the other hand, their incapacity to carry a remanence, they are called *superparamagnetic* (SP) particles.

The grain-size thresholds between the four domain states (SP, SD, PSD and MD) primarily depend on mineralogy. For magnetite the SP/SD transition is at 0.03 μm, the SD/PSD boundary at 0.1 μm and particles larger than 10 - 20 μm show MD behavior (Parry 1965; Dunlop 1973; Bailey and Dunlop 1983). The properties of natural magnetic particles are discussed in detail by Stacey and Banerjee (1974), Dunlop (1981; 1986; 1990; 1995) and Dunlop and Özdemir (1997). The textbook of Chikazumi (1997) gives a detailed treatment of the physics of ferromagnetism.

Experimental Methods

Common rock magnetic parameters are derived from

- magnetic hysteresis loops,
- remanence acquisition and demagnetization experiments,
- magnetic susceptibility measurements,
- thermomagnetic analyses,
- evaluation of magnetic anisotropies.

The last two topics are covered by the following references: Lowrie (1990), Mullender et al. (1993), Hrouda (1994), Hrouda et al. (1997), Hamilton and Rees (1970), Rochette et al. (1992), Borradaile and Stupavsky (1995) and Lehmann et al. (1996). They will not be further discussed here.

Magnetic Hysteresis Loops

The term *magnetic hysteresis* refers to the effect that a sample's magnetization depends not only on the actual magnetizing field, but also on the preceding magnetization states (Fig. 2).

The shape of a hysteresis loop, for which the field cycles between positive and negative extremes, delineates re-magnetization processes. A magnetically hard (*high-coercive*) mineral (e.g., hematite) yields a flat and broad hysteresis loop, while a magnetically soft (*low-coercive*) mineral (e.g., magnetite) displays a steep and narrow loop. In Figure 2a both hysteresis branches merge at medium field strengths, but still increase towards higher fields. From where the outer branch is strictly linear, the increase in magnetization can exclusively be attributed to para- or diamagnetic minerals of the sedimentary matrix. Subtraction of the linear asymptote, i.e., of the *non-ferromagnetic susceptibility* κ_{nf}, results in the slope corrected hysteresis loop (Fig. 2b). In the presence of SP and/or antiferromagnetic particles linearity can generally not be reached as maximum fields are limited to about 1 T in most laboratories. Sophisticated mathematical algorithms allow to estimate the effect of partly unsaturated hard magnetic constituents by the approach to saturation analysis (von Dobeneck 1996).

578 Frederichs et al.

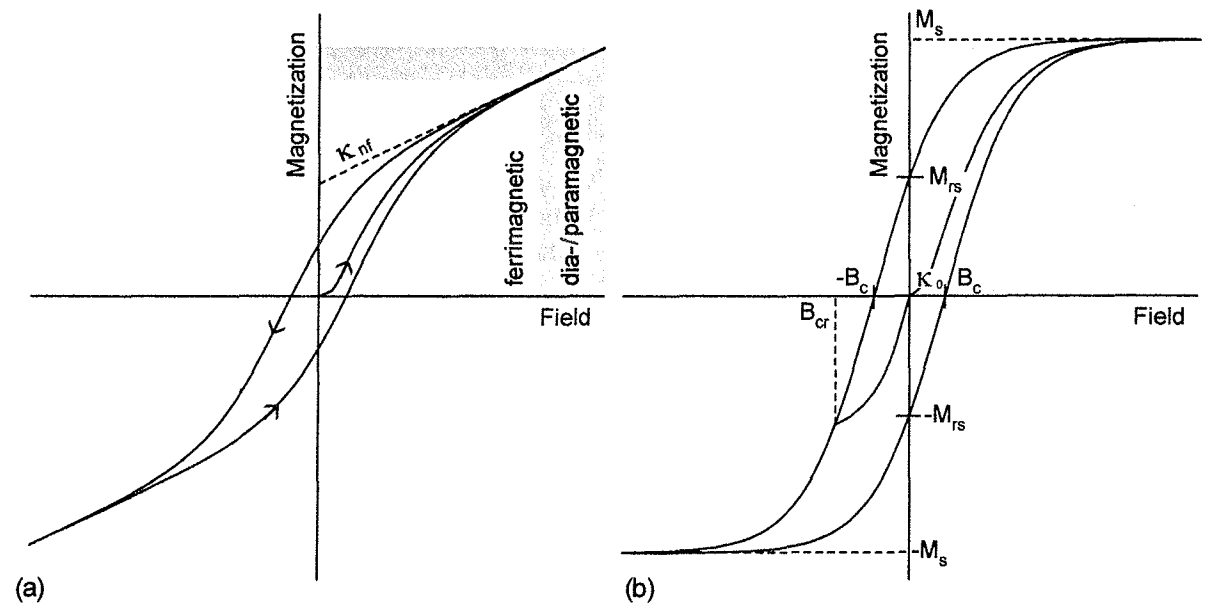

Fig. 2. (a) Schematic hysteresis loop for a mixture of ferrimagnetic and non-ferromagnetic minerals without slope correction, **(b)** slope corrected hysteresis loop with basic hysteresis parameters (see text for details).

A complete hysteresis measurement (Fig. 2b) starts from the demagnetized state (zero remanence) and zero field. The gradient of the curve near the origin defines the *initial susceptibility* κ_0 (per unit volume) or χ_0 (per unit mass). With rising field the magnetization increases up to the *saturation magnetization* M_s (σ_s). M stands for magnetization per unit volume, σ for the magnetization per unit mass. After removal of the field, the *saturation remanent magnetization* M_{rs} (σ_{rs}) remains. An inverse *coercive field* B_c reduces the magnetization to zero. The *coercivity of remanence* B_{cr} is a further increased inverse field which leaves a zero remanent magnetization after its withdrawal. The hysteresis loop is symmetric about the origin.

Remanence Acquisition and Demagnetization Experiments

Imparting a remanence in a stepwise increasing direct field yields the acquisition curve of *isothermal remanent magnetization* M_{ir} (σ_{ir}) which is indicative of the magnetic mineralogy (Fig. 3a). The maximum value, the *isothermal saturation remanent magnetization* M_{sir} (σ_{sir}), is identical with M_{rs} (σ_{rs}). Applying a (reversed) back field of typically 0.3 T results in the *back isothermal remanent magnetization* $M_{-0.3T}$ (Fig. 3b).

Subjecting a sample to an alternating field (AF) of decreasing amplitude in the presence of a weak constant biasing field generates the *anhysteretic remanent magnetization* M_{ar} (σ_{ar}). M_{ar} (σ_{ar}) normalized to the biasing field gives the *anhysteretic susceptibility* κ_{ar} (χ_{ar}).

Stepwise AF demagnetization of M_{ir} and M_{ar} yields two demagnetization curves which are characterized by their *median destructive fields* $B_{1/2}(M_{ar})$ and $B_{1/2}(M_{ir})$.

Modern long-core magnetometers make it possible to perform a set of various remanence based rock magnetic analyses at high resolution in short time (Nagy and Valet 1993; Weeks et al. 1993).

Magnetic Susceptibility Measurements

Volume (κ) or *mass specific* (χ) *magnetic susceptibility* is determined from the induced magnetization in a weak alternating field with an operating frequency of typically some hundred Hz. It is about equivalent to the initial susceptibility κ_0 (χ_0). For details of magnetic susceptibility definitions refer to Chikazumi (1997).

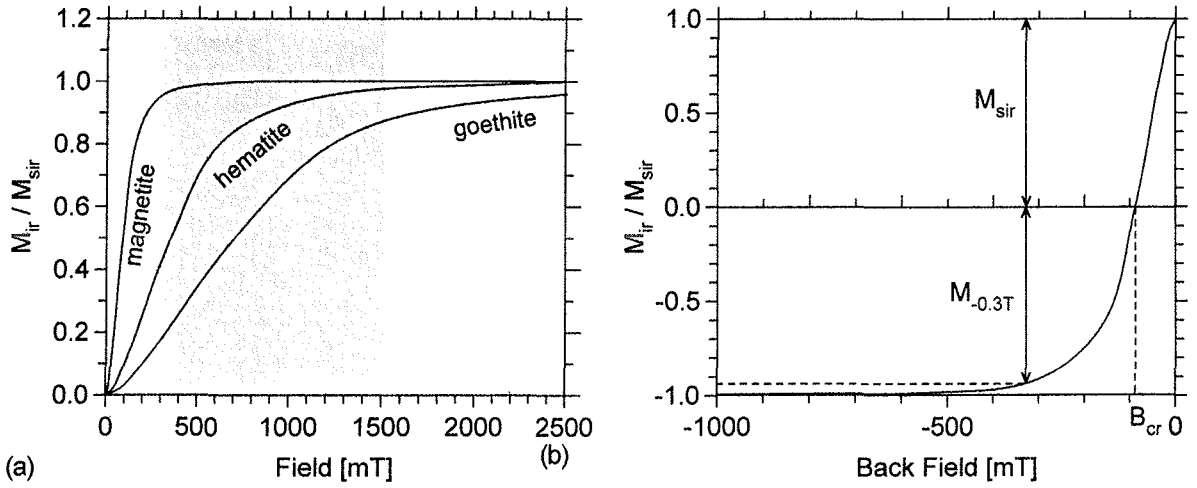

Fig. 3. (a) Schematic acquisition of isothermal remanent magnetization M_{ir} normalized to saturation remanence M_{sir} for magnetic mineral assemblages dominated by magnetite (upper curve), hematite (middle curve) and goethite (lower curve). Within the shaded field limits M_{ir} variations can primarily be attributed to individual mineral components approximately reaching saturation at the respective upper boundaries. **(b)** Schematic back field curve for a mixture of magnetite and hematite. At $M_{ir} / M_{sir} = 0$ the field is equivalent to the coercivity of remanence B_{cr}. M_{ir} left after -300 mT essentially refers to hematite.

By measuring susceptibility at a second, typically one magnitude higher frequency (κ_{hf}) its *frequency dependence* is quantified either as a loss of susceptibility (Dearing et al. 1996)

$$\kappa_{fd} = \kappa - \kappa_{hf}$$

or as percentage

$$\kappa_{fd\%} = 100 \cdot (\kappa - \kappa_{hf}) / \kappa$$

Rock Magnetic Parameters

Concentration Dependent Parameters

Rock magnetic parameters delineate variations in concentration, grain-size and mineralogy of magnetic mineral assemblages. Their sedimentological interpretation is considerably more complex, however, than usually straightforward physical explanations. The respective paleoceanographic proxy character depends on the sedimentary environment and must be evaluated for each individual setting.

From the theoretical viewpoint, saturation magnetization M_s is the only strictly domain state (grain-size) independent parameter to quantify the concentration of the magnetic mineral fraction. Its precise determination requires laborious high-field hysteresis measurements which are not very practicable for large sample series. The next best (and widely accepted) choice is magnetic susceptibility κ, the fastest and most reliably measurable magnetic quantity. Heider et al. (1995) have compiled susceptibility data for various magnetite grain-size fractions and found that a fairly constant value of 3.1 ± 0.4 SI is valid over a wide grain-size range from 0.1 to 10000 μm. Only SP magnetite has up to two times higher susceptibilities of 4 - 6 SI. Other ferri- or antiferromagnetic minerals as well as paramagnetic matrix constituents contribute to κ, but with much lower specific susceptibilities. Diamagnetism must be considered where κ falls below 10^{-4} SI (< 30 ppm magnetite) such as in many calcareous or siliceous biogenic sediments.

Ultra-fine SP particles are unable to carry a permanent magnetization, but show relaxation effects. They are represented by κ_{fd}.

The non-ferromagnetic susceptibility κ_{nf} is determined from high field hysteresis data (Fig. 2a).

Other remanence based parameters are selective for the concentration of specific grain-size fractions (see Table 1 in Example 2).

M_{rs} (= M_{sir}) refers to all components capable of carrying a remanence. It is biased by grain-size

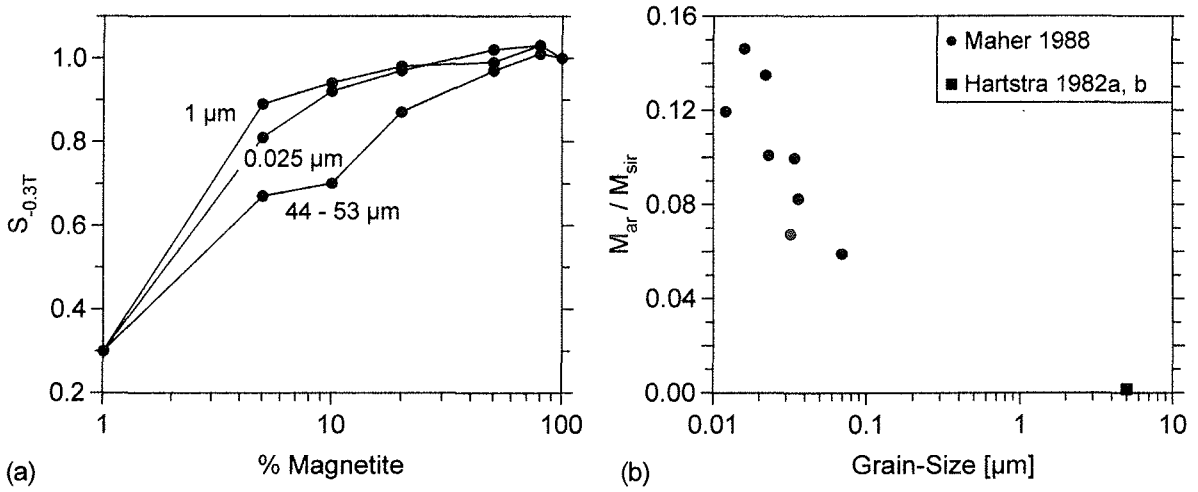

Fig. 4. (a) $S_{-0.3T}$ index for mixtures of hematite and different grain-sized magnetite (Bloemendal et al. 1992). **(b)** Magnetite grain-size dependence of the M_{ar}/M_{sir} ratio (anhysteretic remanent magnetization to isothermal saturation remanent magnetization).

as small SD particles have higher remanences.

Ferrimagnetic minerals are largely saturated in fields of about 0.3 T, while antiferromagnetic minerals need several Tesla to reach M_{rs}. *Hard isothermal remanent magnetization*

$$M_{hir} = 0.5 \cdot (M_{sir} + M_{-0.3T})$$

relates to high-coercive remanences encompassing primarily the concentration of antiferromagnetic minerals (Stoner et al. 1996). Only SD and small PSD particles acquire a significant anhysteretic remanent magnetization (Banerjee 1981) and are therefore quantified by M_{ar}.

Mineralogy Dependent Parameters

The ratio κ_{nf}/κ estimates the contribution of paramagnetically bound iron and diamagnetic compounds to susceptibility separating distinctly different depositional regimes.

The ratio of high- (hematite, goethite) to low-coercive ((titano-)magnetite) mineral concentrations is expressed as

$$S_{-0.3T} = 0.5 \cdot (1 + M_{-0.3T}/M_{sir})$$

varying non-linearly from 0 to 1 (Fig. 4a). Because of much lower specific magnetizations $S_{-0.3T}$ allows a reliable assessment of relative antiferromagnetic mineral concentrations only if their fraction exceeds about 80% (Bloemendal et al. 1992).

Coercivity Parameters

B_c is a measure of bulk magnetic stability (coercivity) and particularly sensitive to grain-size and magnetomineralogy. Other than the following three parameters, B_c is affected by (super-)paramagnetic and diamagnetic components.

B_{cr} quantifies the coercivity of remanence carrying particles.

$B_{1/2}(M_{ar})$ and $B_{1/2}(M_{ir})$ selectivity for mineralogy and grain-size is equivalent to that of M_{ar} and M_{ir}.

Grain-Size Sensitive Parameters

The ratios M_{rs}/M_s and B_{cr}/B_c depend on the dominant (titano-)magnetite domain state and therefore grain-size (Wasilewski 1973). With decreasing grain-size M_{rs}/M_s varies between about 0.01 and 0.5, B_{cr}/B_c between about 10 and 1 (>10 if a considerable SP fraction is present). Both parameters are commonly combined in a diagram (Fig. 5; Day et al. 1977).

Due to the predominant contribution of small PSD/SD particles to anhysteretic remanent mag-

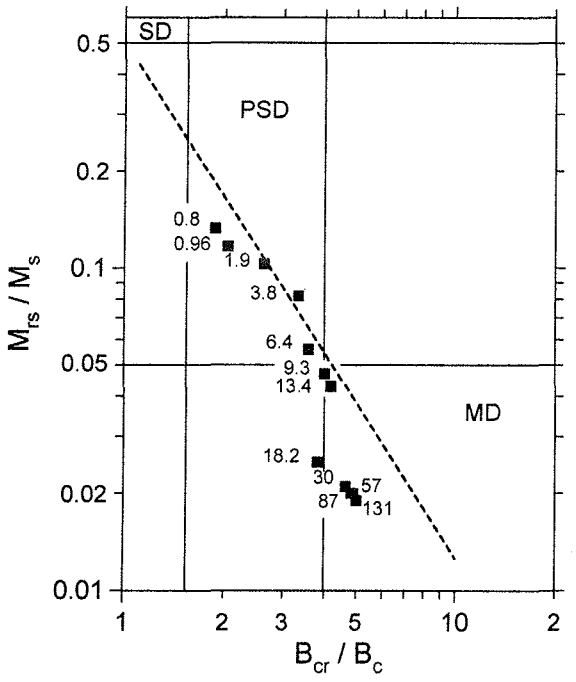

Fig. 5. Logarithmic plot of M_{rs}/M_s ratio (saturation remanent magnetization to saturation magnetization) versus B_{cr}/B_c ratio (coercivity of remanence to coercive field) for magnetite. Data point labels give mean grain-sizes of synthetic sample series (Day et al. 1977). The dashed line indicates an empirical relationship according to Parry (1982). Solid lines delineate fields of magnetically stable single (SD) and pseudo-single-domain (PSD) and magnetically unstable multi-domain (MD) grain-sizes (modified from Dunlop 1986).

netization, the ratios M_{ar}/M_{ir} and κ_{ar}/κ (King et al. 1982) increase for smaller grain-sizes (Fig. 4b). In contrast to κ_{ar}/κ, M_{ar}/M_{ir} is related only to remanence carrying particles.

Case Studies

In the following, three examples demonstrate the potential of environmental magnetism in paleoceanography. The first study presents a statistical approach classifying recent regional sedimentation regimes in the central equatorial Atlantic on the basis of magnetic properties of surface samples. The second illustrates the analysis and interpretation of a complex magnetic mineral assemblage in late Quaternary sediments from the central equatorial Atlantic. The strong effects of reductive diagenesis on the magnetic attributes of sediments from the Benguela upwelling region are discussed in the third example.

Example 1: Rock Magnetic Properties of Equatorial Atlantic Surface Sediments

Rock magnetic analyses are an effective method to identify and characterize marine sedimentation provinces with regard to source regions and transport mechanisms of their magnetic mineral inventories. This study deals with the variability of magnetic sediment properties in the recent equatorial Atlantic delineating regionally distinct magnetic mineralogies and granulometries.

All 53 samples are from the uppermost (0-1 cm) surface sediment layer. Seven of the above introduced accumulation rate independent rock magnetic parameters were determined. They delimit relative contributions of non-ferromagnetic (κ_{nf}/κ) and high-coercive antiferromagnetic minerals ($S_{-0.3T}$) as well as grain-size (M_{rs}/M_s, M_{ar}/M_{ir}) and coercivity (B_c, $B_{1/2}(M_{ar})$) of the ferrimagnetic mineral fraction. Relative concentrations of particles in the superparamagnetic (SP) grain-size range were determined from measurements of the frequency dependent susceptibility ($\kappa_{fd\%}$).

The recent equatorial Atlantic distribution patterns of four of these parameters are shown in Figure 6.

Contributions of non-ferromagnetic minerals to the magnetic susceptibility signal are given by the κ_{nf}/κ ratio (Fig. 6a). Low or even negative values indicate an essentially diamagnetic sediment matrix composed of biogenic carbonate or silica, while a mainly paramagnetic sediment matrix (Fe-rich silicates including clays) result in high positive values. The κ_{nf}/κ ratio is thus a proxy parameter for predominantly pelagic versus terrigenous sedimentation. It has to be taken into account, however, that diamagnetic biogenic sediments with small negative bulk susceptibilities may yield positive κ_{nf}/κ values erroneously implying a paramagnetic sediment matrix. The highest κ_{nf}/κ ratios were encountered off the Congo and Amazon river mouths documenting an enhanced terrigenous influx of paramagnetic materials (Barron and Whitman 1981; Lisitzin 1996). With increasing distance to the continents

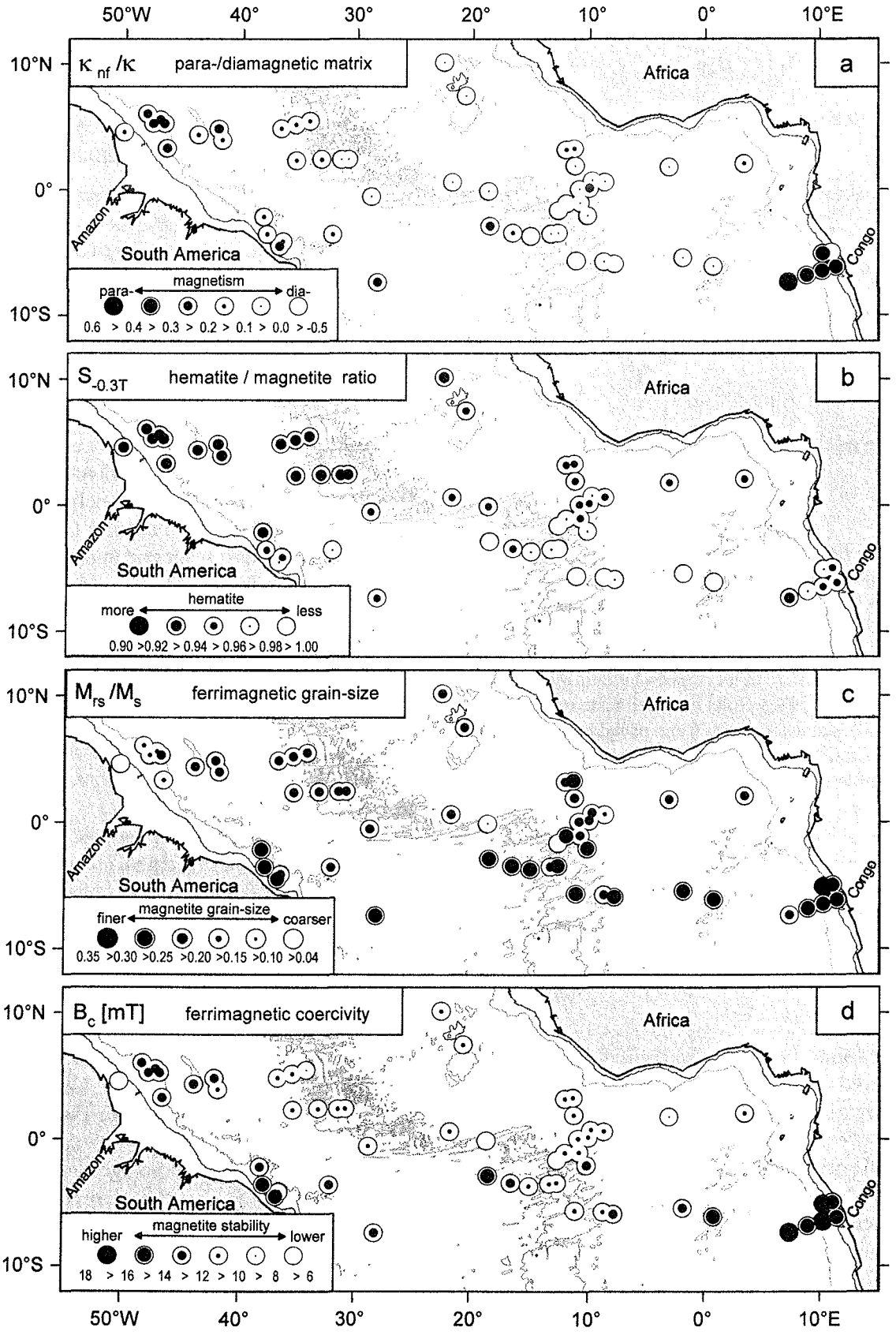
50°W
40°
30°
20°
10°
0°
10°E
10°N
0°
10°S
κ nf /κ para-/diamagnetic matrix
a
Africa
Amazon
South America
Congo
magnetism
para-
dia-
0.6 > 0.4 > 0.3 > 0.2 > 0.1 > 0.0 > -0.5
S-0.3T hematite / magnetite ratio
b
more
hematite
less
0.90 >0.92 > 0.94 > 0.96 > 0.98 > 1.00
Mrs /Ms ferrimagnetic grain-size
c
finer
magnetite grain-size
coarser
0.35 >0.30 >0.25 >0.20 >0.15 >0.10 >0.04
Bc [mT] ferrimagnetic coercivity
d
higher
magnetite stability
lower
18 > 16 > 14 > 12 > 10 > 8 > 6

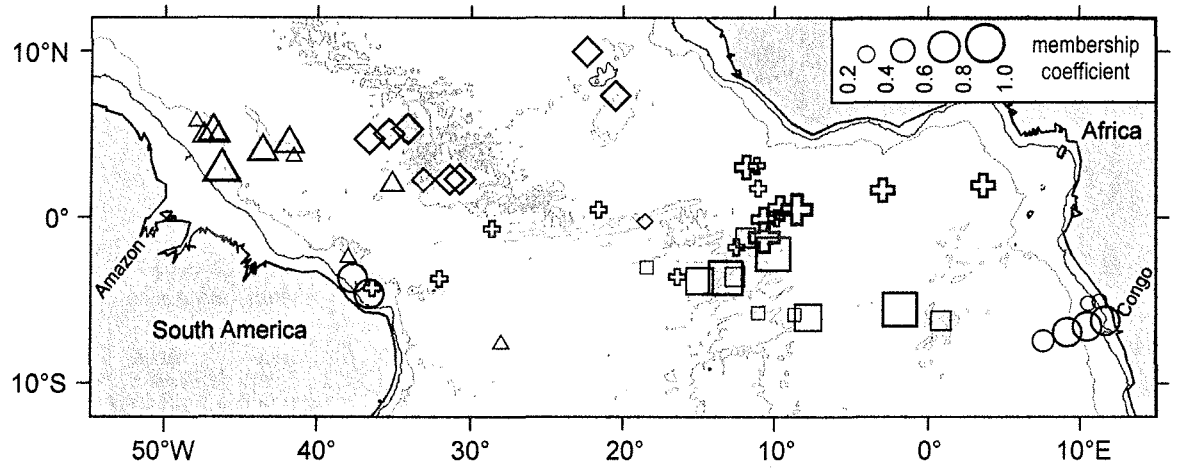

Fig. 7. Results of fuzzy c-means cluster analysis. Each sample is associated to one of five cluster centers (Fig. 8) according to its highest membership coefficient indicated by the symbol size. The data reveal a generally high regionality in characteristics of the dominant magnetic mineral assemblage and outline areas of fluvial input by the Amazon (triangles) and the Congo (circles) Rivers, eolian input from the Sahara (diamonds) and Sahel Zone (crosses) as well as a pelagic environment around 5°S near the mid-Atlantic Ridge (squares).

κ_{nf}/κ decreases to around -0.5 on the mid-Atlantic Ridge (MAR). There, the sample collection represents a typical pelagic sedimentation regime above the carbonate compensation depth (CCD) with almost no supply of terrigenous components. Three samples in this area show high κ_{nf}/κ values. They were recovered from below the CCD, where the sediment matrix mainly consists of paramagnetic deep-sea clays.

The $S_{-0.3T}$ parameter relates high-coercive ($B_{cr} > 0.3$ T) hematite and goethite to magnetite (Fig. 6b). As the maximum field applied was 0.8 T, $S_{-0.3T}$ essentially refers to hematite in this study (see Fig. 3) which specifically forms under arid conditions (Thompson and Oldfield 1986). Highest hematite/magnetite ratios (lowest $S_{-0.3T}$) are found in the northwestern equatorial Atlantic, a region strongly influenced by the Saharan dust plume extending to Central and South America (Pye 1987). The Amazon and Congo Rivers also convey substantial portions of high-coercive antiferromagnetic minerals as indicated by relatively low $S_{-0.3T}$ in their fan areas. Elsewhere, the concentration of high-coercive minerals decreases towards the open ocean.

The magnetogranulometric parameter M_{rs}/M_s (Fig. 6c) reveals a predominance of fine PSD to SD particles in most areas. This is also true for the Congo Fan, whereas the average ferrimagnetic grain-size in the Amazon River realm falls into MD range. Higher concentrations of MD particles at some MAR locations should reflect local volcanic sources. The regional distribution of coercivity B_c is shown in Figure 6d. B_c was measured using a maximum field of 0.3 T saturating most all of the magnetite fraction, but scarcely affecting high-coercive antiferromagnetic hematite. Elevated magnetite coercivities are particularly found in the Congo Fan, on the MAR between about 0° and 8°S and also at some localities on the Brazilian continental slope.

Fig. 6. Regional distribution of rock magnetic properties in surface sediments of the central equatorial Atlantic. **(a)** Ratio of non-ferromagnetic susceptibility to bulk susceptibility, κ_{nf}/κ, discriminating a predominantly paramagnetic, terrigenous versus a predominantly diamagnetic, biogenic sediment matrix. **(b)** $S_{-0.3T}$ parameter, quantifying the relative concentration of high-coercive, terrigenous hematite (and/or goethite) mineral components. **(c)** Grain-size of the magnetite mineral fraction as derived from the ratio of saturation remanence to saturation magnetization, M_{rs}/M_s. **(d)** Coercivity of the magnetite mineral fraction, B_c.

584 Frederichs et al.

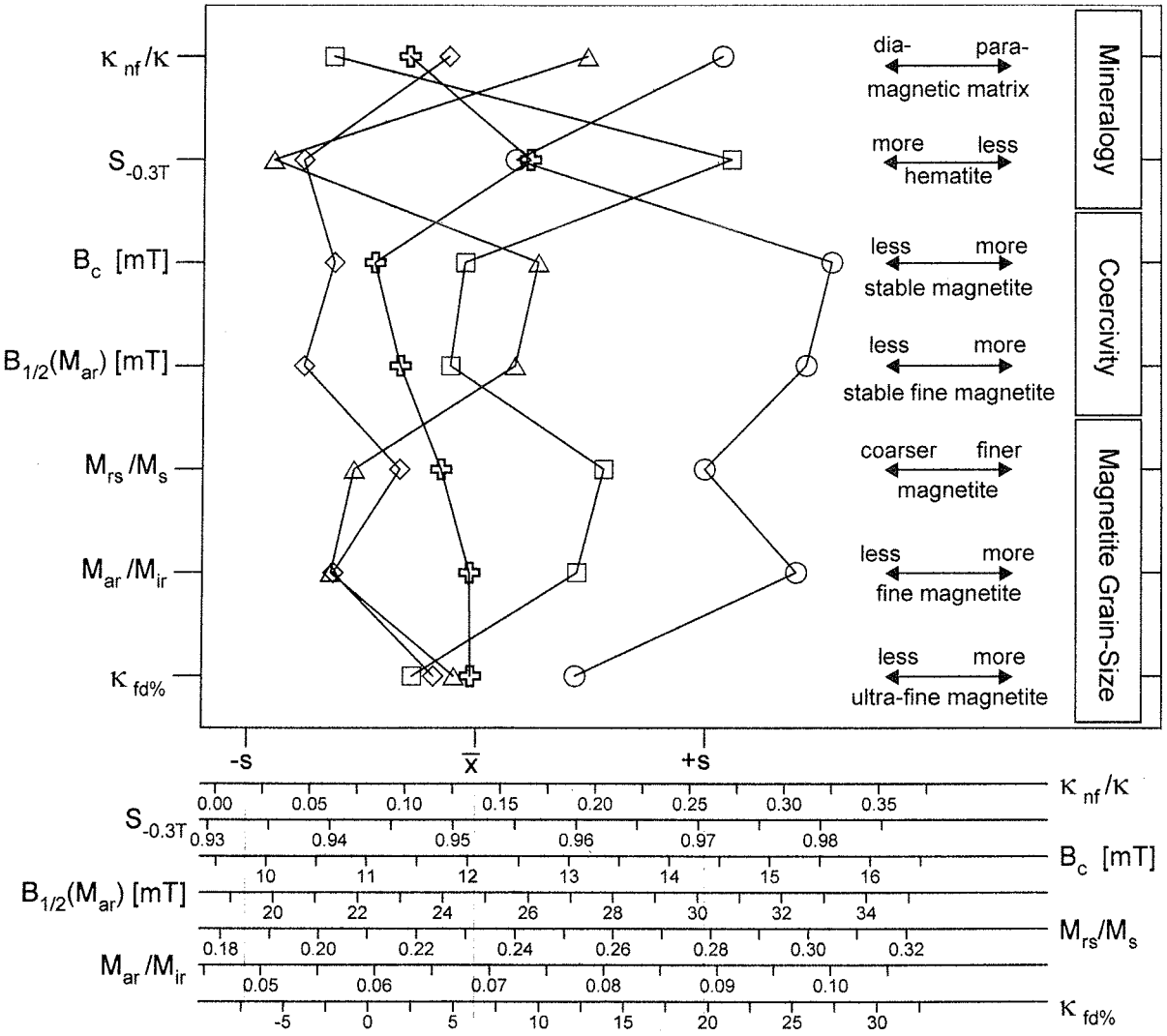

Fig. 8. Rock magnetic properties of the five cluster centers. Symbols correspond to Figure 7. Mean values and standard deviations refer to the total sample set, axes for the individual parameters have been scaled appropriately.

The above presented four and another three rock magnetic parameters form a multivariate data set allowing an outline of sedimentation areas in the equatorial Atlantic. A suitable statistical method for this aim is the cluster analysis initially adapted for rock magnetic purposes by Dekkers et al. (1994).

Detailed introductions to cluster analysis have been compiled by Bezdek (1981) and Bacher (1994). Applications in geochemistry were published by Middleburg and de Lange (1988) and Frapporti et al. (1993). In this study cluster analysis was calculated using the fuzzy logic toolbox (Jang and Gulley 1995) of the computer program Matlab.

The primary aim of cluster analysis is to group a collection of objects (samples) according to their individual characteristics (parameters) into empirically defined categories (clusters) with minimal internal heterogeneity. Among the different cluster analytical techniques, probabilistic fuzzy c-means clustering (FCM; Zadeh 1965; Bezdek and Dunn 1975) is most appropriate for the present application. Specifically, FCM quantifies smooth

transitions between sedimentation areas with fuzzy, gradual or overlapping boundaries by a membership function for each sample.

Figure 7 illustrates the resulting cluster structure of surface sediments in the equatorial Atlantic based on their rock magnetic properties. By its maximum membership function each sample is attributed to one cluster.

The five clusters in the working area reveal a distinct regionality. This strongly suggests a first order interpretation in terms of sedimentation provinces. It has to be pointed out again that no additional information about the sample locations and their sedimentation regimes has been included to attain this result which therefore entirely reflects the variability in rock magnetic sediment characteristics.

The rock magnetic properties of the five cluster centers are depicted in Figure 8. Samples from the Congo Fan area exclusively belong to the cluster marked by circles. High amounts of small, down to SP sized particles and relatively high coercivities of (titano-)magnetites are its most specific features compared to all other clusters. As described by Pak et al. (1984), the Congo detritus consists mainly of fine grain-sizes. Coarser fractions are settled in continental catchments. There is also an important fluvial influx of paramagnetic materials from the African continent by the Congo River. In contrast to this 'Congo Cluster' the sample collection from the Amazon Fan and including the Ceará Rise area (triangles) comprises the coarsest grain-sizes, but again relatively high coercivities suggesting that an elevated coercivity of magnetite is typical of continental sources and perhaps as well for fluvial transport. The 'Amazon Cluster' contains the highest quantities of hematite. Similar, yet slightly lower concentrations of hematite occur in the cluster marked by diamonds. The regional extent of available data for this cluster coincides with the southern portion of the Saharan dust plume. Magnetite is in the PSD/MD grain-size range and has the lowest coercivities encountered, indicating a large scale transport of coarse particles by strong wind systems also carrying substantial amounts of hematite. The cluster which mostly concentrates at the equatorial mid-Atlantic Ridge (squares) represents a typical pelagic sedimentation environment above the CCD without discernible eolian influx of continental material. The content of diamagnetic biogenic carbonate is highest and almost no hematite found. A fifth cluster (crosses) primarily covers the eastern part of the equatorial Atlantic. The characteristics of its cluster center fall approximately in between those of the 'Saharan Dust Plume Cluster' and the 'MAR Cluster' implying a pelagic sedimentation with some terrigenous components which could originate from the African Sahel Zone and are transported by less intense NE trade winds.

The example demonstrates that rock magnetic investigations combined with cluster analysis are an effective tool for empirical classification and identification of marine sedimentation provinces. As illustrated by the samples from the northeastern Brazilian continental margin, sediments collected in a relatively small area may belong to quite different clusters which have their principal occurrence in distant regions. It should generally be more appropriate, therefore, to name clusters according to their major magnetic characteristics instead of using geographic terms.

Example 2: The Analytical Concept of 'Partial Susceptibilities' Applied to a Complex Late Quaternary Magnetic Record from the Western Equatorial Atlantic

Most rock magnetic analyses of marine sedimentary deposits are based only on five or six different bulk sample measurements, each of which can be performed in a few minutes with standard magnetic laboratory equipments (Maher 1986; 1988). Combined data of high- and low-frequency susceptibility (κ_{hf}, κ), anhysteretic and isothermal remanent magnetization (M_{ar}, M_{ir}) of corresponding peak fields (in the present case 0.1 T), as well as saturation and back field isothermal remanent magnetization (M_{sir}, $M_{-0.3T}$) enable a fairly detailed rock magnetic characterization.

These properties represent concentration measures of partly differing, but overlapping magnetic mineral and grain-size fractions. They are more or less modulated by variations of the non-ferromagnetic, biogenic and/or terrigenous major components of the sediment matrix. The generally high

data co-linearity, imparted by the limited potential of individual parameters to discriminate particular components, is to some extent reduced by forming interparametric differences (→ *linear parameters*). The influence of matrix constituents can be eliminated by calculating suitable ratios (→ *relational parameters*) listed in Table 1.

As an example, the data set for central equatorial Atlantic gravity core GeoB 1505-2 (2°16.0'N / 33°0.9'W, 3706 m water depth) is presented. The age model for this sediment sequence has been established by matching its distinct $CaCO_3$ pattern to that of the $\delta^{18}O$ dated core GeoB 1523-1 from the Ceará Rise (Zabel et al. 1998). The paleoclimatically controlled $CaCO_3$ variations, ranging from 40 to 80 weight%, are inversely correlated to major features of the susceptibility log. However, they can neither fully explain the fluctuations in signal amplitude from 50 to $250 \cdot 10^{-6}$ SI nor various details of the susceptibility record. Bloemendal et al. (1988) published similar data for several late Quaternary cores from the eastern equatorial Atlantic and showed that carbonate-free susceptibility logs and respective magnetic mineral accumulation rates maintain a pronounced climatic signal and consequently testify climatically driven variations of terrigenous fluxes.

A compilation of susceptibility, three *per se* carbonate independent magnetic parameters, $\kappa_{fd\%}$, $S_{-0.3T}$, M_{ar}/M_{ir} and the $\delta^{18}O$ SPECMAP stack (Fig. 9) suggests that core GeoB 1505-2 comprises a similar record. The magnetogranulometric ratio M_{ar}/M_{ir} strikingly parallels the SPECMAP stack and lends itself perfectly for age modeling. During warm periods, a systematic fining of the magnetite grain-size distribution is indicated. Likewise, the pattern of magnetomineralogical ratio $S_{-0.3T}$ correlates with global climate, but the relative hematite minima associated to sub-stages 3.3, 6.3, 6.5, 8.3 and 8.5 are much more pronounced than the respective $\delta^{18}O$ minima. The frequency dependence of susceptibility $\kappa_{fd\%}$, denoting ultra-fine superparamagnetic magnetite (< 30 nm), displays no simple climatic pattern and retains a quite high level of about 8% throughout most of the core. Anomalies appear again in several sub-stages (6.3, 6.5, 7.1, 7.5, 8.3) and stage 10. During these intervals either no SP fraction was deposited or it has been dissolved by diagenetic processes. Four narrow horizons of particular lithologies (a sand layer at 30 ka, tephra layers at 247, 256 and 270 ka) peak out as negative or positive spikes in all core logs, demonstrating that specific facies, and in particular ash-rich layers, have their own magnetic signature.

The so far discussed magnetic parameters are relational and therefore independent of the major sediment constituents. They exclusively indicate grain-size and mineralogy shifts within the magnetic mineral assemblage which have to be explained in

Table 1. Linear magnetic parameters characterizing the concentration of specific magnetic fractions and relational magnetic parameters indicating magnetite domain state (and therefore grain-size) and antiferromagnetic constituents. Note that M_{ir}, determined here using a field of 0.1 T does not exclusively refer to multi-domain magnetite. A softer remanence (e.g., M_{ir} of 0.01 T) should generally be preferable for this purpose.

Magnetic Fraction	Linear Parameters	Relational Parameters
SP Magnetite < 0.03 μm	κ_{fd}	$\kappa_{fd\%}$
SD Magnetite 0.03 - 0.1 μm	M_{ar}, κ_{arm}	M_{ar}/M_{ir}, κ_{arm}/κ
(PSD) - MD Magnetite > 0.1 μm	M_{ir}	M_{ar}/M_{ir}
HE Hematite and Goethite	M_{hir}	$S_{-0.3T} = 1 - M_{hir}/M_{sir}$

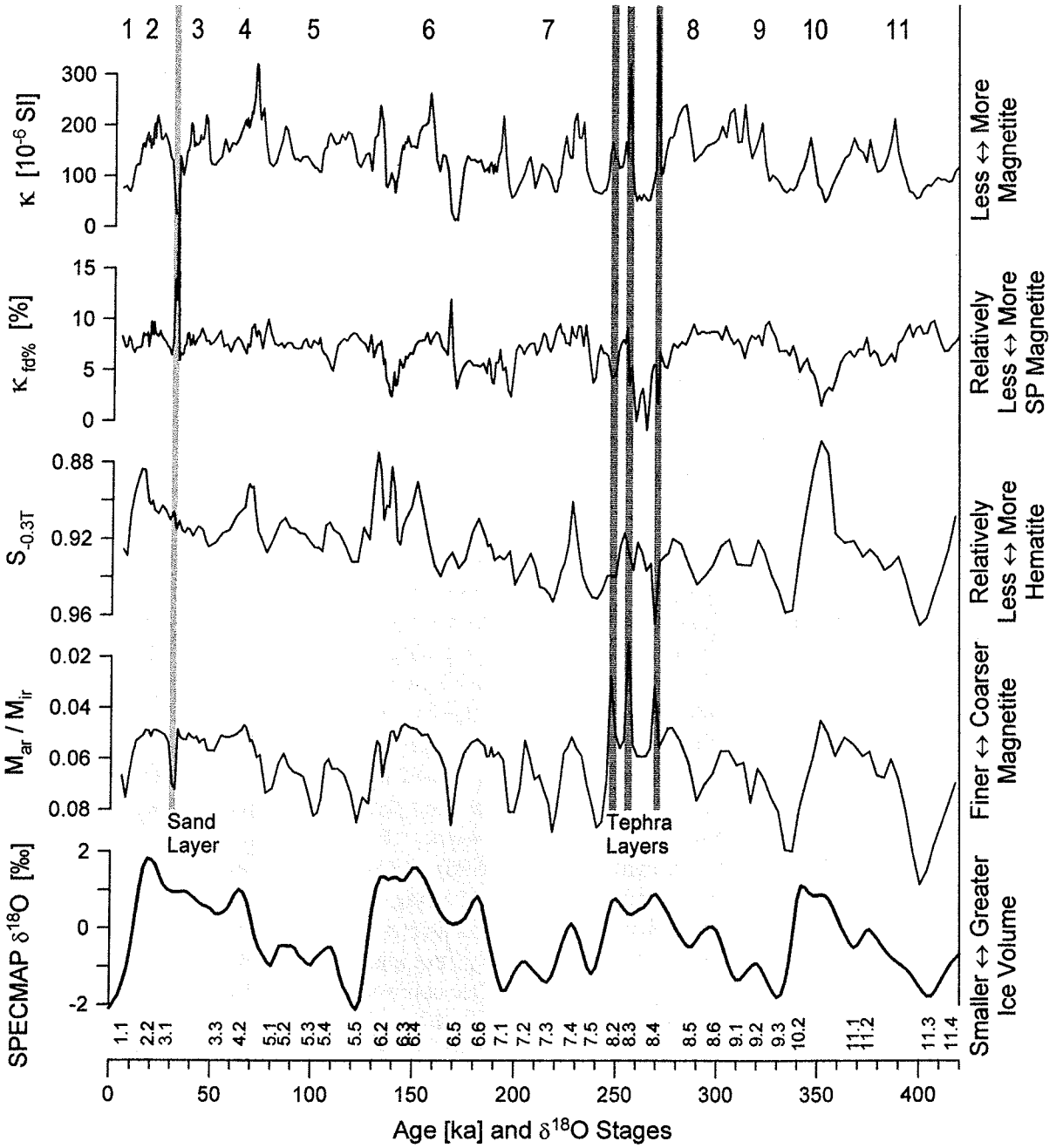

Fig. 9. Central equatorial Atlantic core GeoB 1505-2. Records of susceptibility κ, frequency dependence of susceptibility $\kappa_{fd\%}$, hematite to magnetite index $S_{-0.3T}$ and magnetite grain-size index M_{ar}/M_{ir} compared to the $\delta^{18}O$ SPECMAP stack (Imbrie et al. 1984). The anhysteretic remanence M_{ar} was imparted in a constant field of 0.038 mT and a peak alternating field of 0.1 T. The isothermal remanence M_{ir} has been acquired at a peak field of 0.1 T, the saturating field for $S_{-0.3T}$ was 0.8 T. The trends marked at the right side of each plot denote the 'first-order' significance of the respective parameter. For magnetically complex lithologies these simplified classifications may be inadequate. A sand layer and three tephra layers influence all records. Predominantly cold climatic stages are shaded.

terms of a variable sediment source, transport or alteration.

Magnetic volume susceptibility is the most widely used parameter to quantify concentration changes of the magnetic mineral fraction in marine sediments. Susceptibility records are generally interpreted as proxies for the ratio of terrigenous (magnetite bearing) to biogenic (diamagnetic) deposition. In this respect not only continental sources must be considered. Outcropping weathered ocean floor basalt may also release considerable quantities of titanomagnetite, e.g., in regions of tectonic activity or high bottom current erosion. Magnetite biomineralization and diagenesis may further complicate the situation. With these possibilities in mind, the κ log of core GeoB 1505-2 reads as a basically climate induced signal which carries additional features (pronounced minima) in some of the sub-stages mentioned before.

To unravel such a composite record the following approach has been developed (von Dobeneck 1998). The observed susceptibility κ_{obs} is regarded as the sum of partial susceptibilities corresponding to discrete particle or mineral fractions. These partial susceptibilities are determined by calibrating the concentration related (linear) parameters (Table 1). The scaling coefficients, which link the basically uncalibrated individual parameter to the respective partial susceptibility, can be found by multiple linear regression provided the various signal patterns are sufficiently dissimilar. With indices corresponding to the fractions defined in Table 1 and to paramagnetism and diamagnetism, the observed susceptibility

$$\kappa_{obs} = \kappa_{para} + \kappa_{dia} + \kappa_{sp} + \kappa_{sd} + \kappa_{md} + \kappa_{he}$$

is approximated by a predicted susceptibility

$$\kappa_{pre} = \beta_0 + \beta_1 \cdot \kappa_{fd} + \beta_2 \cdot M_{ar} + \beta_3 \cdot M_{ir} + \beta_4 \cdot M_{hir}$$

It is obvious that κ_{sp} and $\beta_1 \cdot \kappa_{fd}$, κ_{md} and $\beta_3 \cdot M_{ir}$, as well as κ_{he} and $\beta_4 \cdot M_{hir}$ are corresponding terms, whereas κ_{sd} contributes to both $\beta_2 \cdot M_{ar}$ and $\beta_3 \cdot M_{ir}$. Using a more MD particle selective parameter such as low field remanence (e.g., M_{ir} of -0.01 T) would avoid this ambiguity. For the sake of simplicity the original parameter M_{ir} of 0.1 T is retained here, to some extent overestimating κ_{md} at the expense of κ_{sd}. The paramagnetic susceptibility κ_{para} cannot be estimated from the considered remanence parameters, but definitely contributes to κ_{obs} and must have an expression in κ_{pre}.

If the fluxes of paramagnetic minerals are linked to one or several magnetic fractions (e.g., weathering products such as paramagnetic clays and antiferromagnetic hematite are often associated and have proportional concentrations), the regression calculation will include their susceptibility by increasing the coefficient β_i of the respective magnetic fraction. Otherwise κ_{para} will contribute to the constant β_0. The diamagnetic susceptibility κ_{dia} is largely independent of the terrigenous fraction and can therefore be associated with β_0.

The regression results emphasize the sensitivity of this approach. Goodness-of-fit R equals 0.986 and the standard error of the estimate is $8.7 \cdot 10^{-6}$ SI. Predicted and observed susceptibilities (Fig. 11a) match very well, largest discrepancies occur at sharp maxima. The constant $\beta_0 = -12.4 \cdot 10^{-6}$ SI convincingly coincides with κ_{dia} for a mixture of $CaCO_3$ and H_2O. Also the other coefficients β_1 to β_4 (Fig. 10) appear altogether plausible from a rock magnetic point of view. The relation $\kappa_{sp} = 3.97\ \kappa_{fd}$ implies that for purely superparamagnetic particles we should have $\kappa_{fd}/\kappa_{sp} = 1/3.97 = \kappa_{fd}/\kappa = 0.25$, i.e., $\kappa_{fd\%} = 25\%$. Dearing et al. (1996) give a theoretical value of 14-16% for $\kappa_{fd\%}$, suggesting that our regression moderately underestimates κ_{sp}. The relationship $\kappa_{sd} = 35 \cdot 10^{-5}\ M_{ar}/M_0$ (unit magnetization $M_0 = 1$ A/m) results in a SD specific κ_{arm}/κ_{sd} ratio of 94 which is distinctly higher than the expected value (≈ 60; Oldfield 1994). As mentioned before, a too small κ_{sd} is determined here, because the SD fraction also contributes to M_{ir} and therefore to κ_{md}. The hematite susceptibility $\kappa_{he} = 16 \cdot 10^{-5}\ M_{hir}/M_0$ compares fairly well to a $\kappa_{he} = 3 \cdot 10^{-5}\ M_{sir}/M_0$ (Thompson and Oldfield 1986) as the M_{hir} acquired between 0.3 and 0.8 T represents only a portion of the total M_{sir}. Finally, $\kappa_{md} = 9 \cdot 10^{-5}\ M_{ir}/M_0$ corresponds to a reasonable mean MD magnetite grain-size of 10 µm (Thompson and Oldfield 1986).

With the concept of partial susceptibilities, the κ record of core GeoB 1505-2 can now be

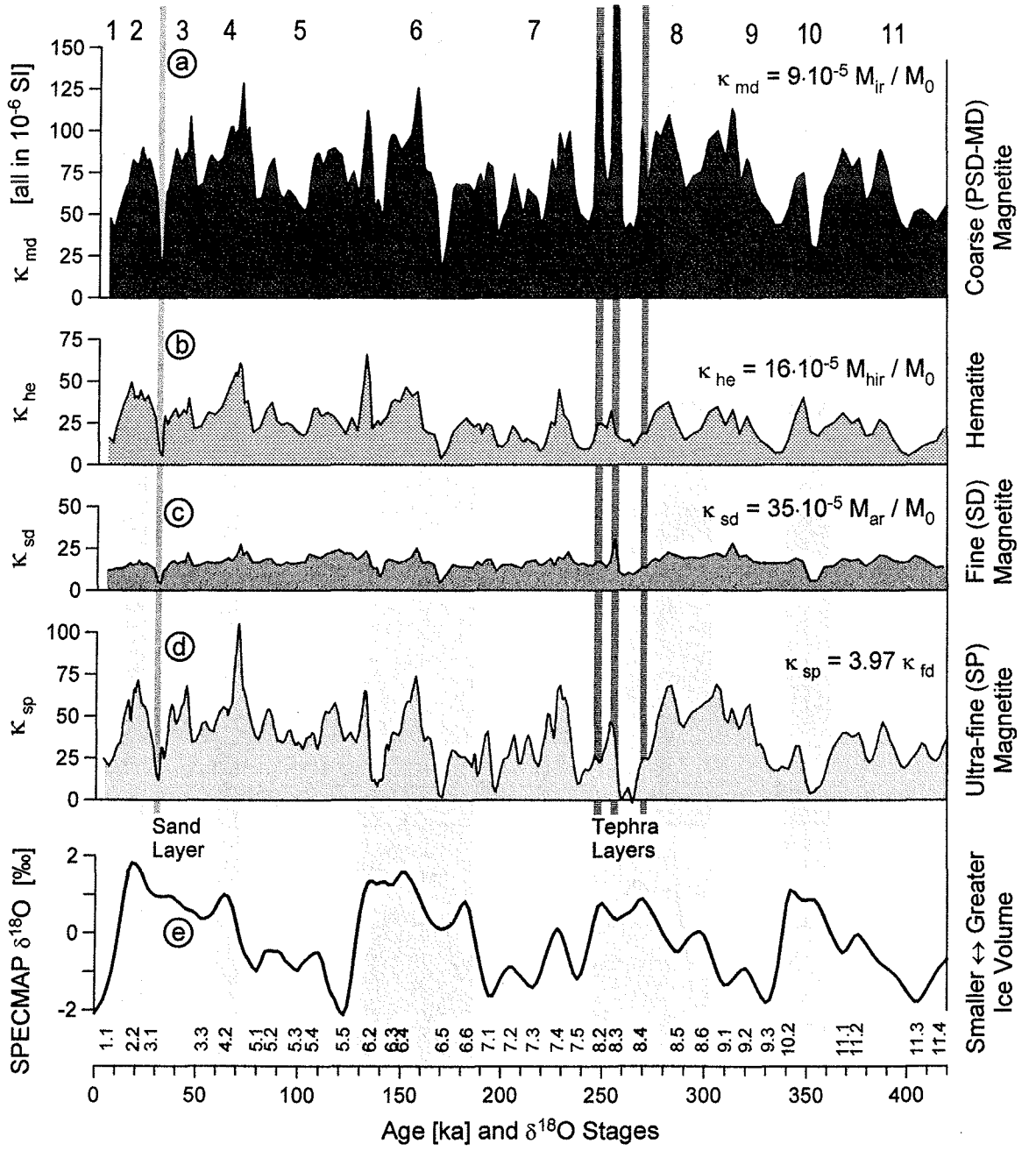

Fig. 10 (a) - (d). Central equatorial Atlantic core GeoB 1505-2. Partial susceptibilities κ_{md}, κ_{sd}, κ_{sp} and κ_{he} estimated by multiple linear regression analysis of three magnetite grain-size selective parameters, M_{ir}, M_{ar}, κ_{fd} and the hematite selective parameter M_{hir}. The calibrations denoted above each plot depend on the average magnetomineralogical composition and magnetite grain-size distribution of the individual sediment sequence and cannot be generalized. To make the coefficients dimensionless, all remanence terms were divided by a unit magnetization M_0 of 1 A/m. The scaling is identical for all four diagrams. Because κ is approximately grain-size independent for magnetite, the κ_{sp}, κ_{sd}, and κ_{md} records can be quantitatively compared. The specific susceptibility of hematite is about 1/1000 that of magnetite. The κ_{he} log therefore represents a proportionally much higher mineral concentration, but probably also associated paramagnetism. **(e)** SPECMAP oxygen isotope stack (Imbrie et al. 1984).

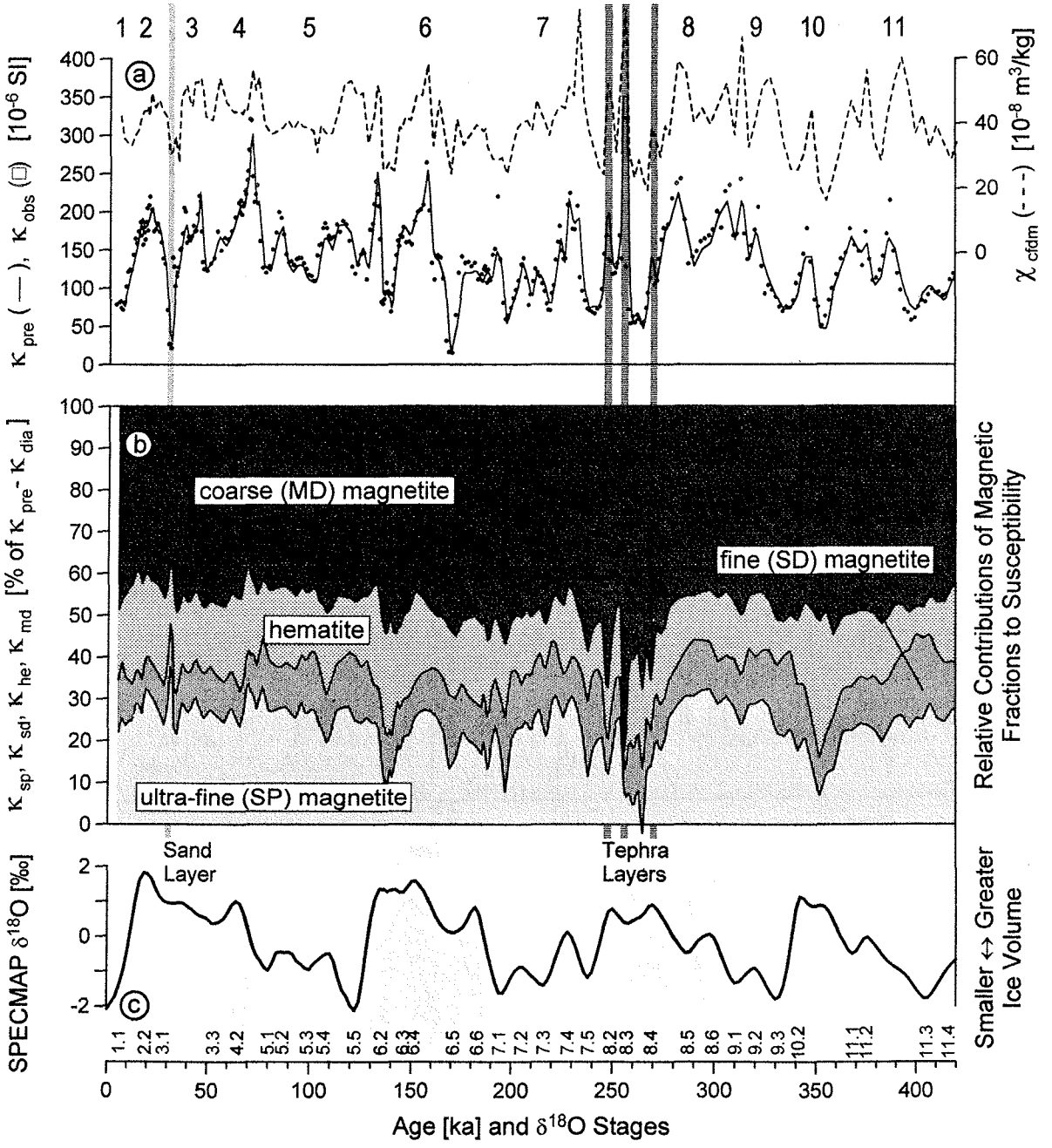

Fig. 11. Central equatorial Atlantic core GeoB 1505-2. **(a)** The predicted susceptibility core log κ_{pre} (solid line) defined as the sum of five estimated partial susceptibilities is in excellent agreement (goodness-of-fit R = 0.986) with the measured susceptibilities κ_{obs} (dots). Carbonate-free dry mass susceptibility χ_{cfdm} (dashed curve), which was determined on the basis of $CaCO_3$ (Zabel et al. 1998) and porosity data, exhibits a similar general pattern as bulk susceptibility. The core GeoB 1505-2 susceptibility record thus largely delineates flux shifts in terrigenous material, whereas variable carbonate dilution of the magnetic mineral assemblage is only a secondary effect. **(b)** Partial susceptibilities κ_{sp}, κ_{sd}, κ_{he}, and κ_{md} as percentages of κ_{pre} - κ_{dia}. The negative diamagnetic term κ_{dia} was excluded to provide a carbonate-free record of relative changes in the magnetic mineral assemblage. Dissolution events in sub-stages 6.3, 6.5, 7.1, 7.5, 8.3 and stage 10 are documented by a distinct coarsening of magnetite grain-size at κ minima. **(c)** SPECMAP oxygen isotope stack (Imbrie et al. 1984).

described quantitatively (Figs. 10, 11; Table 2). Around half of the susceptibility originates from a detrital (MD) magnetite fraction which essentially displays a climatic pattern (Fig. 10a). During $\delta^{18}O$ sub-stages 6.3, 6.5, 7.1, 7.5 and 8.3 this coarser particle fraction is enhanced relative to the finer SD and SP components (Fig. 11b), but in absolute concentrations all magnetite fractions decline sharply in these intervals, even in the carbonate-free signal (Fig. 11a). The SP fraction, which on average is responsible for 24% of the κ signal (Table 2), virtually disappears. Such a simultaneous decrease and coarsening strongly suggests intermittent magnetite dissolution (Tarduno 1994; 1995; see also the following Example 3). Hematite has a mean contribution of 17% to κ and is not as intensely affected by dissolution as magnetite (Fig. 10b). This explains, why κ_{he} reveals higher correlations to the 'terrigenous' elements Al (Pearson's correlation coefficient r = 0.84) and Ti (r = 0.89), but also to $CaCO_3$ (r = -0.78) than the diagenetically overprinted κ_{md} and κ_{sp} records (Table 2). SD particles carry only 11% of the total susceptibility and differ from the three other fractions in so far as their signal is considerably less variable (Fig. 10, standard deviation 24% of the mean as compared to $\approx$50% for MD, SP, HE) and clearly less correlated to Al (r = 0.53), Ti (r = 0.54), $CaCO_3$ (r = -0.41) and to total susceptibility (r = 0.77). This implies that the SD fraction is not part of the terrigenous flux, but was formed *in situ,* presumably by magnetobacteria.

The steady accumulation of the biogenic SD fraction and, on the other hand, a mostly climate controlled sedimentation of the terrigenous MD fraction prompts the MD/SD ratio to be a terrigenous flux proxy at this core location. Because the early diagenetic overprint applies to both and was rather mild, the original signal can be reconstructed by relating the two fractions as shown in Figure 12a. The carbonate independent ratio κ_{md}/κ_{sd} can therefore be regarded as a proxy for terrige-

Table 2. Correlation matrix (Pearson's r) of total and partial susceptibilities together with geochemical data indicative for continental detritus (Zabel 1998). The mean relative contributions of partial susceptibilities to κ refer to $\kappa_{pre} - \kappa_{dia}$ to avoid negative (diamagnetic) percentages (see Fig. 11). $\bar{x}$ denotes the arithmetic parameter means, s their relative standard deviations.

Correlation to	κ	κ_{md}	κ_{he}	κ_{sd}	κ_{sp}	% of κ	$\bar{x}$	s (in %)
$CaCO_3$ [wt%]	-0.72	-0.65	-0.78	-0.41	-0.55		61	17
Al [g/kg]	0.84	0.79	0.84	0.53	0.65		35	30
Ti [g/kg]	0.87	0.81	0.89	0.54	0.71		1.8	33
κ [10^{-6} SI]	1	0.91	0.88	0.77	0.92		140	39
κ_{md} [10^{-6} SI]	0.91	1	0.77	0.75	0.75	48	75	57
κ_{he} [10^{-6} SI]	0.88	0.77	1	0.49	0.77	17	26	46
κ_{sd} [10^{-6} SI]	0.77	0.75	0.49	1	0.72	11	17	24
κ_{sp} [10^{-6} SI]	0.92	0.75	0.77	0.72	1	24	37	49

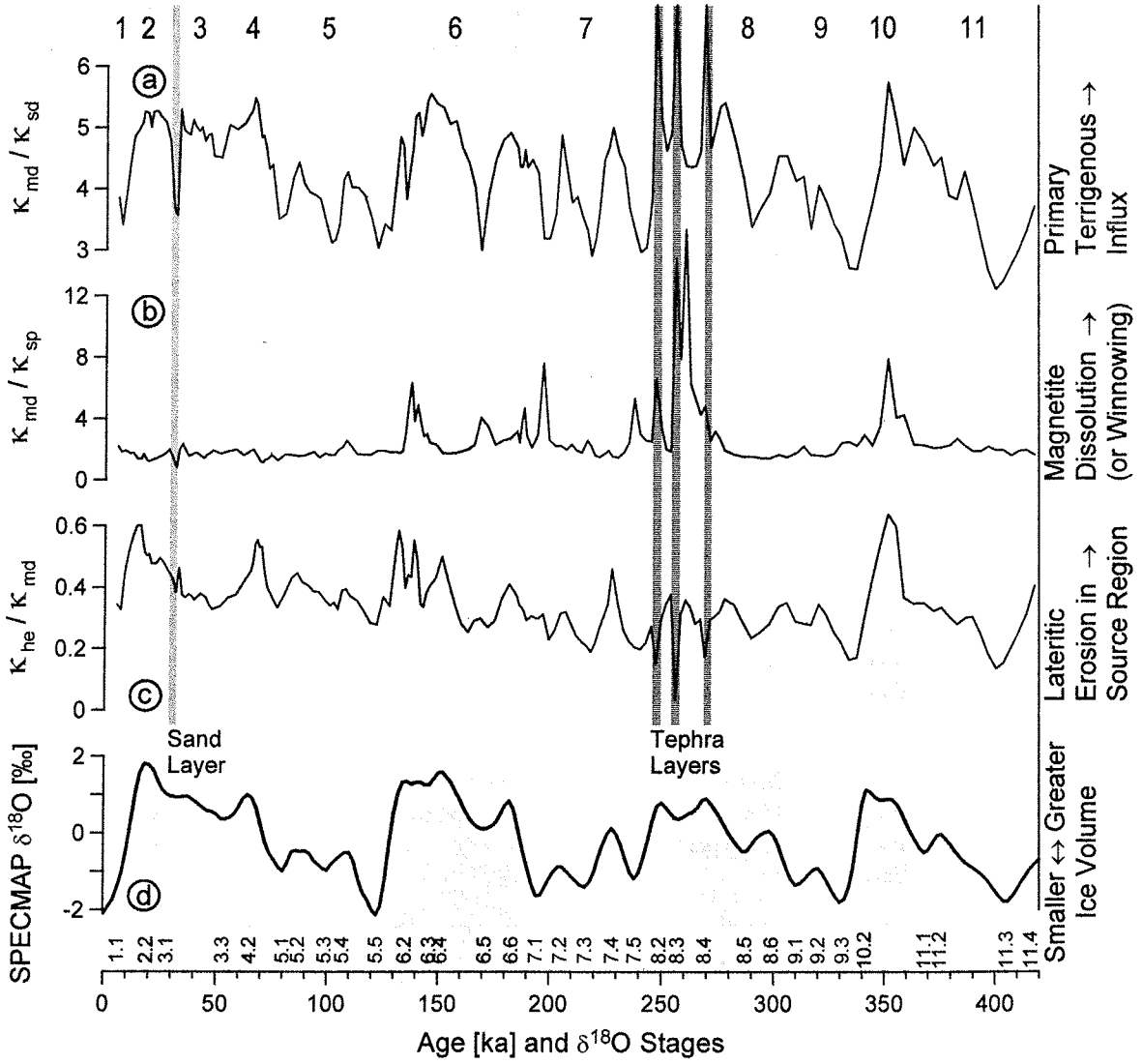

Fig. 12. Central equatorial Atlantic core GeoB 1505-2. Selective proxy parameters defined on the basis of rock magnetic data evaluation. **(a)** κ_{md}/κ_{sd} ratio reflects variations in climatically controlled primary eolian influx from the African continent. **(b)** κ_{md}/κ_{sp} ratio documents intervals of diagenetic overprinting (or, less likely, of winnowing). **(c)** κ_{he}/κ_{md} ratio indicates variations in dust composition related to prevailing weathering style. **(d)** SPECMAP oxygen isotope stack (Imbrie et al. 1984).

nous, in the present case most likely eolian (see Example 1), flux variations. The core sections influenced by partial magnetite dissolution (an alternative explanation could be winnowing) are most easily detected by relating the coarsest, least affected fraction (MD) to the finest, most affected component. The proxy κ_{md}/κ_{sp} (Fig. 12b) pinpoints these events as sharp peaks. Their true nature can only be understood on the basis of additional geochemical and granulometric analyses.

The ratio of hematite to magnetite ($S_{-0.3T}$, Fig. 9), or better κ_{he}/κ_{md} (Fig. 12c), serves as a proxy for variations in dust composition, e.g., the maxima in stages 6 and 10 likely indicate an enhanced erosion of lateritic soils on the African continent.

This example shows that even a relatively small rock magnetic data set allows remarkably detailed reconstructions of the temporal evolution of the terrigenous sedimentation in marine environments. Other selective rock magnetic parameters could be

added to gather additional information, e.g., on diagenetic precipitation of greigite (Roberts and Turner 1993; Roberts 1995). A typical trait of such magnetic analyses is their regional character. The specific significance of rock magnetic proxy parameters has to be carefully evaluated and calibrated for each individual depositional setting.

Example 3: Diagenetic Dissolution of Biogenic Magnetite in a Reducing Marine Environment

Early diagenetic processes in marine sediments are primarily driven by microbially mediated degradation of organic matter. Oxidation of organic compounds provides energy for the microorganisms to maintain their metabolism. Froehlich et al. (1979) identified a systematic depth succession of terminal electron acceptors in the sediment column from oxygen in the top layer to nitrate, Mn(IV)-oxides, Fe(III)-oxides and sulphate at depth. This sequence of oxidants reflects the accessible amount of energy per mole of organic carbon. The depth extent of the early diagenetic zonation critically depends on organic matter supply, sedimentation rate and the availability of reactants (Berner 1981).

It is well known that diagenetic processes also affect the magnetic mineral assemblage. In reducing environments even well crystallized ferrimagnetic oxides may be unstable, e.g., dissolution of magnetite and/or its transformation to iron sulphides is a common phenomenon in suboxic to anoxic sediments (Canfield and Berner 1987; Karlin 1990). As a result, systematic changes in magnetic properties are observed (Karlin and Levi 1983). The present example is to demonstrate the potential of high-resolution rock magnetic analyses to contribute proxy parameters for geochemically induced alterations in near-surface layers of organic-rich sedimentary deposits.

Reducing conditions in the sediment column are widespread, where an intense primary biologic productivity in the surface waters supplies high fluxes of organic material to the sea floor. A representative area for such a depositional regime is the Benguela upwelling system in the eastern South Atlantic. In this region, high abundances of living magnetotactic bacteria have been observed in the uppermost sedimentary layers (Petermann and Bleil 1993). The magnetite crystals synthesized intracellularly by these bacteria are preserved after decomposition of their organic constituents (Petersen et al. 1986). They have been identified as the by far dominant carrier of the magnetic signal in recent sediments at the upper continental slope off southwest Africa, also because the concentration of lithogenic, terrigenous ferrimagnetic mineral components is relatively low compared to other hemipelagic environments. Within a few centimeters sub-bottom an unusually sharp decrease in magnetic susceptibility is observed in numerous cores from this area (Fig. 13a).

A high-resolution rock magnetic study of an 18 cm long sediment sequence, which was recovered with a multicorer at 23°13'S / 13°01'E from about 600 m water depth (core GeoB 1713-5) in the center of the Namibian upwelling cell, aimed at quantifying in full detail this conspicuous feature. The parameters determined provide information about the concentration of ferrimagnetic minerals (χ, σ_{ir}, σ_{ar}, σ_s), their grain-size (σ_{ar}/σ_{ir}, σ_{rs}/σ_s, B_{cr}/B_c) and also contributions of non-ferromagnetic compounds of the sedimentary matrix (κ_{nf}/κ). The objective of supplementary electron microscopy was to identify the magnetic minerals on the basis of their morphology and grain-size as well as corrosion phenomena indicating potential dissolution effects.

Both concentration dependent parameters, the isothermal remanent magnetization σ_{ir}, (acquired in a 0.1 T direct field) and the anhysteretic remanent magnetization σ_{ar} (0.1 T alternating field, 0.04 mT constant biasing field) convincingly testify that the drastic drop in specific susceptibility χ results from a diminishing content of ferrimagnetic components in the uppermost centimeters of core GeoB 1713-5 (Fig. 13b, c). In the narrow depth interval between about 3 and 7 cm contributions of the paramagnetic sediment matrix to the susceptibility signal rise from approximately 20 to 80% (Fig. 13e) at the expense of the ferrimagnetic mineral fraction. Concurrently, the grain-size sensitive parameter σ_{ar}/σ_{ir} (Fig. 13d) reflects a downward coarsening of ferrimagnetic grains from primarily single-domain particles in the top centimeters to multi-domain particles in deeper strata. High σ_{ar}/σ_{ir} ratios in the upper 6 cm and particularly

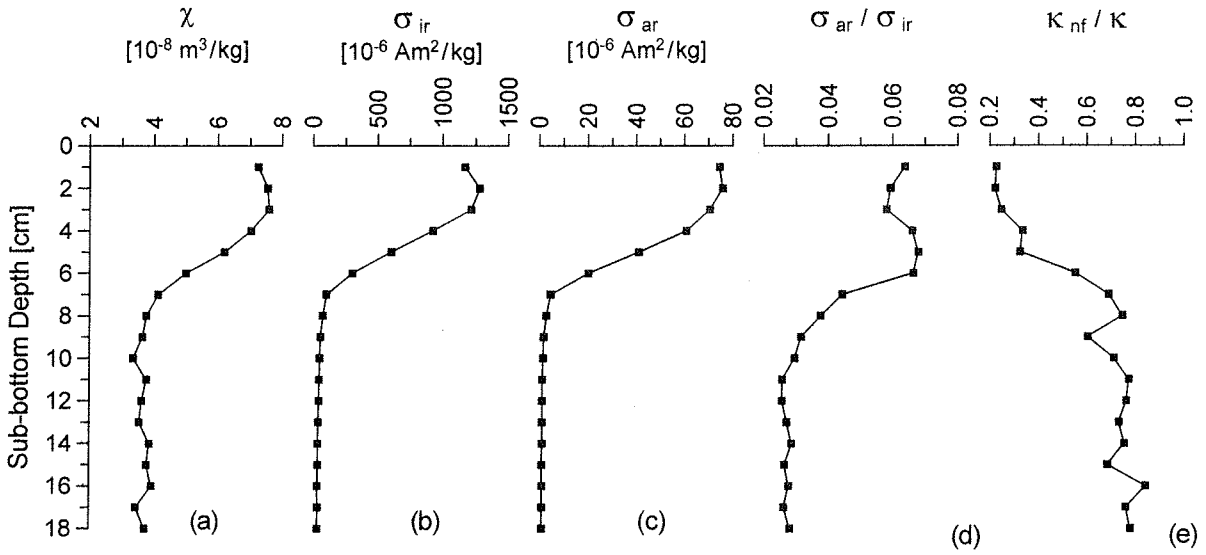

Fig. 13. Rock magnetic properties of core GeoB 1713-5 from the Benguela upwelling system off Namibia. **(a)** Specific susceptibility χ, **(b)** specific isothermal remanent magnetization σ_{ir}, **(c)** specific anhysteretic remanent magnetization σ_{ar}, **(d)** magnetite grain-size sensitive ratio, σ_{ar}/σ_{ir}, **(e)** relative contribution of the non-ferromagnetic sediment matrix to volume susceptibility κ_{nf}/κ.

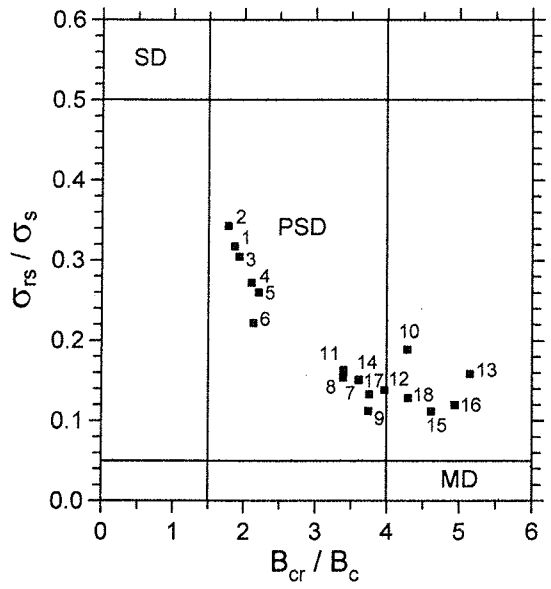

Fig. 14. Variation of the average magnetite grain-size in core GeoB 1713-5 as inferred from ratios of specific saturation remanence to specific saturation magnetization σ_{rs}/σ_s and coercivity of remanence to coercive field B_{cr}/B_c determined from hysteresis measurements to maximum fields of 0.3 T. Note depth succession of data indicated by the sub-bottom position of the samples.

between 4 and 6 cm depth are indicative of a sizeable portion of fine to very fine grained SD particles.

The ratios of specific saturation remanence to specific saturation magnetization, σ_{rs}/σ_s, and coercivity of remanence to coercive field, B_{cr}/B_c, characterize the domain state and thus grain-size of the magnetic mineral assemblage. Figure 14 illustrates this data set determined from hysteresis measurements to maximum fields of 0.3 T. The data points plotted in the standard diagram of Day et al. (1977) depict a clear depth succession according to the position of the samples. From 1 to 6 cm sub-bottom small particles in the PSD to SD range dominate the grain-size distributions, whereas from 7 to 18 cm depth they fall into the coarse PSD to MD field. Ultra-fine superparamagnetic particles which would also lead to lower σ_{rs}/σ_s ratios may be important in the upper half of the core (Fig. 16), but certainly not in deeper parts. The hysteresis loop of the top sample is relatively wide open and its 'rectangular' shape indicates single-domain particles. With increasing sediment depth the hysteresis branches progressively merge reflecting a distinct reduction in the amount of ferrimagnetic compo-

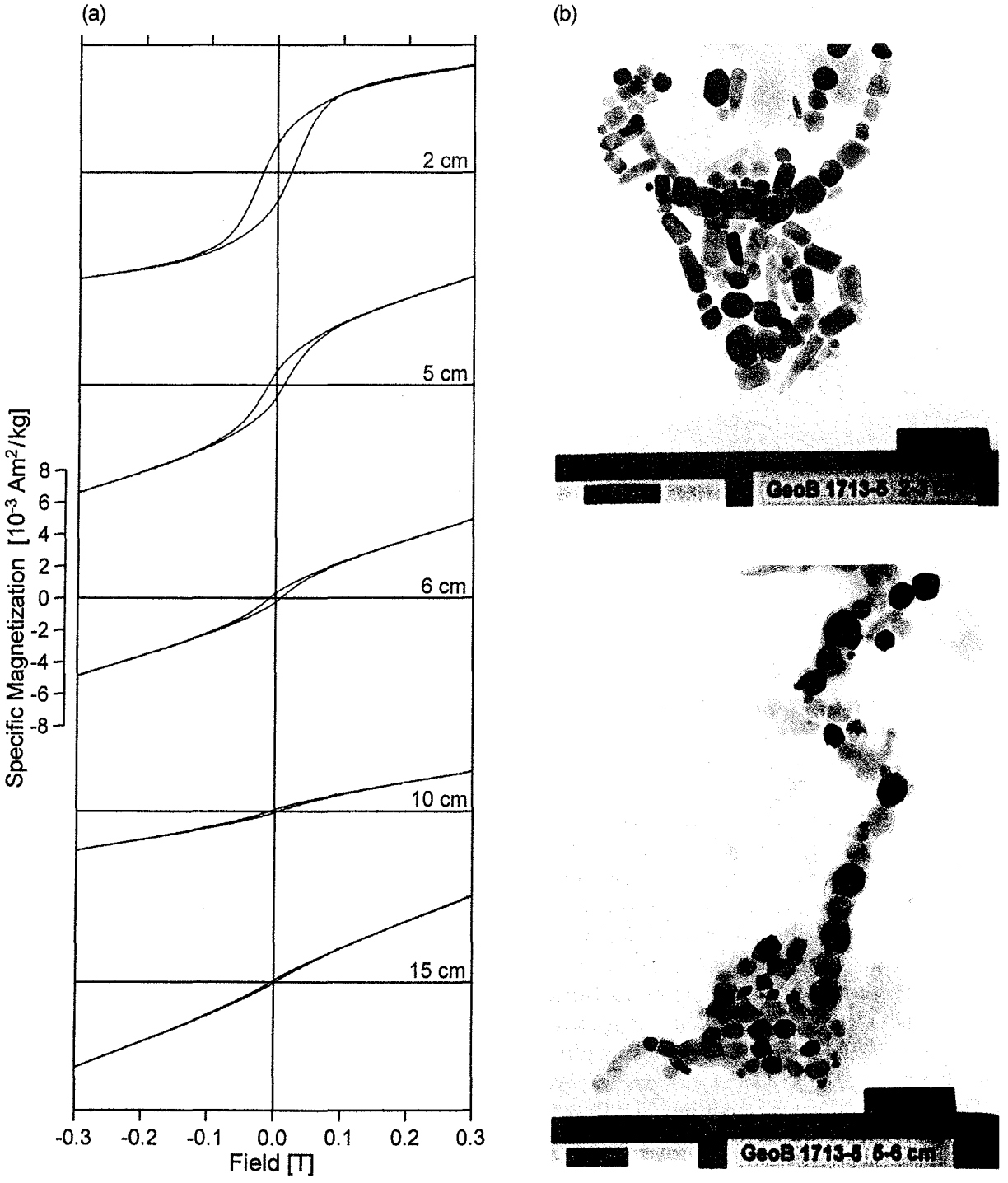

Fig. 15. **(a)** Hysteresis loops to maximum fields of 0.3 T for samples from 2, 5, 6, 10 and 15 cm sub-bottom depth in core GeoB 1713-5. **(b)** Transmission electron micrographs of magnetic extracts from 2-3 and 5-6 cm sub-bottom depth.

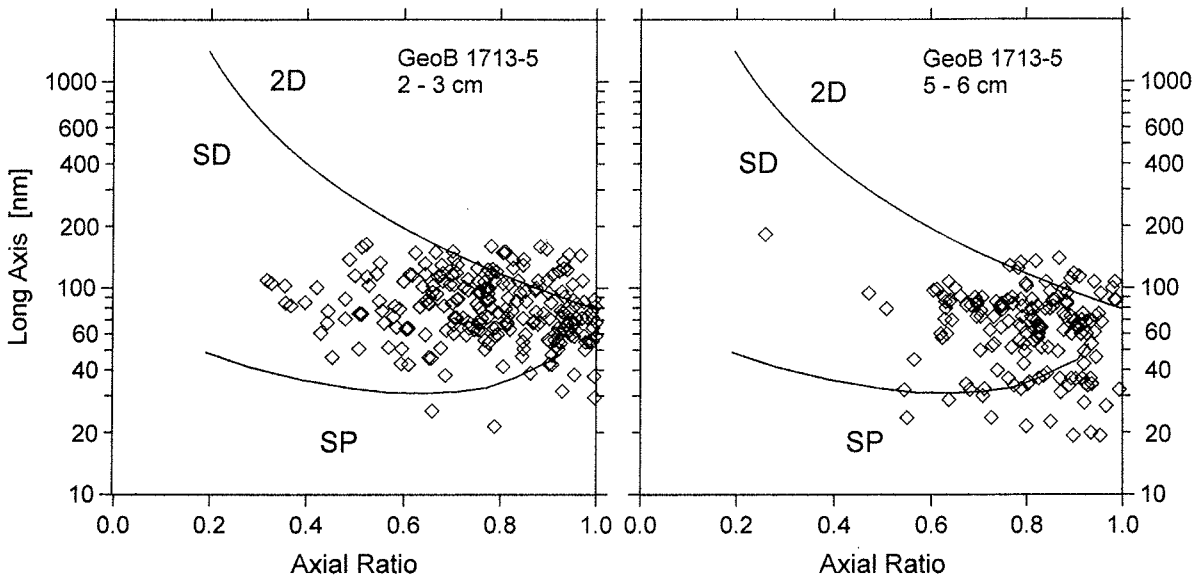

Fig. 16. Grain-sizes of magnetosomes from 2-3 and 5-6 cm sub-bottom depth in core GeoB 1713-5 plotted to the diagram after Butler and Banerjee (1975) outlining the superparamagnetic (SP), single-domain (SD) and two-domain (2D) fields.

nents. The 'sigmoid' shaped loops of the deeper samples clearly imply a coarser grained mineral fraction (Fig. 15a).

Transmission electron micrographs of magnetic extracts (Fig. 15b) show that in the sample from 2-3 cm depth grain-size and morphology of the particles are typical for magnetosomes produced by magnetotactic bacteria. The crystals have perfect regular faces. In contrast, at 5-6 cm depth the magnetosomes exhibit distinct corrosion and dissolution effects. In deeper parts of the core no biogenic magnetites could positively be identified. The downcore shift to smaller grain-sizes is confirmed by direct measurements of magnetic particle dimensions. At 2-3 cm depth their average length amounts to 85 ± 30 nm, the average width to 64 ± 25 nm. At 5-6 cm depth mean grain-sizes are reduced to 67 ± 29 nm in length and 54 ± 22 nm in width. According to Butler and Banerjee (1975), the particles from 2-3 cm depth predominantly fall into the single-domain field (Fig. 16), the sample from 5-6 cm depth contains distinctly higher proportions of smaller, superparamagnetic grains.

Rock magnetic and electron microscopic analyses of recent to sub-recent sediments from the Benguela upwelling center off Namibia reveal that high concentrations of biogenic magnetite, remnants of magnetotactic bacteria, in the uppermost layers entirely disintegrate only a few centimeters beneath. Measurements of various parameters, specifically characterizing the magnetic grain-size distribution, allow to trace this early diagenetic dissolution process in detail. Downcore, it first causes a slight fining of the original, essentially single-domain assemblage followed by a rapid coarsening, as the most abundant, small biogenic grains reach the SD transition and subsequently are completely dissolved. Electron microscope observations provide additional strong support for this interpretation of the rock magnetic measurements. Due to the extremely high supply of organic matter the early diagenetic zonation is evidently confined to a very shallow and narrow depth interval in the study area. This may, of course, be quite different in other depositional settings, but could equally well be documented using the present systematics.

Conclusions

Each of the three studies presented exemplifies an individual approach of employing rock magnetic data sets as sensitive proxy parameters to charac-

terize and distinguish different marine sedimentary environments. They are all entirely based on the sediment matrix magnetic properties and more specifically on mineralogy, concentration, grain-size and domain state of the magnetic mineral assemblages. Though not yet exploited in their full range of capacities, the wide variety of distinct rock magnetic measurements and parameters enables to discriminate primary input mechanisms of terrigenous material by fluvial or eolian transport as well as various source regions and to recognize biogenic or lithogenic magnetic components of marine origin. As demonstrated for the recent equatorial South Atlantic, these *Environmental Magnetism* methods, combined with appropriate statistical data evaluation techniques, efficiently identify particular sedimentary regimes and outline their regional extent. With a sufficiently comprehensive and precisely dated sample collection available, analogous analyses would be possible for any ocean and time slice. Rock magnetic core logs determined as high-resolution time series for a late Quaternary sediment sequence recovered in the central equatorial South Atlantic give an elementary example of this strategy. They yield a detailed reconstruction of sedimentary patterns which reflect pronounced variations of paleoclimatic and paleoceanographic conditions primarily documenting a systematic cyclicity due to orbital forcing. To trace the intense effects of diagenetic processes on the magnetic mineral assemblage in a reducing environment, supplementary transmission electron micrographs proved to be especially useful. It should be mentioned that most magnetic measurements are non-destructive and, compared to other methods, accomplished in a relatively short period of time thereby allowing quite elaborate investigations. Depending on the individual situation, additional rock magnetic techniques, which have not been introduced here, e.g., thermomagnetic, anisotropy or Mößbauer analyses, may be of critical importance. Finally, rock magnetic and paleomagnetic data sets have a great potential in establishing high-resolution chronostratigraphies for marine sediment sequences (see Bleil and von Dobeneck; von Dobeneck and Schmieder this volume).

Acknowledgments

We thank crews and scientific parties of numerous METEOR cruises to the South Atlantic for their cooperation. Contributions of H. Petermann, who was involved in parts of this work, and constructive reviews by J.A. Dearing and E. Petrovský are gratefully acknowledged. This study was funded by the Deutsche Forschungsgemeinschaft (Sonderforschungsbereich 261, contribution no. 185).

Data are available under www.pangaea.de/Projects/SFB261.

References

Bacher J (1994) Clusteranalyse: Anwendungsorientierte Einführung. Oldenbourg Verlag, München, pp 1-424

Bailey ME, Dunlop DJ (1983) Alternating field characteristics of pseudo-single-domain (2-14 μm) and multi-domain magnetite. Earth Planet Sci Lett 63: 333-352

Banerjee SK (1981) Experimental methods of rock magnetism and paleomagnetism. Adv Geophys 23: 25-99

Barron EJ, Whitman JM (1981) Oceanic sediments in space and time. In: Emiliani C (ed) The Sea. Wiley and Sons, New York, pp 689-731

Berner RA (1981) A new geochemical classificication of sedimentary environments. J Sed Petrol 51:359-365

Bezdek JC (1981) Pattern Recognition with Fuzzy Objective Function Algorithms. Plenum Press, New York, pp 1-256

Bezdek JC, Dunn JC (1975) Optimal fuzzy partitions: a heuristic for estimating the parameters in a mixture of normal distributions. IEEE Trans Comp 24:835-838

Bloemendal J, King JW, Hall FR, Doh S-J (1992) Rock magnetism of late Neogene and Pleistocene deep-sea sediments: relationship to sediment source, diagenetic processes, and sediment lithology. J Geophys Res 97:4361-4375

Bloemendal J, Lamb B, King J (1988) Paleoenvironmental implications of rock magnetic properties of late quaternary sediment cores from the eastern equatorial Atlantic. Paleoceanography 3:61-87

Borradaile GJ, Stupavsky M (1995) Anisotropy of magnetic susceptibility: measurement schemes. Geophys Res Lett 22:1957-1960

Butler RF, Banerjee SK (1975) Theoretical single-domain grain size range in magnetite and titanomagnetite. J Geophys Res 80:4049-4058

Canfield DE, Berner RA (1987) Dissolution and

pyritization of magnetite in anoxic marine sediments. Geochim Cosmochim Acta 51:645-659

Chikazumi S (1997) Physics of Ferromagnetism. Oxford University Press, New York, pp 1-655

Day R, Fuller M, Schmidt VA (1977) Hysteresis properties of titanomagnetites: grain-size and compositional dependence. Phys Earth Planet Inter 13:260-267

Dearing JA, Dann RJL, Hay K, Lees JA, Loveland PJ (1996) Frequency-dependent susceptibility of environmental materials. Geophys J Int 124:228-240

Dekkers MJ, Langereis CG, Vriend SP, van Santfort PJM, de Lange GJ (1994) Fuzzy c-means cluster analysis of early diagenetic effects on natural remanent magnetisation acquisition in a 1.1 Myr piston core from the central Mediterranean. Phys Earth Planet Inter 85:155-171

Doh SJ, King JW, Leinen M (1988) A rock magnetic study of Giant Piston Core LL44-GPC3 from the central North Pacific and its paleoceanographic implications. Paleoceanography 3:89-111

Dunlop DJ (1973) Superparamagnetic and SD threshold sizes in magnetite. J Geophys Res 78:1780-1793

Dunlop DJ (1981) The rock magnetism of fine particles. Phys Earth Planet Inter 26:1–26

Dunlop DJ (1986) Hysteresis properties of magnetite and their dependence on particle size: a test of pseudo-single-domain remanence models. J Geophys Res 91: 9569-9584

Dunlop DJ (1990) Developments in rock magnetism. Rep Prog Phys 53:707-792

Dunlop DJ (1995) Magnetism in rocks. J Geophys Res 100:2161-2174

Dunlop DJ, Özdemir Ö (1997) Rock Magnetism: Fundamentals and Frontiers. Cambridge University Press, Cambridge, pp 1-573

Frapporti G, Vriend SP, van Gaans PFM (1993) Hydrogeochemistry of the shallow Dutch groundwater: interpretation of the national groundwater quality monitoring network. Water Res Rev 29:2993-3004

Froehlich PN, Klinkhammer GP, Bender ML, Luedtke NA, Heath GR (1979) Early oxidation of organic matter in pelagic sediments of the eastern equatorial Atlantic: suboxic diagenesis. Geochim Cosmochim Acta 43:1075-1090

Hamilton N, Rees AV (1970) The use of magnetic fabric in paleocurrent estimation. In: Runcorn SK (ed) Paleogeophysics. Academic Press, New York, pp 445-464

Hartstra, RL (1982a) Grain-size dependence of initial susceptibility and saturation magnetization-related parameters of four natural magnetites in the PSD-MD range. Geophys J R astr Soc 71:477-495

Hartstra, RL (1982b) A comparative study of the ARM and I_{SR} of some natural magnetites of MD and PSD grain-size. Geophys J R astr Soc 71:497-518

Heider F, Zitzelsberger A, Fabian K (1995) Magnetic susceptibility and remanent coercive force in grown magnetite crystals from 0.1 μm to 6 mm. Phys Earth Planet Inter 93:239-256

Hrouda F (1994) A technique for the measurement of thermal changes of magnetic susceptibility of weakly magnetic rocks by the CS-2 apparatus and KLY-2 kappabridge. Geophys J Int 118:604-612

Hrouda F, Jelínek V, Zapletal K (1997) Refined technique for susceptibility resolution into ferromagnetic and paramagnetic components based on susceptibility temperature-variation measurement. Geophys J Int 129:715-719

Imbrie J, Hays JD, Martinson DG, McIntyre A, Mix AC (1984) The orbital theory of Pleistocene climate: support from a revised chronology of the marine $\delta^{18}O$ record. In: Berger AL, Imbrie J, Hays J, Kukla G, Saltzman B (eds) Milankovitch and Climate Part I. Kluwer, Dordrecht, pp 269-305

Jang JSR, Gulley N (1995) Fuzzy Logic Toolbox Users Guide. The Math Works Inc, Natick, pp 1-188

Karlin R (1990) Magnetic mineral diagenesis in suboxic sediments at Bettis Site W-N, NE Pacific Ocean. J Geophys Res 95:4421-4436

Karlin R, Levi S (1983) Diagenesis of magnetic minerals in recent hemipelagic sediments. Nature 303:327-330

Kent DV (1982) Apparent correlation of palaeomagnetic intensity and climatic records in deep-sea sediments. Nature 299:538-539

King J, Banerjee SK, Marvin J, Özdemir Ö (1982) A comparison of different magnetic methods for determining the relative grain size of magnetite in natural materials: some results from lake sediments. Earth Planet Sci Lett 59:404-419

King JW, Channell JET (1991) Sedimentary magnetism, environmental magnetism, and magnetostratigraphy. Rev Geophys 29:358–370

Lehmann B, Sagnotti L, Winkler A, Lo Cascio C (1996) Magnetic mineralogy changes in the Pleistocene marine sequence of Montalto di Castro (central Italy) and influences on the magnetic anisotropy. Geophys J Int 127:529-541

Lisitzin AP (1996) Oceanic Sedimentation Lithology and Geochemistry. AGU Special Publication, pp 1- 407

Lowrie W (1990) Identification of ferromagnetic minerals in a rock by coercivity and unblocking temperature properties. Geophys Res Lett 17:159-162

Lund SP, Karlin R (1990) Introduction to the special section on physical and biogeochemical processes responsible for the magnetization of sediments. J Geophys Res 90:4353-4354

Maher BA (1986) Characterisation of soils by mineral magnetic measurements. Phys Earth Planet Inter 42:76-92

Maher BA (1988) Magnetic properties of some synthetic sub-micron magnetites. Geophys J 94: 83–96

Mead GA, Tauxe L, LaBrecque JL (1986) Oligocene paleoceanography of the South Atlantic: paleoclimatic implications of sediment accumulation rates and magnetic susceptibility measurements. Paleoceanography 1:273-284

deMenocal PB, Laine EP, Ciesielski PF (1988) A magnetic signature of bottom current erosion. Phys Earth Planet Inter 51:326–348

Middleburg JJ, de Lange GJ (1988) Geochemical characteristics as indicators of the provenance of Madeira abyssal plain turbidites. A statistical approach. Oceanol Acta 11:1159-1164

Mullender TAT, van Velzen AJ, Dekkers MJ (1993) Continuous drift correction and separate identification of ferrimagnetic and paramagnetic contributions in thermomagnetic runs. Geophys J Int 114:663–672

Nagy EA, Valet JP (1993) New advances for paleomagnetic studies of sediment cores using U-channels. Geophys Res Lett 20:671-674

Oldfield F (1991) Environmental magnetism: a personal perspective. Quat Sci Rev 10:73–85

Oldfield F (1994) Towards the discrimination of fine-grained ferrimagnets by magnetic measurements in lake and near-shore marine sediments. J Geophys Res 99:9045–9050

Pak H, Zanefeld JRV, Spinrad RW (1984) Vertical distribution of suspended particulate matter in the Zaire river, estuary and plume. Neth J Sea Res 17:412-425

Parry LG (1965) Magnetic properties of dispersed magnetite powders. Phil Mag 11:303–312

Parry LG (1982) Magnetization of immobilized particle dispersions with two distinct particle sizes. Phys Earth Planet Inter 28:230–241

Petermann H, Bleil U (1993) Detection of live magnetotactic bacteria in South Atlantic deep-sea sediments. Earth Planet Sci Lett 117:223-228

Petersen N, von Dobeneck T, Vali H (1986) Fossil bacterial magnetite in deep-sea sediments from the South Atlantic Ocean. Nature 320:611-615

Pye K (1987) Aeolian Dust and Dust Deposits. Academic Press, London, pp 1-334

Roberts PR (1995) Magnetic properties of sedimentary greigite (Fe_3S_4). Earth Planet Sci Lett 134:227-236

Roberts PR, Turner GM (1993) Diagenetic formation of ferrimagenetic iron sulphide minerals in rapidly deposited marine sediments, South Island, New Zealand. Earth Planet Sci Lett 115:257-273

Robinson SG (1986) The late Pleistocene palaeoclimatic record of North Atlantic deep-sea sediments revealed by mineral-magnetic measurements. Phys Earth Planet Inter 42:22-47

Rochette P, Jackson M, Aubourg C (1992) Rock magnetism and the interpretation of anisotropy of magnetic susceptibility. Rev Geophys 30:209-226

Sager WW, Hall SA (1990) Magnetic properties of black mud turbidites from ODP Leg 116, distal Bengal Fan, Indian Ocean. In: Cochran JR, Stow DAV et al. (eds) Proceedings of the Ocean Drilling Program, Scientific Results, Ocean Drilling Program, College Station, pp 317-336

Stacey FD, Banerjee SK (1974) The Physical Principles of Rock Magnetism. Elsevier, Amsterdam, pp 1-195

Stoner JS, Channell JET, Hillaire-Marcel C (1996) The magnetic signature of rapidly deposited detrital layers from the deep Labrador Sea: relationship to North Atlantic Heinrich layers. Paleoceanography 11:309-325

Tarduno J (1994) Temporal change of magnetic dissolution in the pelagic realm: gauging paleoproductivity? Earth Planet Sci Lett 123:39-48

Tarduno J (1995) Superparamagnetism and reduction diagenesis in pelagic sediments: enhancement or depletion? Geophys Res Lett 22:1337-1340

Thompson R, Bloemendal J, Dearing JA, Oldfield F, Rummery TA (1980) Environmental applications of magnetic measurements. Science 207:481–486

Thompson R, Oldfield F (1986) Environmental Magnetism. Allen and Unwin, London, pp 1-227

Verosub KL, Roberts AP (1995) Environmental magnetism: past, present, and future. J Geophys Res 100: 2175-2192

von Dobeneck T (1996) A systematic analysis of natural magnetic mineral assemblages based on modeling hysteresis loops with coercivity-related hyperbolic basis functions. Geophys J Int 124:675-694

von Dobeneck T (1998) The concept of 'partial susceptibilities'. Geol. Carpathica 49: 228-229

Wasilewski PJ (1973) Magnetic hysteresis in natural materials. Earth Planet Sci Lett 20:67-72

Weeks R, Laj C, Endignoux L, Fuller M, Roberts A (1993) Improvements in long-core measurement techniques: applications in palaeomagnetism and paleoceanography. Geophys J Int 114:651-662

Zabel M, Bickert T, Dittert L, Haese R (1998) The significance of the sedimentary Al/Ti ratio as indicator for reconstructions of the terrestrial and fluvial input to the equatorial Atlantic. Submitted to Paleoceanography

Zadeh LA (1965) Fuzzy sets. Inf Contr 8:338-353

PALEOCEANOGRAPHY, VOL. 14, NO. 4, PAGES 465-481, AUGUST 1999

Magnetic characterization of Holocene sedimentation in the South Atlantic

Andrea M. Schmidt, Tilo von Dobeneck, and Ulrich Bleil

Fachbereich Geowissenschaften, Universität Bremen, Bremen, Germany

Abstract. Surface sediment samples representative for the tropical and subtropical South Atlantic (15°N to 40°S) were investigated by isothermal magnetic methods to delineate magnetic mineral distribution patterns and to identify their predominant Holocene climatic and oceanographic controls. Individual parameters reveal distinct, yet frequently overlapping, regional sedimentation characteristics. A probabilistic ("fuzzy c-means") cluster analysis was applied to five concentration independent magnetic properties assessing magnetite to hematite ratios and diagnostic of bulk and fine-particle magnetite grain size and coercivity spectra. The resultant 10 cluster structures establish an oceanwide magnetic sediment classification scheme tracing the major terrigenous eolian and fluvial fluxes, authigenic biogenic magnetite accumulation in high-productivity areas, transport by ocean current systems, and effects of bottom water velocity on depositional regimes. Distinct dissimilarities in magnetic mineral inventories between the eastern and western basins of the South Atlantic reflect prominent contrasts of both oceanic and continental influences.

1. Introduction

Magnetic mineral assemblages of marine sediments are controlled by lithospheric, hydrospheric, and atmospheric conditions. Concentration, mineralogy, and grain size (more precisely, domain state) of the magnetic fraction reflect geology and climate in the source regions, means and pathways of transport, and sedimentation milieus in the deposition areas. Among others, *Kobayashi and Nomura* [1974] and *Bloemendal et al.* [1992] published pioneer work illustrating these links. The general concept of "environmental magnetism" was advanced by *Thompson et al.* [1980] and *Thompson and Oldfield* [1986]. Recent reviews were compiled by *Lund and Karlin* [1990], *King and Channell* [1991], *Oldfield* [1991], and *Verosub and Roberts* [1995]. *Frederichs et al.* [1999] discussed specific applications to paleoceanographic research.

In this study, South Atlantic surface sediments (Figure 1) have been analyzed with the objective of delineating regional magnetic mineral distribution patterns and documenting their predominant Holocene climatic and oceanographic controls. The results provide a reference frame for ongoing paleoceanographic time slice analyses. In this respect the actualistic approach bears a peculiarity as all surface sediments sampled are oxic and therefore unaffected by early diagenesis. Even in the Benguela upwelling system, where the supply of degradable organic matter is highest in the South Atlantic, oxygen penetrates 0.5 cm to typically several centimeters into the top layers [*Glud et al.*, 1994; *Schulz et al.*, 1996]. There the shallowest zone of magnetic mineral alteration observed starts at ~3 cm sediment depth [*Dăumler*, 1996]. Electron microscope element analyses (energy dispersive analysis: EDAX) failed to trace any iron sulfides in surface sediments, and all bacterial magnetosomes were identified as magnetite [*Petermann*, 1994; this study]. Numerous investigations have shown [e.g., *Karlin and Levi*, 1983; *Karlin*, 1990; *Leslie et al.*, 1990a, b; *Tarduno*, 1994, 1995; *Tarduno and Wilkinson*, 1996] that reductive diagenesis may greatly modify magnetic mineral inventories in deeper strata by dissolution of primary iron oxides and authigenic formation of magnetic iron sulfides such as greigite. These effects must be a major concern in time slice studies but can be excluded in the present context. Since typical lock-in depths range from a few centimeters to several tenths of centimeters in marine sediments [e.g., *Hyodo*, 1984; *Yamazaki*, 1984; *Løvlie*, 1989, 1994; *deMenocal et al.*, 1990; *Quidelleur et al.*, 1995], no natural remanent magnetization properties have been determined.

We rely on a large (194), representative sample collection and a relatively small number of well-established isothermal magnetic parameters derived from nondestructive bulk sample measurements of magnetic susceptibility, frequency dependence of susceptibility, isothermal and anhysteretic remanent magnetization, magnetic hysteresis, and back field magnetization. This deliberate analytical limitation is appropriate for the basic magnetic characterization of a vast, barely known area. Its scope exceeds other published large data sets [*Bloemendal et al.*, 1992; *Dearing et al.*, 1996b] and can serve as a foundation for detailed studies invoking more advanced experimental techniques.

Regional variations of magnetic properties enable tracking of different particle fluxes and their sedimentation areas. The complexity of superimposing influences is analyzed by multivariate classification methods. Probabilistic (fuzzy c-means) cluster analysis [*Bezdek*, 1973; *Bezdek and Dunn*, 1975], based on the theory of fuzzy sets [*Zadeh*, 1965], proved to be the most efficient way of objectively establishing magnetically defined sediment classes and of quantifying individual sample affinities. Applications of fuzzy c-means cluster analysis (FCM) in geochemistry have been published by *Middleburgh and de Lange* [1988] and *Frapporti et al.* [1993] and in paleomagnetism and environmental magnetism by *Dekkers et al.* [1994] and *Frederichs et al.* [1999].

Paper number 1999PA900020
0883-8305/99/1999PA900020$12.00

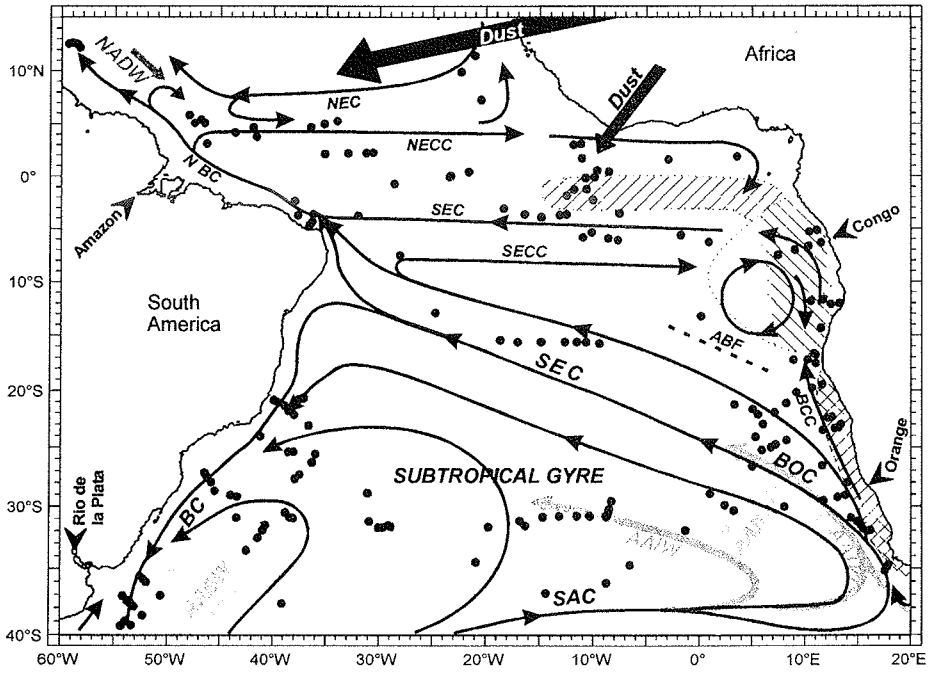

Figure 1. Sample locations (solid dots) in the tropical and southern subtropical Atlantic are given. Surface currents (solid arrows) are North Equatorial Current (NEC), North Equatorial Countercurrent (NECC), North Brazil Current (NBC), South Equatorial Current (SEC), South Equatorial Countercurrent (SECC), South Atlantic Current (SAC), Benguela Ocean Current (BOC), Benguela Coastal Current (BCC), and Brazil Current (BC). The Angola-Benguela Front (ABF) is indicated by a broken line. Deep water currents (lightly shaded arrows) are North Atlantic Deep Water (NADW), Antarctic Intermediate Water (AAIW), and Antarctic Bottom Water (AABW). Modified after *Shannon and Nelson* [1996], *Talley* [1996], *Peterson and Stramma* [1991], and *Reid* [1996]. Darkly shaded arrows denote main dust trajectories by midtropospheric zonal winds and NE trades [*Glaccum and Prospero*, 1980; *Pye*, 1987], and darkly shaded areas denote high-productivity upwelling regions [*Schneider et al.*, 1996]. The Amazon and Congo Rivers are the major fluvial sources of continental detritus to the tropical South Atlantic, and the La Plata and Orange Rivers are the major fluvial sources to the subtropical South Atlantic [*Milliman and Meade*, 1983].

2. Materials and Methods

The 194 surface sediment samples (uppermost centimeter) were recovered by multicorer and box corer devices on several cruises of the German research vessels *Meteor* and *Sonne* (Figure 1). All relevant data of the sampling locations are available from the Internet (http://www.mtu.uni-bremen.de/geomarin/index.htm). Bulk sediment samples (6.4 cm^3) were taken to determine susceptibility and laboratory-imparted remanent magnetizations. Mass specific measurements refer to dry sediment weights. For hysteresis measurements, miniature samples (< 50 mg) were prepared using a technique described by *von Dobeneck* [1996].

2.1. Magnetic Analyses

Mass-specific magnetic susceptibility χ determined with a Geofyzika Kappabridge KLY-2 primarily outlines ferrimagnetic mineral concentrations. Without iron sulfides present, χ is a fairly grain size independent [*Heider et al.*, 1995] measure of ferrimagnetic iron oxides in South Atlantic surface sediments. They are summarized as "magnetites" as no information is available about their titanium content or oxidation state. The nonferrimagnetic susceptibility χ_{nf} derived from the approach-to-saturation analysis of hysteresis data [*von Dobeneck*, 1996] combines contributions of paramagnetic and diamagnetic sediment matrix constituents, and the ferrimagnetic susceptibility $\chi_{fer} = \chi_{tot} - \chi_{nf}$ (χ_{tot} defined as the hysteresis loop gradient at $B = 0$) quantifies magnetite concentrations. The relative abundance of ultrafine superparamagnetic (SP) magnetite (≤ 0.03 μm) [*Dunlop and Bina*, 1977] was estimated from the frequency dependence of susceptibility $\chi_{fd\%}$ [*Stephenson*, 1971; *Mullins and Tite*, 1973; *Maher*, 1988; *Dearing et al.*, 1996a] measured with a Bartington Instruments MS2 bridge.

The *S* ratio [*Stober and Thompson*, 1979] compares concentrations of high-coercive (e.g., hematite and goethite) to low-coercive (e.g., magnetite) fractions. $S_{-0.3T}$, as defined by *Bloemendal et al.* [1992], relates the back field magnetization $M_{-0.3T}$ to the saturation remanence M_{sir}, imparted at our maximum available laboratory field of 0.9 T. Our data exclusively refer to the hematite/magnetite ratio since goethite, a magnetic mineral that apparently has never been unequivocally documented in marine realms, does not acquire a remanence up to fields of 1 T [*Heller*, 1978]. The distinct grain size dependence of magnetite M_{sir} limits a quantitative interpretation of the $S_{-0.3T}$ parameter in terms of mineral proportions. Present estimates assume M_{sir} of 1 kA m^{-1} for hematite and 50 kA m^{-1} for single-domain (SD) magnetite [*Thompson and Oldfield*, 1986].

A PMC M2900 alternating-gradient magnetometer

[*Flanders*, 1988] was used for hysteresis and back field measurements to peak fields of 0.3 and 1 T. Further processed with the "HYSTEAR" program of *von Dobeneck* [1996], the resulting standard hysteresis parameters saturation magnetization M_s and saturation remanence M_{rs} compose the magnetite grain size ratio M_{rs}/M_s [*Bean and Livingston*, 1959; *Wasilewski*, 1973; *Day et al.*, 1977; *Dunlop and Özdemir*, 1997], while the coercive field B_c depicts the magnetic stability of magnetite. The 0.3 T peak field data were ultimately preferred for this purpose as they proved to be less influenced by hematite and SP magnetite than 1 T results.

Isothermal remanent magnetizations M_{ir}, imparted in 200 mT pulsed fields and anhysteretic remanences M_{ar}, effected by superimposing a decaying alternating field of 200 mT to the ambient laboratory field of 35 μT, were measured with a Molspin and Cryogenic Consultants and 2G Superconducting Quantum Interference Device (SQUID) magnetometer, respectively. Fine SD magnetite (0.03 μm < ∅ < 0.1 μm) [*Dunlop*, 1973; *Butler and Banerjee*, 1975] and intermediate pseudo-single-domain (PSD) magnetite (0.1 μm < ∅ < ~5-10 μm) [*Parry*, 1965] particles carry higher isothermal magnetization than coarse multidomain (MD) magnetite (∅ > ~5-10 μm) fractions. As for M_{ar}, an even stronger grain size dependence applies that is most pronounced in the SD/PSD range [*Banerjee et al.*, 1981; *King et al.*, 1982]; the M_{ar}/M_{ir} ratio assesses fine-particle magnetite variations [*Maher*, 1988; *Heider et al.*, 1995]. Incremental triaxial alternating field (AF) demagnetization of M_{ar} primarily delimits the (micro)coecivity spectrum of the magnetite fraction [*Jackson et al.*, 1988]. The median destructive field $B_{1/2}(M_{ar})$ necessary to randomize half of the initial M_{ar} characterizes its average magnetic stability.

2.2. Statistical Analyses

The "Komolgorow-Smirnow test" and the more stringent "chi-square test" [*Davis*, 1986] were applied to evaluate all magnetic data sets for normal or lognormal distributions. Knowledge of these statistical parameters is crucial for the characterization of sediment populations and the applicability of multivariate analyses.

Cluster analysis FCM [*Bezdek*, 1973; *Bezdek and Dunn*, 1975] establishes fuzzy partitions on the basis of multivariate similarity. A multiparameter data set **X** is represented as the scatter of sample specific data points $\mathbf{x} \in \mathbf{X}$ in an n-dimensional vector space spanned by n parameters. As they may greatly vary in range, each value is standardized by subtracting the respective parameter mean and dividing by its standard deviation. The Euclidean distance between any two samples $\mathbf{x}, \mathbf{y} \in \mathbf{X}$

$$D(\mathbf{x},\mathbf{y}) = \sqrt{\sum_{i=1}^{n} (x_i - y_i)^2}$$

can be used to quantify their multiparametric similarity. The FCM algorithm verifies whether and where data points form clusters in the multidimensional parameter space. If the appropriate cluster number is m (determined from validity indicators such as partition coefficient and partition entropy [*Bezdek*, 1981]), a cluster structure is defined in which the affinity of each sample $\mathbf{x} \in \mathbf{X}$ to every individual cluster k ($k = 1...m$) is quantified by its membership function $p_k(\mathbf{x})$:

$$\sum_{k=1}^{m} p_k(\mathbf{x}) = 1, \quad 0 \le p_k(\mathbf{x}) \le 1$$

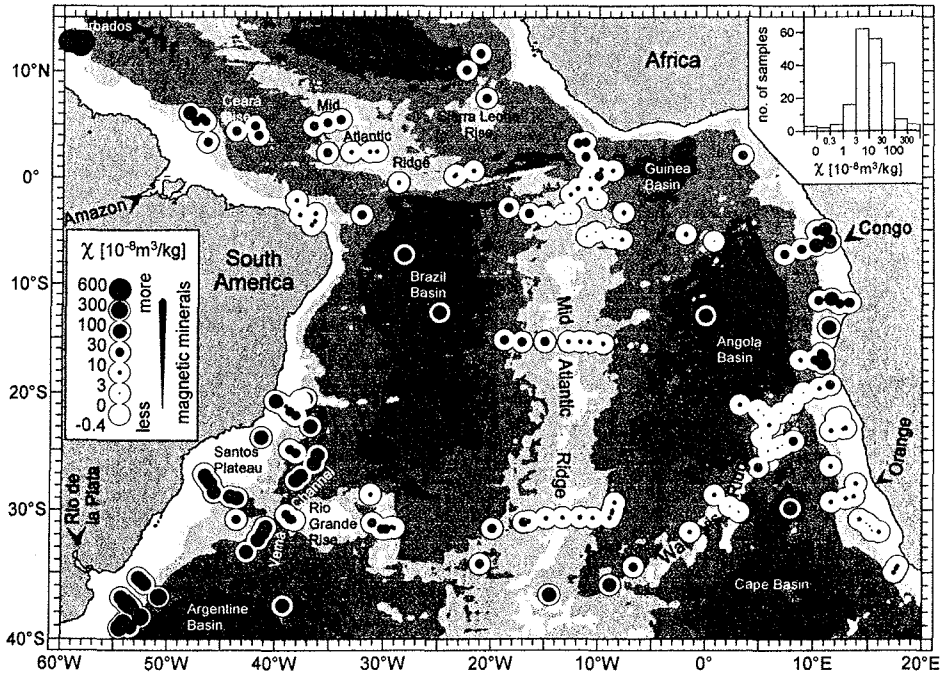

Figure 2. Elevated susceptibilities at continental margins, particularly in the realm of major river estuaries, document a predominantly terrigenous origin of the magnetic mineral fraction. Susceptibility signals in the open ocean strongly depend on water depth increasing with intensified dissolution of the diamagnetic $CaCO_3$ fraction. The statistical data distribution is lognormal.

The cluster centers c_k are determined as weighted arithmetic means and represent the characteristic properties of every cluster k. For each magnetic property i and cluster k, mean $\bar{x}_{ik}$ and standard deviation s_{ik} are calculated with the squared membership $p_k(\mathbf{x})$ acting as a weight factor:

$$\bar{x}_{ik} = \sum_{\mathbf{x}\in\mathbf{X}} p_k^2(\mathbf{x}) x_i \Big/ \sum_{\mathbf{x}\in\mathbf{X}} p_k^2(\mathbf{x})$$

$$s_{ik} = \sqrt{\sum_{\mathbf{x}\in\mathbf{X}} p_k^2(\mathbf{x})(x_i - \bar{x}_i)^2 \Big/ \sum_{\mathbf{x}\in\mathbf{X}} p_k^2(\mathbf{x})}$$

3. Results

3.1. Magnetite Content

To a first-order approximation, bulk magnetic susceptibility refers to the magnetite content ($\chi_{Magn} \approx 50{,}000\times10^{-8}$ $m^3\ kg^{-1}$) in almost all marine deposits. For paramagnetic matrix minerals, typically, iron-bearing silicates, χ varies from 5 to 100×10^{-8} $m^3\ kg^{-1}$, while diamagnetic matrix constituents, mostly calcareous and siliceous microfossils, have negative susceptibilities of $\sim -0.5\times10^{-8}$ $m^3\ kg^{-1}$ [*Dunlop and Özdemir*, 1997]. The contribution of matrix minerals to bulk susceptibility cannot be neglected as common magnetite concentrations in marine sediments are considerably <1%.

Susceptibilities of South Atlantic surface sediments range from -0.4 to 600×10^{-8} $m^3\ kg^{-1}$ (Figure 2). These extremes, observed at the Walvis Ridge and off Barbados, correspond to magnetite concentrations of ~0.0002 and 1.2 wt %, respectively. Along most of the South American continental margin high χ document an enhanced deposition of terrigenous components, largely supplied by the La Plata and Amazon Rivers. In the Argentine Basin, material transported by intense deep water currents from Antarctic regions should also be important [*Ledbetter*, 1986]. Ashes of nearby, recently active Caribbean volcanoes are responsible for particularly high susceptibilities in the Barbados area. On the African side a substantial inflow of terrigenous material from the Congo and other rivers is confined to the Angola Basin, whereas surface sediments in the Cape Basin contain only very minor concentrations of lithogenic magnetic minerals.

A distinct correlation to water depth characterizes the distribution of susceptibilities in the pelagic open ocean areas. On submarine elevations like the Walvis Ridge (WR) and Mid-Atlantic Ridge (MAR) negative to slightly positive values ($\chi \le +10\times10^{-8}$ $m^3\ kg^{-1}$) indicate both low concentrations of ferrimagnetic minerals and a predominant sedimentation of biogenic carbonates ($CaCO_3$). Similar conditions prevail in the high-productivity Benguela upwelling region off Namibia and at the South American continental slope around 5°S. Notably high susceptibilities at several shallow sites along the MAR apparently originate from magnetite-rich debris of eroding deep-sea basalt, an assumption that is supported by grain size and coercivity analyses. Because of progressive calcite dissolution, χ systematically increases to deep waters and reaches relative maxima in the pelagic clays of abyssal plains.

The χ_{nf} (Figure 3) and χ_{fer} (Figure 4) data clearly underline a close affinity of elevated ferrimagnetic and paramagnetic mineral contents, implying that both components frequently have a common lithogenic origin. This relationship is particularly well developed at those continental margins, where

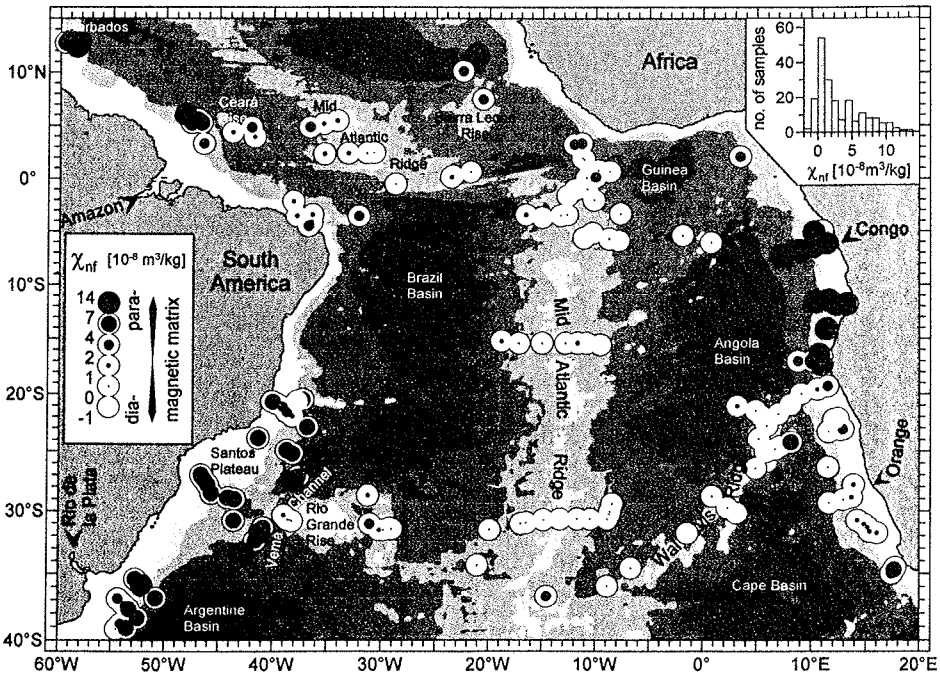

Figure 3. High positive nonferrimagnetic susceptibilities χ_{nf} indicate an enrichment of paramagnetic matrix minerals because of a primarily terrigenous sedimentation at continental margins or carbonate dissolution in abyssal plains. Low to negative χ_{nf} in open ocean and upwelling regions denote a diamagnetic sediment matrix of biogenic calcareous or siliceous constituents. The statistical data distribution is lognormal.

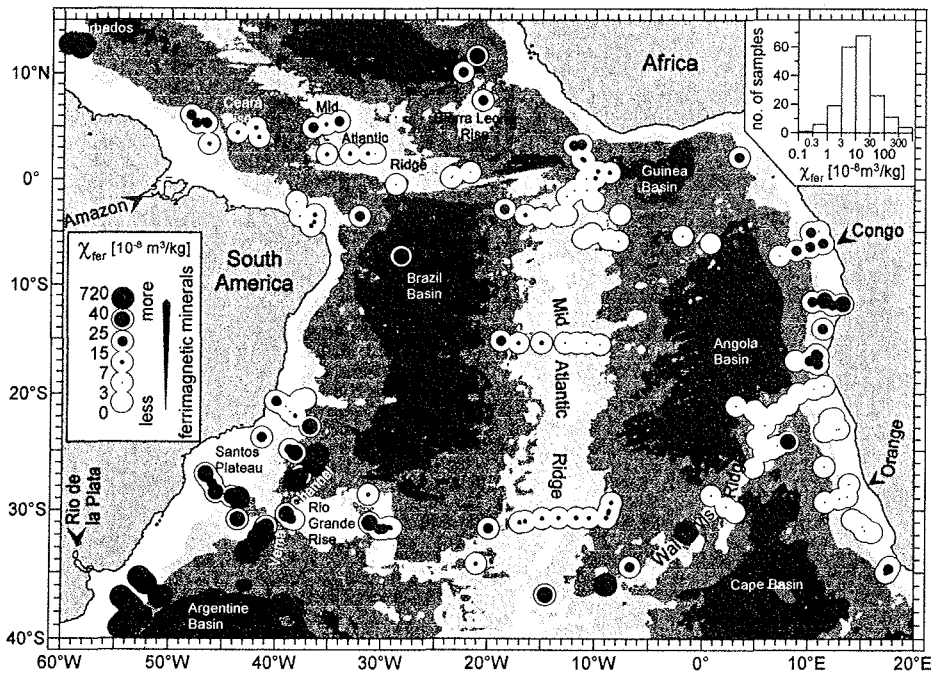

Figure. 4. High ferrimagnetic susceptibilities χ_{fer} are closely associated with paramagnetic (high χ_{nf}) terrigenous sediments; low χ_{fer} are associated with diamagnetic (low χ_{nf}) biogenic deposits (see Figure 3). The statistical data distribution is lognormal.

massive fluvial sediment loads are discharged, but also extends into the open ocean north of the equator delineating African dust plumes. Calcareous sediments deposited above the calcium compensation depth (CCD) and at a sufficient distance from the continents as on the MAR and WR are highly depleted in ferrimagnetic minerals [*Balsam and McCoy*, 1987]. A similar situation at the Cape Basin continental margin is explained by the regional high-productivity system and a general lack of significant fluvial or eolian influx. In contrast, deposits in the deep-sea basins are characterized by a paramagnetic sedimentary matrix and high ferrimagnetic contents.

3.2. Hematite Content

Hematite is primarily regarded as a product of continental weathering and is diagnostic of fluvial or eolian influxes [*Robinson*, 1986; *Bloemendal et al.*, 1988; *Frederichs et al.*, 1999]. The upper limit of $S_{-0.3T} < 0.98$ in the western South Atlantic suggests that hematite is ubiquitous and accounts for over 50% of the magnetic mineral assemblages (Figure 5). Particularly high hematite/magnetite ratios > 8:2 ($S_{-0.3T} < 0.94$) prevail in an east-west oriented tropical belt at ~5°N. The Amazon River, the main fluvial source of terrigenous material to the equatorial South Atlantic [*Holeman*, 1968], supplies large amounts of hematite to this region. At present most of its particulate load is deflected northwestward by the North Brazil Current (NBC). Parts of the Amazon Plume are retroflected eastward to join the North Equatorial Countercurrent (NECC) [*Muller-Karger et al.*, 1988]. Sediment suspended by turbulent processes in the Amazon Canyon and Fan is distributed by deeper southeastward flowing waters summarized as North Atlantic Deep Water (NADW) [*Reid*, 1996].

The arid regions of North Africa are potentially even more important sources of hematite in the equatorial Atlantic. Transported as dust by midtropospheric zonal winds, this eolian sedimentation reaches far into the western equatorial Atlantic and Caribbean [*Pye*, 1987]. Less intense NE trades carry dust into the eastern equatorial Atlantic [*Glaccum and Prospero*, 1980]. The $S_{-0.3T}$ parameter clearly traces this dust plume pattern. Elevated hematite concentrations in the northern Argentine and southern Brazil Basins to which fluvial, possibly also eolian, components originating from the hematite-rich kaolinitic soils of Brazil [*Schwertmann and Kämpf*, 1985] contribute correspond to high terrigenous contents in the surface sediments (Figure 3). Along the southwest African continental margin, fluvial input of hematite is mainly restricted to the Congo Fan region. Its scarcity in the Cape Basin is in agreement with a general lack of terrigenous matter in the sediments and implies that dust flux from the Namib Desert is of minor importance [e.g., *Chester et al.*, 1972; *Aston et al.*, 1973]. It is interesting to note that hematite concentrations are relatively low at most abyssal plain sites.

3.3. Magnetite Domain State and Grain Size

The broad range of M_{rs}/M_s ratios (Figure 6) from 0.04 (MD) up to 0.37 (fine-grained PSD) does not reach the theoretical value ≥0.5 of ideal, noninteracting SD grains [*Stoner and Wohlfahrt*, 1948; *Joffe and Heuberger*, 1974], a common observation for natural sample collections. *Jackson* [1990] and *Gee and Kent* [1995] assume that an omnipresent ultrafine-grained SP fraction causes a drop of the M_{rs}/M_s ratio. At

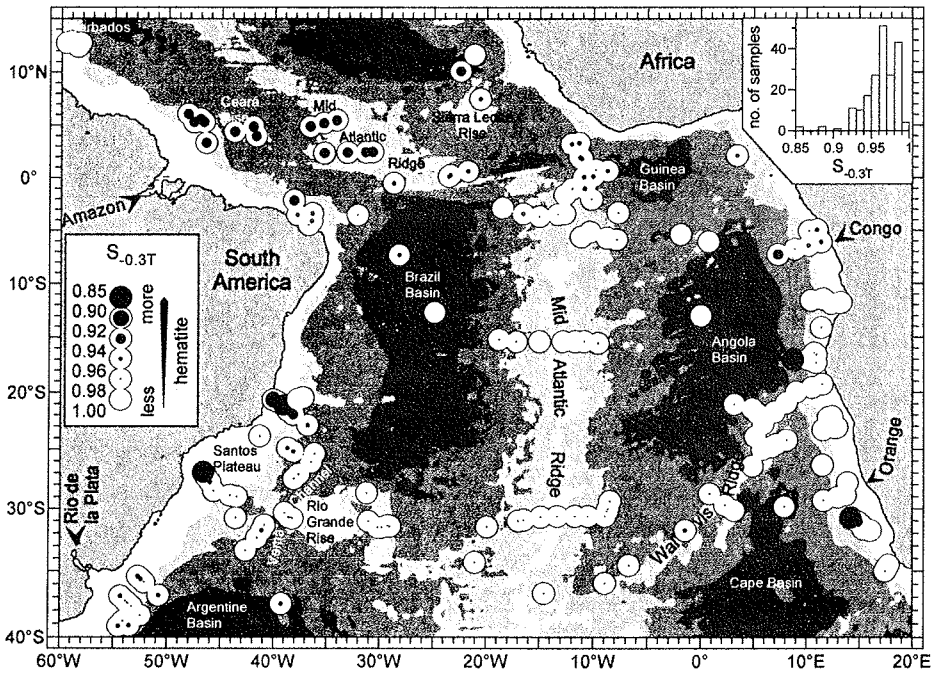

Figure 5. $S_{-0.3T}$ <0.96 (hematite/magnetite > 7/1) document dust fluxes from the African continent and fluvial discharge of terrigeneous material by major river systems. The about normal statistical data distribution is skewed because of the nonlinear definition of $S_{-0.3T}$.

odds with theory it is therefore plausible to accept a SD predominance for $M_{rs}/M_s > 0.3$. The bimodal distribution of M_{rs}/M_s features a primary mode centered in the PSD range at 0.25, while a much less abundant MD-sized population responsible for the second mode at ~0.1 is restricted to a few locations with coarse fluvial (La Plata and Amazon) or volcanic (Barbados and MAR) input.

The most prominent feature revealed by the M_{rs}/M_s data set is a general coarsening of magnetic grain sizes from the eastern to the western half of the South Atlantic. The pre-

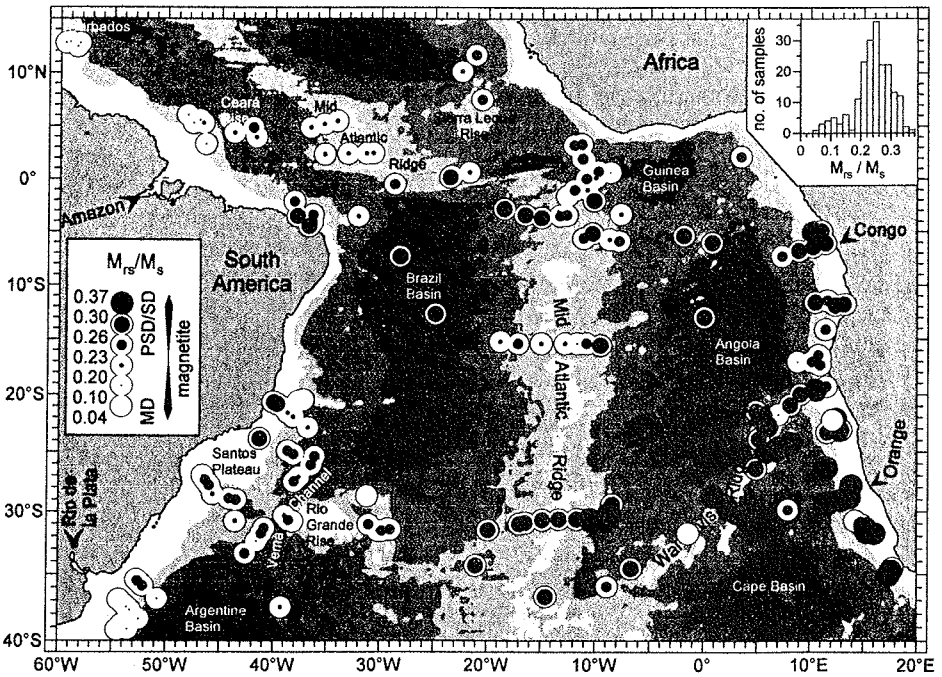

Figure 6. The M_{rs} / M_s ratio outlines a general coarsening of magnetite grain-sizes from east to west. Only deposits of the Amazon and La Plata Rivers and SE Caribbean volcanogenic sediments exhibit multidomain (MD) properties. The bimodal statistical data distribution has a prominent maximum in the pseudo-single-domain (PSD) range and a secondary mode with MD characteristics.

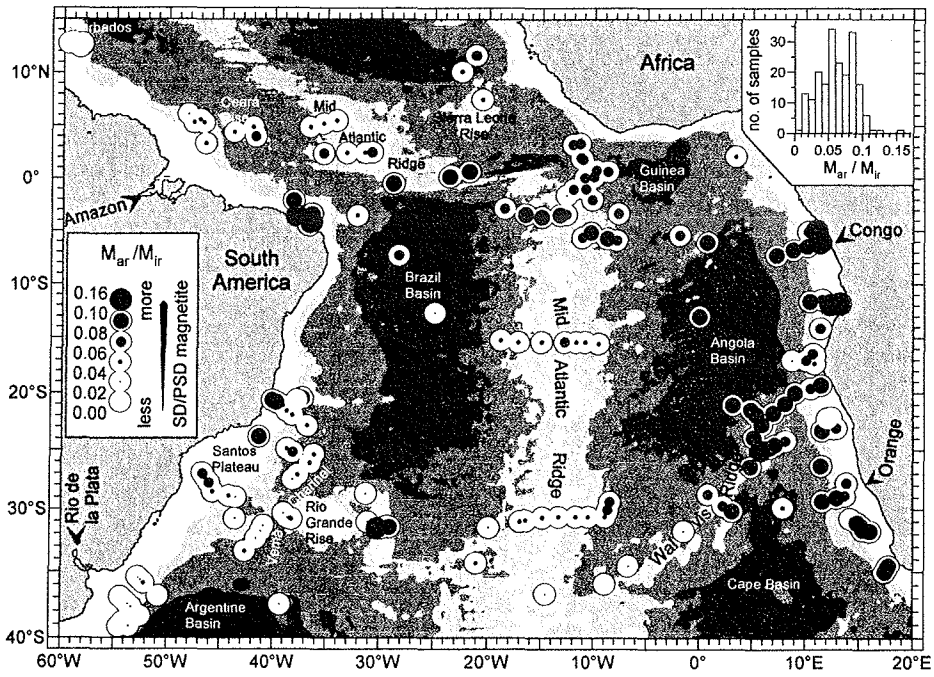

Figure 7. The M_{ar} / M_{ir} ratio assesses relative contributions of SD/PSD grain-size fractions to the total magnetite content. Abundant fine SD-sized (0.03 - 0.1 μm) bacterial magnetite results in elevated M_{ar} / M_{ir} along the African continental margin and in the equatorial high productivity region. The Congo and other African rivers discharge fine-grained material that is dispersed by surface currents into the equatorial and possibly also the western South Atlantic. The large South American rivers deliver significantly coarser magnetite. The statistical data distribution is slightly bimodal.

dominance of fine particles in the high-productivity Benguela upwelling system and on the eastern Walvis Ridge reflects a high abundance of magnetite formed by magnetotactic bacteria [*Petersen et al.*, 1986; *Petermann and Bleil*, 1993]. These magnetofossils are precisely limited by biological growth control to a fairly narrow SD size range. The fine-grained magnetic mineral deposition on the Walvis Ridge could partly also originate from particle advection by intermediate Antarctic water masses such as Circumpolar Deep Water (CDW) or Antarctic Intermediate Water (AAIW) [e.g., *Reid*, 1989; *Petschick et al.*, 1996]. According to the present data it should extend northward to 30°S on the MAR and possibly to the Rio Grande Rise and Santos Plateau areas. *Johnson* [1984] described the sediments in the vicinity of the Vema Channel below 4000 m water depth as deposits from Antarctic Bottom Water (AABW) suspended matter. *Bornhold and Summerhayes* [1977] assume the same origin for the fine-grained lithogenic sediment fractions at the southern foot of the Walvis Ridge. Fluvial particles discharged by the Congo and other African rivers into the Angola and Cape Basins are equally fine-grained. Contrasting conditions dominate at the South American continental margin, where the Amazon and La Plata supply comparatively coarse material. *Ledbetter* [1986] attributes the deposition of coarse-grained magnetite in the NW Argentine Basin to winnowing effects of intense AABW currents, whereas *Sachs and Ellwood* [1988] favor downslope transport of terrigenous detritus.

In general, the M_{ar}/M_{ir} distribution (Figure 7) follows that of M_{rs}/M_s, with notable regional discrepancies [*Schmidt*, 1995]. Most high ratios of ~0.1 indicating SD/PSD predominance are observed in the eastern and equatorial sectors. Two mechanisms, biomineralization and sorting, should be responsible for the abundance of small (SD/PSD) particles in a belt reaching from the SW African continental margin to the Congo region and into the central equatorial South Atlantic. Along the African continental slopes, high population densities of living magnetotactic bacteria were detected [*Petermann and Bleil*, 1993]. Using transmission electron microscopy, we also identified bacterial magnetosomes in surface sediments from the equatorial high productivity zone. A second major source of fine magnetic particles is the Congo River. The coarser fractions of its detrital load are either retained in upstream depocenters or are channeled by the submarine Congo Canyon and released as turbidite flows into the deep Angola Basin [*Peters*, 1978; *Pak et al.*, 1984]. The finer Congo sediments remain suspended and are transported in NW direction to form the Congo Plume [*Eisma and van Bennekom*, 1978]. They appear to follow the South Equatorial Current (SEC) all the way across the tropical South Atlantic.

Throughout the South Atlantic, $\chi_{fd\%}$ indicates high amounts of SP particles in central open ocean areas (Figure 8). Apparently, African rivers to the Angola Basin are the only major fluvial sources of ultrafine grained magnetite. As this fraction may be transported over large distances by currents, its relative absence should be at least as conclusive as its occurrence. Strong currents will prevent settling in many coastal regions, for example, the Benguela system in the Cape Basin. Off the Amazon and La Plata River mouths, where similar conditions prevail, large amounts of fluvial MD mag-

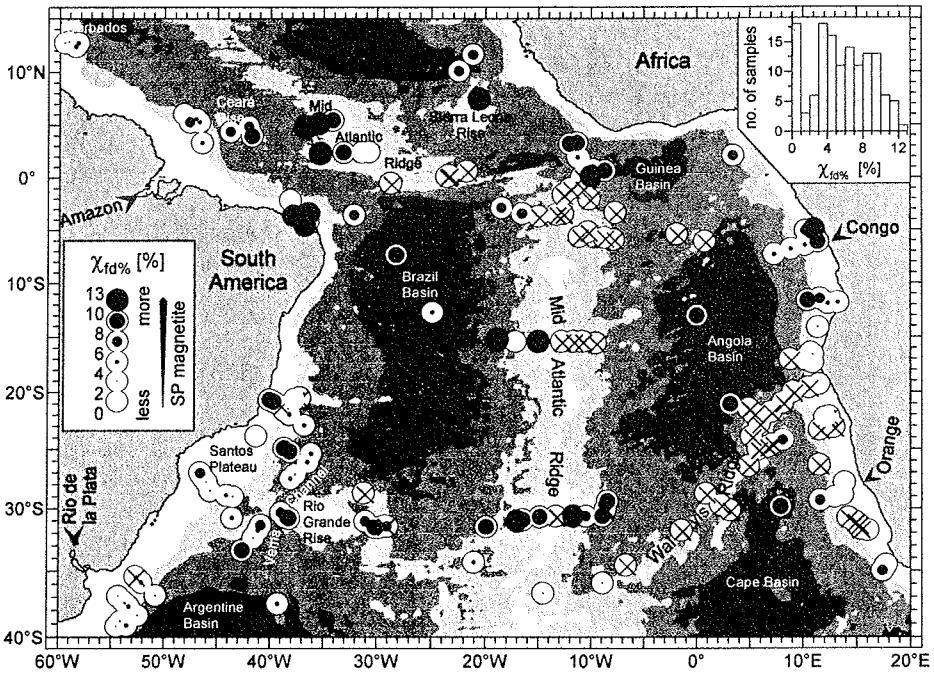

Figure 8. Relative concentrations of ultrafine SP magnetite indicated by the frequency dependence of susceptibility $\chi_{fd\%}$. Crosses mark locations where susceptibilities are too low to reliably quantify $\chi_{fd\%}$. High amounts of coarse-grained MD magnetite may mask SP components in parts of the western South Atlantic (see Figure 6).

netite (see Figure 6) could totally mask SP components. An efficient deposition of this grain size fraction requires particle aggregation and is only conceivable at low bottom current velocities as in the central parts of the South Atlantic Ocean. The $\chi_{fd\%}$ pattern strongly deviates from the M_{rs}/M_s and M_{ar}/M_{ir} grain size ratios, implying that origin, transport, and deposition of the ultrafine-grained magnetite fraction are fairly independent and commonly unrelated to that of the coexisting SD to MD-sized particles.

3.4. Magnetite Coercivity

Except for central equatorial sites, B_c patterns (Figure 9) comply entirely with the M_{rs}/M_s data set (Figure 6), indicating that both parameters are essentially controlled by grain size variations. The bimodal distribution of B_c has maxima at 10 and 15 mT. The two populations roughly represent the tropical and subtropical parts of the South Atlantic.

Highest B_c values of up to 23 mT are encountered in the Benguela upwelling region corresponding to the abundance of biogenic SD magnetite. A noteworthy feature is the remarkably low coercivity in the central equatorial region, where the predominance of fine-grained magnetite (Figures 6 and 7) would actually imply relatively high magnetic stability. A plausible interpretation of these low coercivities should be superparamagnetism. $\chi_{fd\%}$ data (Figure 8) support this assumption. On the other hand, no constricted, so-called wasp-waisted, hysteresis loops were observed diagnostic of magnetic mineral assemblages containing SP and SD/PSD grain sizes in appropriate proportions [*Tauxe et al.*, 1996]. If the SP explanation holds in spite of these controversial findings, an important magnetite fraction should have grain sizes close to the SP/SD transition and quite unstable remanent magnetizations.

The South Atlantic $B_{1/2}(M_{ar})$ pattern (Figure 10) is largely compatible with regional distributions of previously shown parameters. Along the African continental margin, abundant very stable SD components result in high median destructive fields of up to 48 mT. As indicated by M_{rs}/M_s (Figure 6) and M_{ar}/M_{ir} (Figure 7), this grain size fraction should be much less important at the South American continental margin. However, some high $B_{1/2}(M_{ar})$, for example, off the La Plata River mouth, suggest regionally substantial PSD concentrations. In this area, grain size and coercivity parameters exhibit MD characteristics. The deposition of SD/PSD particles is probably prevented by high bottom current velocities [*Ledbetter*, 1986]. This paradox of large magnetic grain sizes and high coercivities may be explained by SD-simulating domains within MD particles. Such behavior has been observed for pinned closure domains or domain walls in grains with high surface stresses like volcanogenic particles [*Özdemir et al.*, 1995; *Özdemir and Dunlop*, 1998]. Most of the La Plata feeders drain the Paraná Basin, where vast formations of Jurassic flood basalts crop out [*Clapperton*, 1993] and should convey large amounts of volcanic detritus into the Argentine Basin. With increasing distance to the continents, M_{ar} is carried by less coercive components. Substantial M_{ar} losses within the first steps of the demagnetization curves cause particularly low $B_{1/2}(M_{ar})$ in the central equatorial region, on the whole MAR, and more locally, on the west flank of the Rio Grande Rise and in the SW Brazil Basin. They hint at important magnetic fractions with grain sizes around the SP/SD transition [*Özdemir and Banerjee*, 1982]. $\chi_{fd\%}$ reaches > 8%

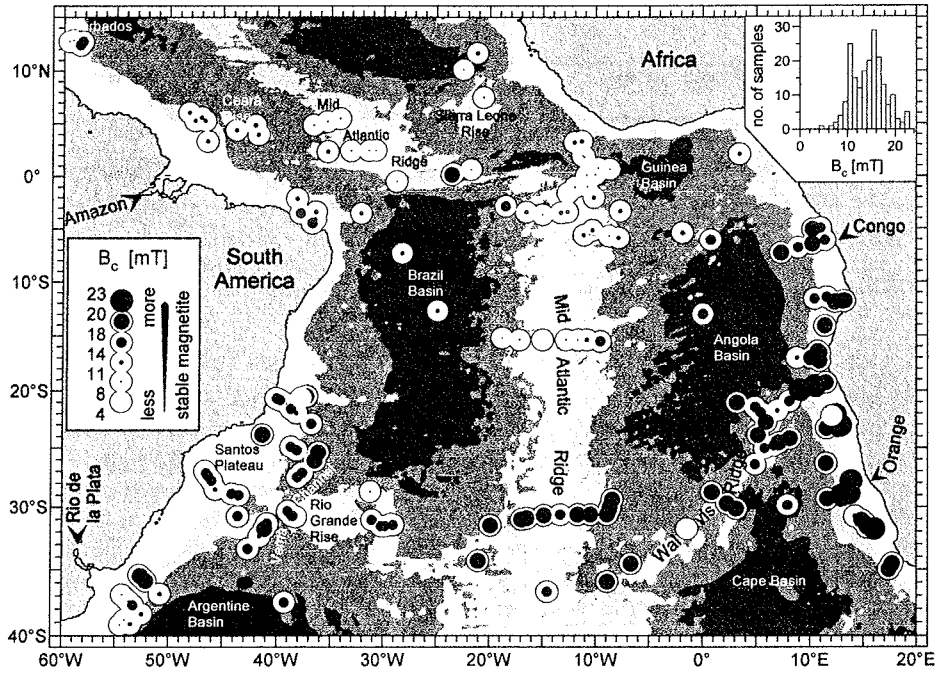

Figure 9. With the exception of the central equatorial region, coercive field B_c and grain-size parameter M_{rs} / M_s patterns (Figure 6) are essentially identical. The statistical data distribution is bimodal.

in most of these samples (Figure 8). Especially on the southern MAR, constricted hysteresis loops that *Pick and Tauxe* [1994] and *Tauxe et al.* [1996] reported for submarine basaltic glasses and modeled for various SP/SD mixtures indicate a mixture of magnetically hard (SD/PSD) and soft components of SP/SD transitional size. These magnetically soft particles may be advected by eolian or current transport, but in view of the large concentrations necessary to produce the particular demagnetization effects, an alternative interpretation shall be considered.

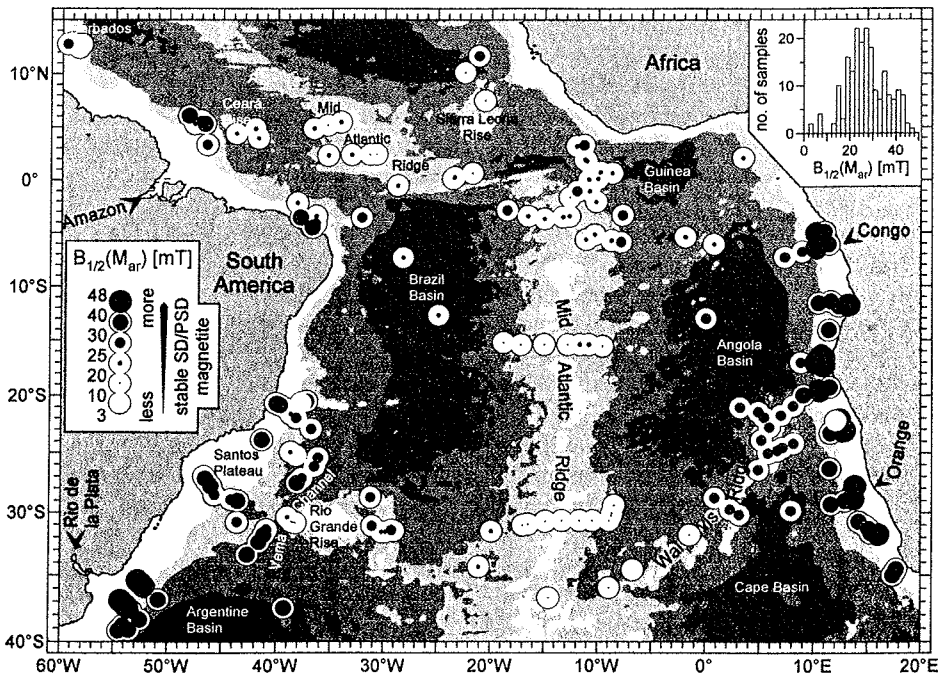

Figure 10. Median destructive fields $B_{1/2}(M_{ar})$ delineate high M_{ar} stabilities in continental realms considerably decreasing toward open ocean areas. The slightly bimodal statistical data distribution has maxima at ~25 mT representative of pelagic regions and at around 40 mT representative of continental margins.

Table 1. Average Rock Magnetic Properties of the Ten Clusters, Weighted by Respective Sample Memberships

	Cluster 1	Cluster 2	Cluster 3	Cluster 4	Cluster 5	Cluster 6	Cluster 7	Cluster 8	Cluster 9	Cluster 10
$S_{-0.3T}$	0.931	0.956	0.976	0.963	0.981	0.980	0.964	0.963	0.961	0.959
M_{rs}/M_s	0.21	0.22	0.26	0.27	0.31	0.30	0.28	0.23	0.22	0.10
M_{ar}/M_{ir}	0.054	0.064	0.073	0.081	0.075	0.086	0.044	0.033	0.045	0.011
B_c, mT	11.9	11.0	12.1	16.3	21.1	16.2	16.3	15.2	13.5	9.7
$B_{1/2}(M_{ar})$, mT	23.0	22.0	24.0	34.0	39.9	29.0	16.6	29.2	24.8	36.7

Deutsch et al. [1981] and *Radhakrishnamurty et al.* [1981] reported SP-simulating properties of synthetic Ti-rich titanomagnetites and oceanic basalts, which they explained as "spin glass" behavior. A relatively small number of coarse-grained (titano)magnetites of basaltic origin with such SP-simulating characteristics could account for the observed phenomenon. According to *Johnson* [1983] the western flank of the Rio Grande Rise above 3600 m water depth is under the influence of southward flowing NADW with relatively high velocities of 2-8 cm s^{-1}. Above 1400 m, *Johnson* [1984] described outcropping Eocene basaltic rocks, and *Melguen and Thiede* [1974] found volcanic glass in surface sediments on the west Rio Grande Rise flank below 4050 m water depth. On the MAR, young oceanic crust should also form common basaltic outcrops.

4. Discussion

4.1. Magnetic Sediment Classification Using Fuzzy C-means Cluster Analysis

So far, it has been demonstrated that specific magnetic properties of surface sediments delineate distinct Holocene particle sources and transport patterns in the South Atlantic. Each parameter develops a somewhat different scheme of magnetic mineralogy and grain size provinces, bounded by sharp or gradual transitions. To condense and refine this information, a synthesis of the different geographical distributions has to be drawn. This task is much too complex to be carried out by visual and descriptive comparison and requires analytical statistics. Among applicable multivariate methods, cluster analysis is particularly suitable for large, heterogeneous natural systems and provides a detailed empirical classification from relatively few parameters. The most appropriate clustering algorithm for many geological problems is FCM [*Bezdek*, 1973; *Bezdek and Dunn*, 1975].

Magnetic mineral contents of marine sediments depend both on their specific accumulation rates and on dilution by calcareous or siliceous matrix components. While magnetic mineral fluxes mostly trace the origin and lateral transport of terrigenous sediment fractions, biogenic particle fluxes primarily reflect surface water productivity and water depth. The interference of these two basic deposition systems complicates the environmental magnetic evidence. To eliminate such dilution effects, exclusively concentration independent quantities were combined in the cluster analysis. Five previously discussed parameters, quantifying hematite to magnetite proportions ($S_{-0.3T}$), magnetite domain state (M_{rs}/M_s, M_{ar}/M_{ir}), and coercivity (B_c, $B_{1/2}(M_{ar})$), have been selected. The restriction to a small number of diagnostic parameters underlines the intention to keep results and interpretations as transparent as possible. Successively more detailed cluster analyses postulating 2-20 cluster centers were performed. By evaluating statistical validity criteria as well as the oceanographic interpretability of each solution the ten cluster partition presented in the following was established for the South Atlantic.

The magnetic cluster characteristics are summarized in Table 1. A most instructive graph for analytical purposes is Figure 11 in which each cluster center position is depicted along the respective parameter axis. All clusters are denoted by symbols in the figures to formally separate statistical classifications from rock magnetic, sedimentological, and oceanographic associations: cluster 1, solid triangle; cluster 2, open triangle; cluster 3, half-solid invented triangle; cluster 4, half-solid circle; cluster 5, solid circle; cluster 6, solid star; cluster 7, open box; cluster 8, plus; cluster 9; cross; and cluster 10, solid diamond. Table 1 and Figure 11 serve as a common platform for all following interpretations.

4.2. Geographical Distribution of Cluster Affinities

Considering that the database comprises only concentration independent magnetic parameters and bears no geographical information, the remarkably clear regional delimitation of most clusters is a striking result. Only cluster 9 cannot be regionalized.

Convincing sedimentological interpretations of magnetic cluster characteristics under present oceanographic settings are indispensable for environmental magnetic conclusions and future paleoceanographic applications in the South Atlantic. To identify the geological and oceanographic controls responsible for the grouping of individual clusters, it is advantageous to map and analyze the geographical distribution of each individual cluster on the basis of membership functions. The results are given in Figure 12 with symbol sizes quantifying respective membership coefficients. Samples without a single prominent membership occupy intermediate positions between two or more clusters. Four such transitions have been specified by roman numbers: I, transition between clusters 1 and 2; II, transition between clusters 2, 3, 9, and 7; III, transition between clusters 4 and 6; and IV, transition between clusters1, 9, and 8.

Samples with close affinities to cluster 1 are primarily found in the NW equatorial Atlantic. The unusually high mean hematite/magnetite ratio of ~9:1 ($S_{-0.3T}$ = 0.931) results from dust originating in the Saharan desert. M_{rs}/M_s = 0.21 and

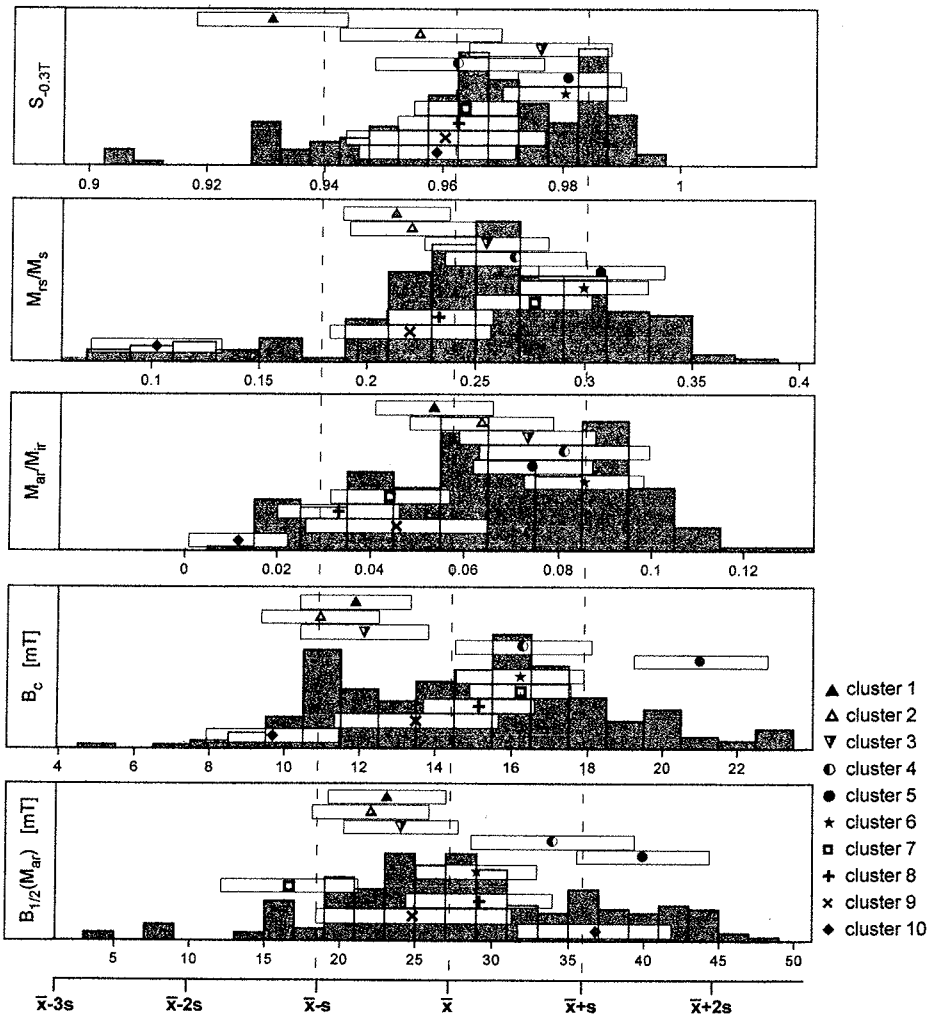

Figure 11. Magnetic fuzzy c-means cluster analysis (FCM) classification of South Atlantic surface sediments are presented. Cluster center positions projected onto the five parameter axes and marked by symbols depict the characteristic magnetic properties of the 10 clusters. Horizontal bars quantify means $\bar{x}_{ik}$ and standard deviations s_{ik} for each parameter i and cluster k. The bottom axis refers to the overall parameter arithmetic means $\bar{x}_i$ and standard deviations s_i after parameter standardization. Shadded histograms represent frequency distributions of the complete sample set.

an intermediate $M_{ar}/M_{ir} = 0.054$ indicate domain states in the coarser PSD range. The low coercivity ($B_c = 11.9$ mT) and stability of anhysteretic ($B_{½}(M_{ar}) = 23.0$ mT) remanence suggest even larger grain sizes. On the Ceará Rise and in the Amazon Fan, where the terrigenous fraction is mainly supplied by the Amazon River, similar characteristics apply. SP or basaltic material on the MAR (Figures 8 and 10) may reduce the average coercivities.

The highest affinities to cluster 1 are not found near the African continent but farther west. *Balsam and Otto-Bliesner* [1995] reported a similar distribution for their factor 2 score, which they primarily relate to hematite. The specific characteristic of this cluster, low $S_{-0.3T}$, obviously combines both influences, the African dust and the Amazon detritus. A high-resolution cluster analysis based on a subset of equatorial Atlantic samples and seven magnetic parameters [*Frederichs et al.*, 1999] separates clusters of Amazon and Saharan influence. The large diversity and scatter within the present sample set prevents discrimination of the relatively similar magnetic signatures of the Amazon and Sahara.

An affinity to cluster 1 is also observed for samples along the Brazilian coast between 20° and 30°S. The fluvial sediment supply to this area [*Petschick et al.*, 1996] originates from catchments that pedologically resemble the Amazon Basin. According to *Schwertmann and Kämpf* [1985], hematite and goethite are the main iron oxides in kaolinitic soils of southern and central Brazil.

The highest memberships to cluster 2 are found in the western Guinea Basin with elevated affinities extending northwestward to the Sierra Leone Rise and westward to the South American coast. The magnetic properties are comparable to cluster 1 (Figure 11) and suggest a similar particle source. *Pye* [1987] and *Westerhausen et al.* [1993] describe a southward transport of Sahel Zone-derived particles via NE trade winds into this area. The flux is less intense than in the Saharan dust plume and finds its expression in a lower hema-

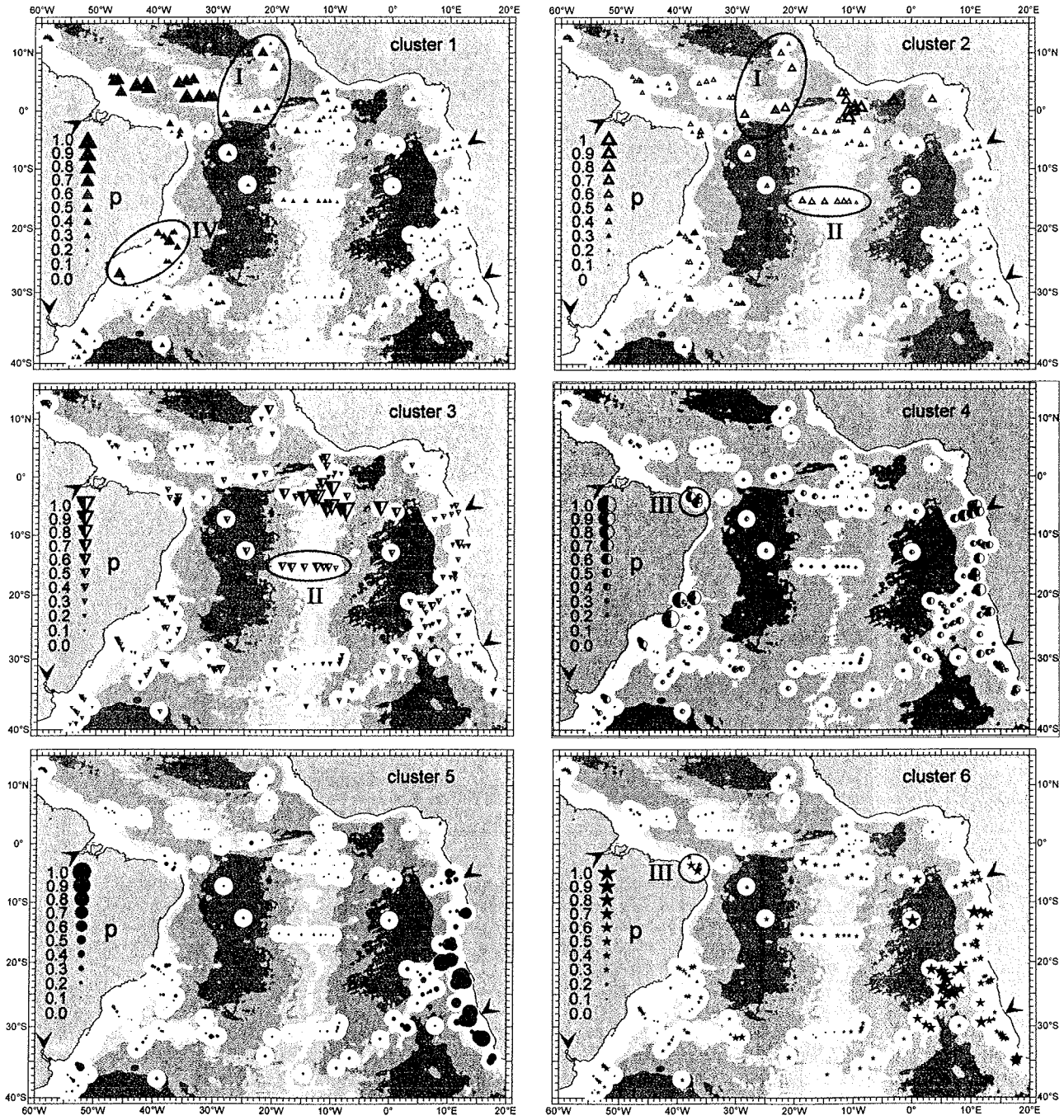

Figure 12. Geographic distribution of magnetic 10-cluster FCM classification of South Atlantic surface sediments. Respective membership functions p are represented by symbol sizes. Most clusters display distinct regional centers. Samples with less prominent memberships delineate transitional regimes I-IV.

tite/magnetite ratio of ~7:3 ($S_{-0.3T} = 0.956$) and slightly finer grain sizes ($M_{rs}/M_s = 0.22$ and $M_{ar}/M_{ir} = 0.064$). Coercivities ($B_c = 11$ mT and $B_{1/2}(M_{ar}) = 22.0$ mT) are moderately lower than in cluster 1. The contrasting high M_{ar}/M_{ir} and low $B_{1/2}(M_{ar})$ should best be explained by a relatively high amount of ultrafine SP material (Figure 8).

Cluster 3 characteristics prevail in the region between the equator to 6°S and 0° to 20°W. They apparently represent a combination of magnetic constituents. Together with a comparatively low hematite to magnetite ratio of ~ 3:2 ($S_{-0.3T} = 0.976$), high $M_{ar}/M_{ir} = 0.073$ indicates biogenesis of SD magnetite resulting from elevated productivity in the equatorial upwelling [*Schneider et al.*, 1996]. A low $M_{rs}/M_s = 0.26$ and reduced coercivities ($B_c = 12.1$ mT and $B_{1/2}(M_{ar}) = 24.0$ mT) hint at an additional, magnetically soft fraction. The puzzle with high M_{ar}/M_{ir} and low $B_{1/2}(M_{ar})$

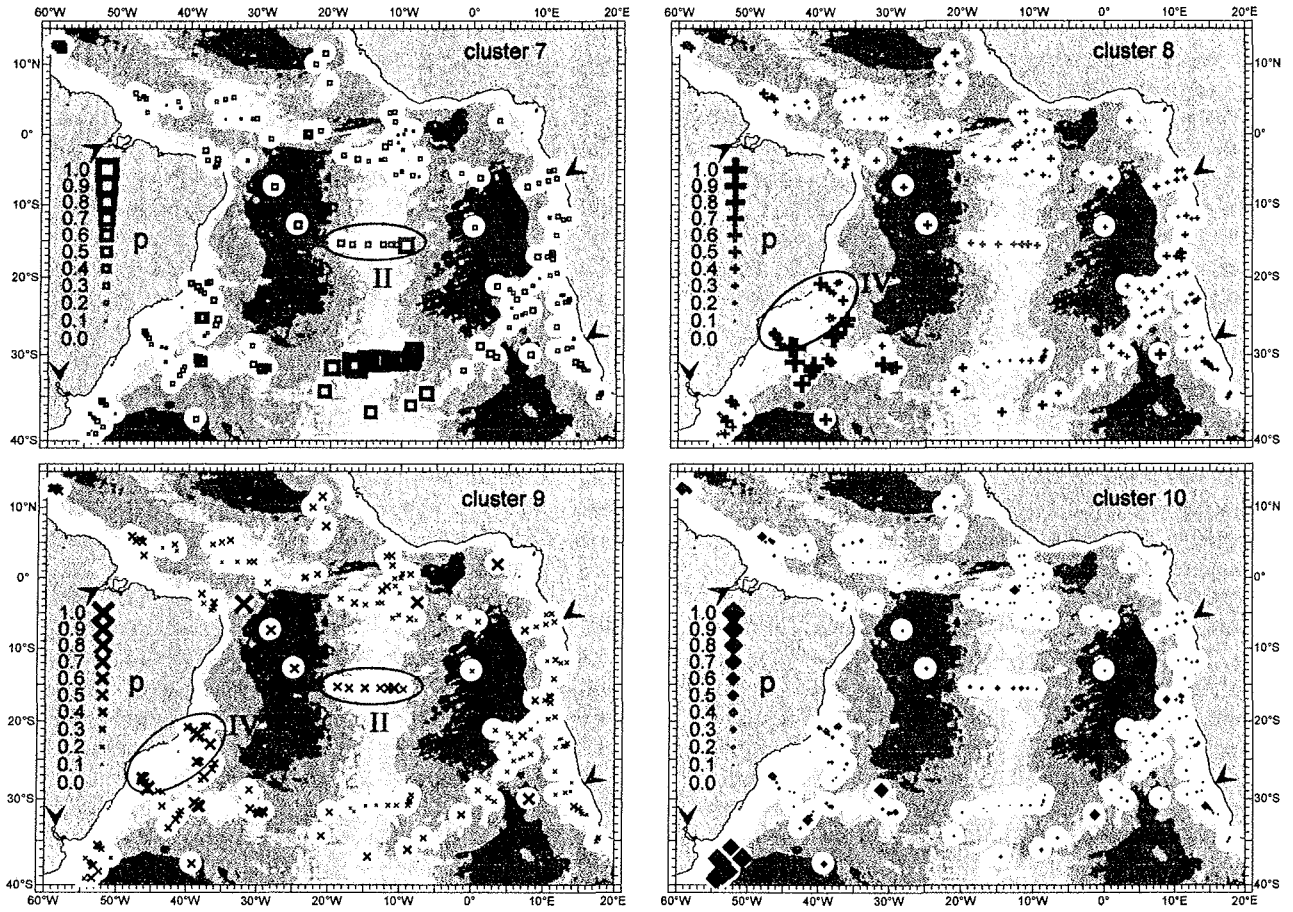

Figure 12. (continued)

resembles that of Sahel Zone-influenced cluster 2. Considering the geographical closeness of clusters 3 and 2, both sediment classes presumably receive ultrafine Sahel dust. An additional source of fine material could be the Congo Plume, which extends northward along the African coast and merges with SEC to cross the Atlantic.

Cluster 4 mainly traces the coastal areas of South America and Africa south of the equator. A dominant SD/PSD fraction ($M_{ar}/M_{ir} = 0.081$ and $M_{rs}/M_s = 0.27$), high stability of M_{ar} ($B_{1/2}(M_{ar}) = 34$ mT), and a relatively high average coercivity ($B_c = 16.3$ mT) indicate biogenic SD magnetite due to elevated near-coast productivity. This should also be true for samples from the Congo Plume and Angolan continental margin, where oceanic upwelling is related to the convergence of warm South Equatorial Countercurrent (SECC) and colder nutrient-rich Benguela Coastal Current (BCC) waters in the Angola-Benguela Front (ABF) [*Shannon et al.*, 1987]. *Petermann* [1994] detected living magnetotactic bacteria in most of these sediments, although in much lower concentrations than in the Benguela upwelling system. In view of this authigenic magnetite production an average hematite/magnetite ratio of ~7:3 ($S_{-0.3T} = 0.962$), which coincides with the major peak of the bimodal frequency distribution of $S_{-0.3T}$, implies additional continental hematite influx from the Congo and smaller African and South American rivers.

High affinities to the extreme magnetic characteristic of cluster 5 are almost entirely confined to the Benguela upwelling system. The low mean hematite/magnetite ratio of ~1:1 ($S_{-0.3T} = 0.981$) reflects a lack of continental material and an intense authigenic production of magnetite. Near-SD characteristics ($M_{rs}/M_s = 0.31$) and very high coercivities ($B_c = 21$ mT and $B_{1/2}(M_{ar}) = 40$ mT) attest to a largely biogenic origin of the magnetite fraction. In view of the fact that these M_{rs}/M_s ratios are the highest within the sample set, $M_{ar}/M_{ir} = 0.075$ is relatively low. *Cisowski* [1981] reported a reduction of M_{ar}/M_{ir} with increasing grain interactions that certainly applies to the characteristic chains of biogenic SD magnetite crystals.

Cluster 6 has a low hematite/magnetite ratio of ~1:1 ($S_{-0.3T} = 0.98$) and predominant SD magnetite properties ($M_{rs}/M_s = 0.30$ and $M_{ar}/M_{ir} = 0.086$) indicative of magnetite biomineralization on the Walvis Ridge under the distal influence of the Benguela upwelling system. Reduced coercivities ($B_c = 16.2$ mT and $B_{1/2}(M_{ar}) = 29.0$ mT) relative to cluster 5 suggest the presence of a second mineral fraction. As there is no significant hematite contribution, eolian dust transport from the African continent to the Walvis Ridge is unlikely [*Chester et al.*, 1972; *Aston et al.*, 1973]. Although the top of the Walvis Ridge is under NADW influence [*Reid*, 1989], the lack of hematite is a strong argument against a NADW parti-

cle transport. Alternatively, this fraction could be advected by AAIW, which is higher in the water column and originates partly in the South Atlantic Current (SAC) and partly in the Indian Ocean and follows the Benguela Ocean Current (BOC) across the Walvis Ridge [*Shannon and Nelson*, 1996]. Elevated memberships also occur along the Angolan and Namibian coast and in the Angola Basin north of the ABF.

Prominent memberships to cluster 7 concentrate on a 30°S MAR transect in the center of the Subtropical Gyre. The mean hematite/magnetite ratio of ~7:3 ($S_{-0.3T} = 0.964$) implies no particular hematite or magnetite enrichment. $M_{rs}/M_s = 0.28$ and $B_c = 16.3$ mT correspond to average domain states in the fine PSD range with a tendency to SD, presumably an indication of AAIW particle transport. Low $M_{ar}/M_{ir} = 0.044$, low coercivity of anhysteretic remanence ($B_{1/2}(M_{ar}) = 16.6$ mT), and constricted hysteresis loops of these samples hint at an important SP or basaltic fraction.

Samples with a high affinity to cluster 8 are concentrated in the southern Brazil Basin, on the southwestern flanks of the Vema Channel, on the southern Santos Plateau, and on the eastern flanks of the Rio Grande Rise. Similar to cluster 7, the average $S_{-0.3T}(= 0.963)$ (hematite/magnetite ~ 7:3) matches the total mean. The domain states are in the coarser PSD range ($M_{rs}/M_s = 0.23$ and $M_{ar}/M_{ir} = 0.033$). According to *Johnson* [1984], sediments deposited in the vicinity of the Vema Channel below 4000 m water depths should primarily contain suspended AABW matter. Samples collected at depths below 3500 m on the SW Santos Plateau are under the influence of the AABW/NADW transition zone. The coercivities ($B_c = 15.2$ mT and $B_{1/2}(M_{ar}) = 29.2$ mT) are slightly above the total mean and show no evidence of a SP fraction (Figure 8). This should be related to relatively high current velocities between 1.1 and 9.6 cm s^{-1} of northward flowing AABW along the western flanks of the Vema Channel [*Hogg et al.*, 1982].

Little regional grouping is observed for cluster 9. The cluster center is characterized by intermediate positions and the largest standard deviations of all parameters. Domain states in the PSD range ($M_{rs}/M_s = 0.22$ and $M_{ar}/M_{ir} = 0.045$) are in agreement with average coercivities of $B_c = 13.5$ mT and $B_{1/2}(M_{ar}) = 24.8$ mT. The lack of regionality and specific characteristics does not permit unambiguous interpretations. Some similarity to cluster 8 may indicate bottom current influence.

Magnetic attributes of cluster 10 deviate significantly from all other cluster centers. The largest parameter space distance is to cluster 5 implying that the primary magnetic particle source must be very different from the fine-grained bacterial magnetite of the Benguela upwelling region. Very "coarse" $M_{rs}/M_s = 0.10$ and $M_{ar}/M_{ir} = 0.011$ as well as a low mean coercivity $B_c = 9.7$ mT indicate predominant PSD/MD properties, most likely of La Plata detritus as proposed by *Sachs and Ellwood* [1988]. However, the coercivity of the M_{ar} carrying fraction ($B_{1/2}(M_{ar}) = 36.7$ mT) almost reaches the high mean value (39.9 mT) of SD-dominated cluster 5. As high current velocities in the western Argentine Basin should prevent the deposition of fine SD magnetite, the contradictory coercivities are believed to originate from stressed and/or nonstoichiometric volcanogenic (titano)magnetites of weathered Paraná Basin flood basalts.

A quantitative and synoptic differentiation of cluster characteristics is obtained by evaluating Euclidean distances between cluster centers in the parameter space. The results are summarized in a dissimilarity matrix (Table 2). Distances to the nearest and farthest class are marked for each cluster center. The mean distance to all other clusters is given in the last line.

A suitable method for extracting information from such high-dimensional distances is multidimensional scaling, here performed with the computer program STATISTICA (StatSoft, Inc.) using algorithms of *Kruskal* [1964] and *Guttman* [1968]. This procedure allows for the projection of multidimensional objects into a lower-dimensional space with a minimum of distortion. The data points are arranged such that an integral stress index based on the differences between observed and reproduced distances is minimized. The five-dimensional 10-cluster solution projected to the plane is shown in Figure 13. Although this visualization produces some deformation, the calculated cluster center distances (Table 2) are generally well reproduced. Yet there is no simple mathematical convertibility between this configuration and measured parameters. Physical axes were therefore omitted.

The cluster center positions delineate prevailing and com-

Table 2. Euclidean Distances Between Cluster Centers in the Five-Dimensional Parameter Space

	Cluster 1	Cluster 2	Cluster 3	Cluster 4	Cluster 5	Cluster 6	Cluster 7	Cluster 8	Cluster 9	Cluster 10
Cluster 1	0.0	1.2	2.3	2.7	4.3	3.2	2.4	2.0	1.5	3.2
Cluster 2	1.2[a]	0.0	1.2[a]	2.3	4.0	2.5	2.0	1.9	1.1	3.2
Cluster 3	2.3	1.2	0.0	1.8	3.3	1.6	1.9	1.9	1.4	3.8
Cluster 4	2.7	2.3	1.8	0.0	1.9[a]	1.1[a]	1.4[a]	1.9	2.0	4.2
Cluster 5	4.3[b]	4.0[b]	3.3	1.9	0.0	1.9	3.3	3.0[b]	3.4[b]	5.3[b]
Cluster 6	3.2	2.5	1.6	1.1[a]	1.9	0.0	2.2	2.3	2.3	4.8
Cluster 7	2.4	2.0	1.9	1.4	3.3	2.2	0.0	1.7	1.6	4.3
Cluster 8	2.0	1.9	1.9	1.9	3.0	2.3	1.7	0.0	0.9[a]	2.9[a]
Cluster 9	1.5	1.1[a]	1.4	2.0	3.4	2.3	1.6	0.9	0.0	2.9[a]
Cluster 10	3.2	3.2	3.8[b]	4.2[b]	5.3[b]	4.8[b]	4.3[b]	2.9	2.9	0.0
$\bar{D}$	2.3	1.9	1.9	1.9	3.0[b]	2.2	2.1	1.9	1.7	3.5[b]

The mean distance $\bar{D}$ to all other clusters is listed in the last line.
a Minimal distances
b Maximal distances.

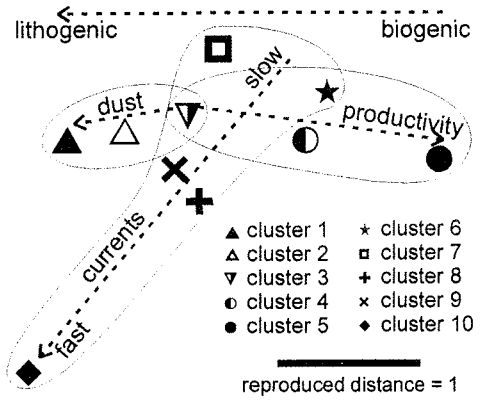

Figure 13. Relative cluster center positions after projection from the five-dimensional parameter space into the plane by multidimensional scaling. Mutual distances (Table 2) are preserved with very minor distortion. Dashed trend arrows indicate gradients of prominent common influences.

peting influences in the sedimentation areas. Clusters related to common oceanographic and sedimentological conditions are encircled. Within each of these sets a trend arrow represents the intensity gradient of the major control factors, dust fall, current strength, and productivity. The trends compose a general tendency from biogenic to lithogenic magnetic characteristics.

The two most extreme clusters represent volcanic particles deposited under high bottom current velocities off the La Plata (cluster 10) and nearly pure bacterial magnetite accumulated in the Benguela upwelling system (cluster 5). The positions of clusters 4, 6, and 3, characterizing coastal upwelling and the Congo Plume, the Walvis Ridge, and the equatorial upwelling, respectively, depict the declining importance of bacterial magnetite with increasing distance to cluster 5. The equatorial upwelling (cluster 3) additionally receives African dust. The cluster joining Saharan dust and Amazon detritus (cluster 1) is the third cornerstone of the cluster structure. Interestingly, the three major rivers, Amazon (cluster 1), Congo (cluster 4), and La Plata (cluster 10), show large mutual distances, emphasizing that there is no common magnetic signature of fluvial influx.

5. Conclusions

This environmental magnetic study illustrates how magnetic mineral inventories of surface sediments delineate Holocene particle sources, pathways, and depositional regimes in the South Atlantic Ocean. It forms a reference for regional paleoceanographic and paleoclimatic work and a guideline for analogous analyses on a global scale.

Concentration dependent magnetic parameters like susceptibility primarily reflect calcareous and/or siliceous major sediment component variability controlled by productivity and dissolution. Elevated susceptibilities prevail in most coastal areas documenting terrigeneous sedimentation of ferrimagnetic, antiferromagnetic, and paramagnetic minerals. In the open ocean, high values are characteristic for deep basins below the CCD. Concentrations of "magnetic" and "nonmagnetic" iron minerals are clearly correlated, implying that generally, both have a common lithogenic origin. Significant fractions of biogenic magnetite in high-productivity regions may cause a deviation from this trend.

Hematite is ubiquitous and the absolutely dominant magnetic mineral in the western South Atlantic. The $S_{-0.3T}$ parameter also indicates hematite/magnetite mixing ratios > 4:1 in a tropical belt at ~5°N combining eolian Saharan and fluvial Amazonian hematite. High hematite contents at most continental margins correspond to an enhanced terrigeneous influx.

Magnetite grain sizes systematically increase from east to west. In highly productive eastern areas the abundance of magnetofossils and a fine-grained particle discharge by the Congo River account for predominant SD/PSD properties. South American rivers supply coarser-grained magnetite in the PSD/MD size range. Origin, transport, and deposition of the ultrafine-grained SP fraction is mostly unrelated to that of SD to MD size components. Except for central equatorial sites, where SP magnetite markedly reduces the magnetite stability, mean coercivity complies entirely with grain size.

A statistical classification with fuzzy cluster analysis, applied to five concentration independent magnetic parameters, discerned ten clusters, with a single exception clearly related to particular regions and environments.

Our results support and extend available broad-scale information on Holocene sedimentation of magnetic minerals in the South Atlantic [*Balsam and McCoy*, 1987]. A hematite distribution map by *Balsam and Otto-Bliesner* [1995], derived from factor analysis of color reflectance, largely agrees with our $S_{-0.3T}$ results, which also correspond to dust collection data from the African continent [*Chester et al.*, 1972; *Aston et al.*, 1973; *Glaccum and Prospero*, 1980]. Some disagreement arises from biogenic magnetite accumulation in highly productive areas, shifting the hematite/magnetite ratio and therefore masking elevated hematite contents. *Petschick et al.* [1996] described recent South Atlantic clay mineral provinces, sources, and transport patterns that generally conform with our magnetic analyses, although a proposed NADW influence as far south as 40°S and a modern southwest African terrigenous influx are not discernible in the present data set.

Acknowledgments. We thank J. Bloemendal and two anonymous reviewers for valuable suggestions for improving the manuscript. Financial support was provided by the Deutsche Forschungsgemeinschaft (Sonderforschungsbereich 261 at Bremen University, contribution 274).

References

Aston, S. R., R. Chester, L. R. Johnson, and R. C. Padgham, Eolian dust from the lower atmosphere of the eastern Atlantic and Indian Oceans, China Sea and Sea of Japan, *Mar. Geol.*, *14*, 15-28, 1973.

Balsam, W. L., and F. W. McCoy Jr., Atlantic sediments: Glacial/interglacial comparisons, *Paleoceanography*, *2*, 531-542, 1987.

Balsam, W. L., and B. L. Otto-Bliesner, Modern and Last Glacial Maximum eolian sedimentation patterns in the Atlantic Ocean interpreted from sediment iron oxide content, *Paleoceanography*, *10*, 493-507, 1995.

Banerjee, S. K., J. King, and J. Marvin, A rapid method of magnetic granulometry with applica-

tions to environmental studies, *Geophys. Res. Lett.*, *8*, 333-336, 1981.

Bean, C. P., and J. D. Livingston, Superparamagnetism, *J. Appl. Phys.*, *30*, 1205-1295, 1959.

Bezdek, J. C., Fuzzy mathematics in pattern classification, Ph.D. thesis, Cornell Univ., Ithaca, N. Y., 1973.

Bezdek, J. C., *Pattern Recognition With Fuzzy Objective Function Algorithms*, 256 pp., Plenum, New York, 1981.

Bezdek, J. C., and J. C. Dunn, Optimal fuzzy partitions: A heuristic for estimating the parameters in a mixture of normal distributions, *IEEE Trans. Comp., C24*, 835-838, 1975.

Bloemendal, J., B. Lamb, and J. King, Paleoenvironmental implications of rock-magnetic properties of late Quaternary sediment cores from the eastern equatorial Atlantic, *Paleoceanography*, *3*, 61-87, 1988.

Bloemendal, J., J. W. King, F. R. Hall, and S. J. Doh, Rock magnetism of late Neogene and Pleistocene deep-sea sediments: Relationship to sediment source, diagenetic processes, and sediment lithology, *J. Geophys. Res.*, *97*, 4361-4375, 1992.

Bornhold, B. D., and C. P. Summerhayes, Scour and deposition at the foot of the Walvis Ridge in the northernmost Cape Basin, South Atlantic, *Deep Sea Res.*, *24*, 743-752, 1977.

Butler, R. F., and S. K. Banerjee, Theoretical single-domain grain-size range in magnetite and titanomagnetite, *J. Geophys. Res.*, *80*, 4049-4058, 1975.

Chester, R., H. Elderfield, J. J. Griffin, L. R. Johnson, and R. C. Padgham, Eolian dust along the eastern margins of the Atlantic Ocean, *Mar. Geol.*, *13*, 91-105, 1972.

Cisowski, S., Interacting vs. non-interacting single domain behavior in natural and synthetic samples, *Phys. Earth Planet. Inter.*, *26*, 56-62, 1981.

Clapperton, C., *Quaternary Geology and Geomorphology of South America*, 779 pp., Elsevier, New York, 1993.

Däumler, K., Diagenetische Auflösung von biogenem Magnetit, M.S. thesis, Fachbereich Geowissenschaften, Univ. Bremen, Bremen, Germany, 1996.

Davis, J.C., *Statistics and Data Analysis in Geology*, 646 pp., John Wiley, New York, 1986.

Day, R., M. Fuller, and V. A. Schmidt, Hysteresis properties of titanomagnetites: Grain-size and compositional dependence, *Phys. Earth Planet. Inter.*, *13*, 260-267, 1977.

Dearing, J. A., R. J. L. Dann, K. Hay, J. A. Lees, P. J. Loveland, B. A. Maher, and K. O'Grady, Frequency-dependent susceptibility of environmental materials, *Geophys. J. Int.*, *124*, 228-240, 1996a.

Dearing, J. A., K. L. Hay, S. M. J. Baban, A. S. Huddleston, E. M. H. Wellington, and P. J. Loveland, Magnetic susceptibility of soil: An evaluation of conflicting theories using a national data set, *Geophys. J. Int.*, *127*, 728-734, 1996b.

Dekkers, M. J., C. G. Langereis, S. P. Vriend, P. J. M. van Santvoort, and G. J. de Lange, Fuzzy c-means cluster analysis of early diagenetic effects on natural remanent magnetisation acquisition in a 1.1 Myr piston core from the central Mediterranean, *Phys. Earth Planet. Inter.*, *85*, 155-171, 1994.

deMenocal, P. B., W. F. Ruddiman, and D. V. Kent, Depth of post-depositional remanence acquisition in deep-sea sediments: A case study of the Brunhes-Matuyama reversal and oxygen isotopic Stage 19.1, *Earth Planet. Sci. Lett.*, *99*, 1-13, 1990.

Deutsch, E. R., R. R. Pätzold, and C. Radhakrishnamurty, Apparent superparamagnetic behavior of some coarse-grained synthetic titanomagnetite, *Phys. Earth Planet. Inter.*, *26*, 27-36, 1981.

Dunlop, D. J., Superparamagnetic and SD threshold sizes in magnetite, *J. Geophys. Res.*, *78*, 1780-1793, 1973.

Dunlop, D. J., and M. M. Bina, The coercive force spectrum of magnetite at high temperatures: Evidence for thermal activation below the blocking temperature, *Geophys. J. R. Astron. Soc.*, *51*, 121-147, 1977.

Dunlop, D. J., and Ö. Özdemir, *Rock Magnetism: Fundamentals and Frontiers*, 573 pp., Cambridge Univ. Press, New York, 1997.

Eisma, D., and A. J. van Bennekom, The Zaire River and estuary and the Zaire outflow in the Atlantic Ocean, *Neth. J. Sea Res.*, *12*, 255-272, 1978.

Flanders, P. J., An alternating-gradient magnetometer, *J. Appl. Phys.*, *63*, 3940-3945, 1988.

Frapporti, G., S. P. Vriend, and P. F. M. van Gaans, Hydrogeochemistry of the shallow Dutch groundwater: Interpretation of the national groundwater quality monitoring network, *Water Resour. Res.*, *29*, 2993-3004, 1993.

Frederichs, T., U. Bleil, K. Däumler, T. von Dobeneck, and A. Schmidt, The magnetic view on the marine paleoinvironment: Parameters, techniques, and potentials of rock magnetic studies as a key to paleoclimatic and paleoceanographic changes, in *Use of Proxies in Paleoceanography: Examples From the South Atlantic*, edited by G. Fischer and G. Wefer, Springer, Berlin, in press, 1999 .

Gee, J., and D. V. Kent, Magnetic hysteresis in young mid-ocean ridge basalts: Dominant cubic anisotropy?, *Geophys. Res. Lett.*, *22*, 551-554, 1995.

Glaccum, R. A. and J. M. Prospero, Saharan aerosols over the tropical north Atlantic - Mineralogy, *Mar. Geol.*, *37*, 295-321, 1980.

Glud, R. N., J. K. Gundersen, B. B. Jørgensen, N. P. Revsbech, and H. D. Schulz, Diffuse and total oxygen uptake of deep-sea sediments in the eastern South Atlantic Ocean: in situ and laboratory measurements, *Deep Sea Res., Part I*, *41*, 1767-1788, 1994.

Guttman, L., A general nonmetric technique for finding the smallest coordinate space for a configuration of points, *Pyrometrical*, *33*, 469-506, 1968.

Heider, F., A. Zitzelsberger, and K. Fabian, Magnetic susceptibility and remanent coercive force in grown magnetite crystals from 0.1 μm to 6 mm, *Phys. Earth Planet. Inter.*, *93*, 239-256, 1995.

Heller, F., Rock magnetic studies of Upper Jurassic limestones from southern Germany, *J. Geophys.*, *44*, 525-543, 1978.

Hogg, N. G., P. Biscaye, W. Gardner, and W. J. Schmitz Jr., On the transport and modification of Antarctic Bottom Water in the Vema Channel, *J. Mar. Res.*, *40*, *suppl.*, 231-263, 1982.

Holeman, J. N., The sediment yield of major rivers of the world, *Water Res.*, *4*, 737-747, 1968.

Hyodo, M., Possibility of reconstruction of the past geomagnetic field from homogeneous sediments, *J. Geomgn. Geoelectr.*, *36*, 45-62, 1984.

Jackson, M., Diagenetic source of stable remanence in remagnetized Paleozoic cratonic carbonates: A rock magnetic study, *J. Geophys. Res.*, *95*, 2753-2762, 1990.

Jackson, M., W. Gruber, J. Marvin, and S. K. Banerjee, Partial anhysteretic remanence and its anisotropy: Applications and grainsize dependence, *Geophys. Res. Lett.*, *15*, 440-443, 1988.

Joffe, I., and J. Heuberger, Hysteresis properties of distributions of cubic single-domain ferromagnetic particles, *Philos. Mag.*, *29*, 1051-1059, 1974.

Johnson, D. A., Regional oceanographic setting of the southwestern Atlantic, *Initial Rep. Deep Sea Drill. Proj.*, *72*, 15-35, 1983.

Johnson, D. A., The Vema Channel: Physiography, structure, and sediment - current interactions, *Mar. Geol.*, *58*, 1-34, 1984.

Karlin, R., Magnetite diagenesis in marine sediments from the Oregon continental margin, *J. Geophys. Res.*, *95*, 4405-4419, 1990.

Karlin, R., and S. Levi, Diagenesis of magnetic minerals in recent haemipelagic sediments, *Nature*, *303*, 327-330, 1983.

King, J. W., and J. E. T. Channell, Sedimentary magnetism, environmental magnetism, and magnetostratigraphy, *Rev. Geophys.*, *29*, 358-370, 1991.

King, J., S. K. Banerjee, J. Marvin, and Ö. Özdemir, A comparison of different magnetic methods for determining the relative grain-size of magnetite in natural materials: Some results from lake sediments, *Earth Planet. Sci. Lett.*, *59*, 404-419, 1982.

Kobayashi, K., and M. Nomura, Ferromagnetic minerals in the sediment cores collected from the Pacific Basin, *J. Geophys.*, *40*, 501-512, 1974.

Kruskal, J. B., Nonmetric multidimensional scaling: A numerical method, *Pyrometrical*, *29*, 1-27, 115-129, 1964.

Ledbetter, M. T., Bottom-current pathways in the Argentine Basin revealed by mean silt particle size, *Nature*, *321*, 423-425, 1986.

Leslie, B. W., S. P. Lund, and D. E. Hammond, Rock magnetic evidence for the dissolution and authigenic growth of magnetic minerals within anoxic marine sediments of the California continental borderland, *J. Geophys. Res.*, *95*, 4437-4452, 1990a.

Leslie, B. W., D. E. Hammond, W. M. Berelson, and S. P. Lund, Diagenesis in anoxic sediments from the California continental borderland and its influence on iron, sulfur, and magnetite behavior, *J. Geophys. Res.* *95*, 4453-4470, 1990b.

Løvlie, R., Magnetization of sediments and depositional environment, in *Geomagnetism and Paleomagnetism*, edited by F. J. Lowes et al., pp. 243-252, Kluwer Acad., Norwell, Mass., 1989.

Løvlie, R., Field-dependent postdepositional grain realignment in the PDRM process: Experimental evidence and implications, *Phys. Earth Planet. Inter.*, *85*, 101-111, 1994.

Lund, S. P., and R. Karlin, Introduction to the special section on physical and biogeochemical processes responsible for the magnetization of sediments, *J. Geophys. Res.*, *95*, 4353-4354, 1990.

Maher, B., Magnetic properties of some synthetic sub-micron magnetites, *Geophys. J. Int.*, *94*, 83-96, 1988.

Melguen, M., and J. Thiede, Facies distribution and dissolution depths of surface sediment components from the Vema Channel and the Rio Grande Rise (southwest Atlantic Ocean), *Mar. Geol.*, *17*, 341-353, 1974.

Middleburgh, J. J., and G. J. de Lange, Geochemical characteristics as indicators of the provenance of Madeira abyssal plain turbidites: A statistical approach, *Oceanol. Acta*, *11*, 159-165, 1988.

Milliman, J. D., and R. H. Meade, World-wide delivery of river sediment to the oceans, *J. Geol.*, *91*, 1-21, 1983.

Muller-Karger, F., C. R. McClain, and P. L. Richardson, The dispersal of the Amazon's water, *Nature*, *333*, 56-59, 1988.

Mullins, C. E., and M. S. Tite, Magnetic viscosity, quadrature susceptibility and frequency dependence of susceptibility in single-domain assemblies of magnetite and maghemite, *J. Geophys. Res.*, *78*, 804-809, 1973.

Oldfield, F., Environmental magnetism: A

personal perspective, *Quat. Sci. Rev., 10*, 73-85, 1991.

Özdemir, Ö., and S. K. Banerjee, A preliminary magnetic study of soil samples from west-central Minnesota, *Earth Planet. Sci. Lett., 59*, 393-403, 1982.

Özdemir, Ö., and D. J. Dunlop, Single-domain-like behavior in a 3-mm natural single crystal of magnetite, *J. Geophys. Res., 103*, 2549-2562, 1998.

Özdemir, Ö., S. Xu, and D. J. Dunlop, Closure domains in magnetite, *J. Geophys. Res., 100*, 2193-2209, 1995.

Pak, H., J. R. V. Zanefeld, and R. W. Spinrad, Vertical distribution of suspended particular matter in the Zaire river, estuary and plume, *Neth. J. Sea Res., 17*, 412-425, 1984.

Parry, L. G., Magnetic properties of dispersed magnetite powders, *Philos. Mag., 11*, 303-312, 1965.

Petermann, H., Magnetotaktische Bakterien und ihre Magnetosome in Oberflächensedimenten des Südatlantiks, Ph.D. thesis, Fachbereich Geowissenschaften, Univ. Bremen, Bremen, Germany, 1994.

Petermann, H., and U. Bleil; Detection of live magnetotactic bacteria in South Atlantic deep-sea sediments, *Earth Planet. Sci. Lett., 117*, 223-228, 1993.

Peters, J. J., Discharge and sand transport in the braided zone of the Zaire estuary, *Neth. J. Sea Res., 12*, 273-292, 1978.

Petersen, N., T., von Dobeneck, and H. Vali, Fossil bacterial magnetite in deep-sea sediments from the South Atlantic Ocean, *Nature, 320*, 611-615, 1986.

Peterson, R. G., and L. Stramma, Upper-level circulation in the South Atlantic Ocean, *Prog. Oceanogr.*, 26, 1-73, 1991.

Petschick, R., G. Kuhn, and F. Gingele, Clay mineral distribution in surface sediments of the South Atlantic: Sources, transport and relation to oceanography, *Mar. Geol., 130*, 203-229, 1996.

Pick, T., and L. Tauxe, Characteristics of magnetite in submarine basaltic glass, *Geophys. J. Int., 119*, 116-128, 1994.

Pye, K., *Eolian Dust and Dust Deposits*, 334 pp., Academic, San Diego, Calif., 1987.

Quidelleur, X., J.-P. Valet, M. LeGoff, and X. Bouldoire, Field dependence on magnetization of laboratory-redeposited deep-sea sediments: First results. *Earth Planet. Inter., 133*, 311-325, 1995.

Radhakrishnamurty, C., S. D. Likhite, E. R. Deutsch, and G. S. Murthy, A comparison of the magnetic properties of synthetic titanomagnetites and basalts, *Phys. Earth Planet. Inter., 26*, 37-46, 1981.

Reid, J. L., On the total geostrophic circulation of the South Atlantic Ocean: Flow patterns, tracers and transports, *Prog. Oceanogr., 23*, 149-244, 1989.

Reid, J. L., On the circulation of the South Atlantic Ocean, in *The South Atlantic: Present and Past Circulation*, edited by G. Wefer et al., pp. 13-44, Springer, New York, 1996.

Robinson, S. G., The late Pleistocene paleoclimatic record of North Atlantic deep-sea sediments revealed by mineral-magnetic measurements, *Phys. Earth Planet. Inter., 42*, 22-47, 1986.

Sachs, S. D., and B. B. Ellwood, Controls on magnetic grain-size variations and concentration in the Argentine Basin, South Atlantic Ocean, *Deep Sea Res., Part A, 35*, 929-942, 1988.

Schmidt, A. M., Gesteinsmagnetische Analyse und Kartierung rezenter Sedimentationsräume im Südatlantik, M.S. thesis, Fachbereich Geowissenschaften, Univ. Bremen, Bremen, Germany, 1995.

Schneider, R. R., P. J. Müller, G. Ruhland, G. Meinecke, H. Schmidt, and G. Wefer, Late Quaternary surface temperatures and productivity in the east-equatorial South Atlantic: Response to changes in trade/monsoon wind forcing and surface water advection, in *The South Atlantic: Present and Past Circulation*, edited by G. Wefer et al., pp. 527-551, Springer, New York, 1996.

Schulz, H. D., et al., Report and preliminary results of *Meteor* cruise M34/2, *report*, 167 pp., Fachbereich Geowissenschaften, Univ. Bremen, Bremen, Germany, 1996.

Schwertmann, U., and N. Kämpf, Properties of goethite and hematite in kaolinitic soils of southern and central Brazil, *Soil Sci., 139*, 344-350, 1985.

Shannon, L. V., and G. Nelson, The Benguela: Large scale features and processes and system variability, in *The South Atlantic: Present and Past Circulation*, edited by G. Wefer et al., pp. 163-210, Springer, New York, 1996.

Shannon, L. V., J. J. Agenbag, and M. E. L. Buys, Large- and mesoscale features of the Angola-Benguela Front, *S. Afr. J. Mar. Sci., 5*, 11-34, 1987.

Stephenson, A., Single-domain grain-size distribution, I, A method for the determination of single-domain grain distributions, *Phys. Earth Planet. Inter., 4*, 353-360, 1971.

Stober, J. C., and R. Thompson, Magnetic remanence acquisition in Finnish lake sediments, *Geophys. J. R. Astron. Soc., 57*, 727-739, 1979.

Stoner, E. C., and E. P. Wohlfahrt, A mechanism of magnetic hysteresis in heterogeneous alloys, *Philos. Trans. R. Soc. London, Ser. A, 240*, 599-642, 1948.

Talley, L. D., Antarctic Intermediate Water in the South Atlantic, in *The South Atlantic: Present and Past Circulation*, edited by G. Wefer et al., pp. 219-238, Springer, New York, 1996.

Tarduno, J. A., Temporal trends of magnetic dissolution in the pelagic realm: Gauging paleoproductivity?, *Earth Planet. Sci. Lett., 123*, 39-48, 1994.

Tarduno, J. A., Superparamagnetism and reduction diagenesis in pelagic sediments: Enhancement or depletion?, *Geophys. Res. Lett., 22*, 1337-1340, 1995.

Tarduno, J. A., and S. L. Wilkinson, Non-steady state magnetic mineral reduction, chemical lock-in, and delayed remanence acquisition in pelagic sediments, *Earth Planet. Sci. Lett., 144*, 315-326, 1996.

Tauxe, L., T. A. T. Mullender, and T. Pick, Potbellies, wasp-waists, and superparamagnetism in magnetic hysteresis, *J. Geophys. Res., 101*, 571-583, 1996.

Thompson, R., and F. Oldfield, *Environmental Magnetism*, 227 pp., Allen and Unwin, Winchester, Mass., 1986.

Thompson, R., J. Bloemendal, J. A. Dearing, F. Oldfield, T. A. Rummery, J. C. Stober, and G. M. Turner, Environmental applications of magnetic measurements, *Science, 207*, 481-486, 1980.

Verosub, K. L., and A. P. Roberts, Environmental magnetism: Past, present and future, *J. Geophys. Res., 100*, 2175-2192, 1995.

von Dobeneck, T., A systematic analysis of natural magnetic mineral assemblages based on modeling hysteresis loops with coercivity-related hyperbolic basis functions, *Geophys. J. Int., 124*, 675-694, 1996.

Wasilewski, P. J., Magnetic hysteresis in natural materials, *Earth Planet. Sci. Lett., 20*, 67-72, 1973.

Westerhausen, L., J. Poynter, G. Eglinton, H. Erlenkeuser, and M. Sarnthein, Marine and terrigeneous origin of organic matter in modern sediments of the equatorial east Atlantic: The d13C and molecular record, *Deep Sea Res., Part I, 40*, 1087-1121, 1993.

Yamazaki, T., Thickness of the lock-in zone of post-depositional remanent magnetization in deep-sea siliceous clay, *Rock Magn. Paleogeophys., 11*, 85-90, 1984.

Zadeh, L. A., Fuzzy sets, *Inf. Control., 8*, 338-353, 1965.

U. Bleil, A.M. Schmidt, and T. von Dobeneck, Fachbereich Geowissenschaften, Universität Bremen, Postfach 330440, 28334 Bremen, Germany. (aschmidt@geomarin.uni-bremen.de)

(Received October 8, 1998;
revised February 25,1999;
accepted March 30, 1999.)

Monitoring Termination II by environmental magnetic records from subtropical South Atlantic sediments

Andrea M. Schmidt

Fachbereich Geowissenschaften, Universität Bremen, Bremen, Germany

Abstract. Termination II, the transition from oxygen isotope substage 6.2 to 5.5 around 130 ka is the penultimate drastic change from extreme glacial to interglacial climatic conditions, invoking shifts in terrigenous and biogenous influx and deep ocean currents. Environmental magnetic methods are applied to reveal these shifts in an ocean-spanning W-E gravity core transect in an oceanographic key region, the subtropical South Atlantic. Rock magnetic parameters like magnetic mineralogy, grain size, and coercivity reflect intensified eolian inflow of volcanogenic material from the Andes due to enhanced continental aridity and wind intensity during substage 6.2. An African dust supply is only observable in continental vicinity. On the Santos Plateau magnetic attributes indicate fluvial influx of eroded flood basalts. Layers of reductive magnetic mineral diagenesis were identified only in westernmost cores and appears to reflect paleoredox boundaries related to enhanced C_{org} deposition at the termination and stage 5.5. In all unaltered sections, stage 5.5 is magnetically similar to the Holocene.

1. Introduction

Climatic changes during major deglaciation periods or terminations [*Broecker*, 1984] are an important issue of current paleoceanographic and paleoenvironmental research [e.g., *Bauch*, 1996; *Oppo et al.*, 1997; *Broecker and Henderson*, 1998]. The recent completion of the Vostok drilling in East Antarctica now extends the southern hemisphere ice record to the past four glacial/interglacial cycles [*Petit et al.*, 1999]. Its dust component indicates that during glacial climates continental aridity and particle mobilization and transport were enhanced due to a more turbulent atmospheric circulation at southern latitudes. Especially Termination II, the rapid climate transition between marine isotope substage 6.2 and 5.5, arouses special interest as it may represent a climatic analogue to Termination I, the deglaciation towards the present Holocene interglacial [e.g., *Kellogg*, 1980]. *Clapperton* [1993] reported a more humid climate on the South American continent during substage 5.5 compared to the preceding glacial. *Oppo et al.* [1997] found that in the North Atlantic winter sea surface temperatures were 2-3 °C above present values by the middle of 5.5. Numerous studies have shown that oceanic circulation patterns largely changed in the course of the 6.2 to 5.5 deglaciation due to enhanced interglacial North Atlantic Deep Water (NADW) production [e.g., *Duplessy and Shackleton*, 1985; *Oppo et al.*, 1997; *Broecker and Henderson*, 1998]. *Schmiedl and Mackensen* [1997] and *Broecker and Henderson* [1998] described elevated glacial productivity related to intensified upwelling in the eastern South Atlantic.

Environmental magnetic methods, introduced by *Thompson et al.* [1980] and *Thompson and Oldfield* [1986], investigate sedimentary assemblages of magnetic iron minerals as paleoenvironmental archives. Their distinct lithogenic, authigenic or biogenic (biominerali-

zation by magnetotactic bacteria) origin and accumulation are mirrored in rock magnetic mineralogy, grain size (more precisely, domain recent reviews [e.g., *Lund and Karlin*, 1990; *King and Channell*, 1991; *Oldfield*, 1991; *Verosub and Roberts*, 1995] document, their usability as climatic proxies has been repeatedly demonstrated. *Frederichs et al.* [1999] and *von Dobeneck and Schmieder* [1999] discuss specific environmental methods and applications in paleoceanography. *Schmidt et al.* [1999] established systematic sediment classifications for the Holocene South Atlantic based on a multivariate environmental magnetic approach. This study delineates glacial/interglacial changes in magnetic mineral sources and transport media across Termination II for a paleoceanographic key region of the subtropical South Atlantic.

2. Study area and core locations

The 8 gravity cores selected for this investigation (Figure 1), GeoB 1034-3 [*Wefer et al.*, 1988], GeoB 1211-3 [*Wefer et al.*, 1990], GeoB 1313-2 [*Pätzold et al.*, 1993], GeoB 1729-3 [*Schulz et al.*, 1992], GeoB 2109-1 and 2110-4 [*Bleil et al.*, 1993], GeoB 2821-1 [*Bleil et al.*, 1994], and GeoB 3805-3 [*Wefer et al.*, 1996] were recovered during several R/V *Meteor* cruises. They form an West-East transect over the oligotrophic South Atlantic between 20 and 32°S crossing the deep water barriers Rio Grande Rise, mid-Atlantic Ridge, and Walvis Ridge. The water depths at the core sites range between 2504 and 4401 m. The study area is a prime region to trace glacial/interglacial variations in the extent of northern and southern deep water masses. [Zitat(e)?] Circumpolar Deep Water (CPDW) and North Atlantic Deep Water (NADW) drive the modern abyssal circulation in the South Atlantic. Lower CPDW fills the deep Cape Basin below 4000 m [*Witworth and Nowlin*, 1987]. In the West, below 4000 m water depth, southern source bottom water flows northwards through the Vema and Hunter channels and along the lower Santos Plateau [e.g., *Johnson*, 1983]. At odds with this general assumption, *Hogg* [1996] reported Antarctic Bottom Water (AABW) up to 3000 m water depth from direct current measurements in this area. Southward flowing NADW takes up the depth range from 4000 to 2000 m in the West and to 1200 m in the East. North of the Walvis Ridge also the deepest parts of the Angola Basin are filled with NADW [*Diekmann et al.*, 1996]. These water bodies are overlain by southern source Upper Circumpolar Water (UCPW) and Antarctic Intermediate Water (AAIW) forming by injection of Falkland Current [*Talley*, 1996], Benguela Ocean Current (BOC), and Brazil Current (BC) [*Peterson and Stramma*, 1991] surface waters into the subtropical gyre.

The $\delta^{13}C$ signal and faunal fluctuations of benthic foraminifera [e.g., *Schmiedl and Mackensen*, 1997] suggest, that during glacials NADW production weakened, resulting in a shallowing and northward retreat of NADW. This diminished NADW injection to the Southern Ocean was attended by a decreasing generation of southern source bottom water compared to interglacial conditions. In the Vema Channel area, grain size data imply a more vigorous AABW passage during interglacials [*Ledbetter*, 1984; *Ledbetter*, 1986].

The South American Rio de la Plata and Rio Doce and the Southwest African Orange rivers are the main fluvial suppliers of continental detritus to the South Atlantic between about 20 and 40°S. *Gingele et al.* [1999] recently described the glacial/

Termination II

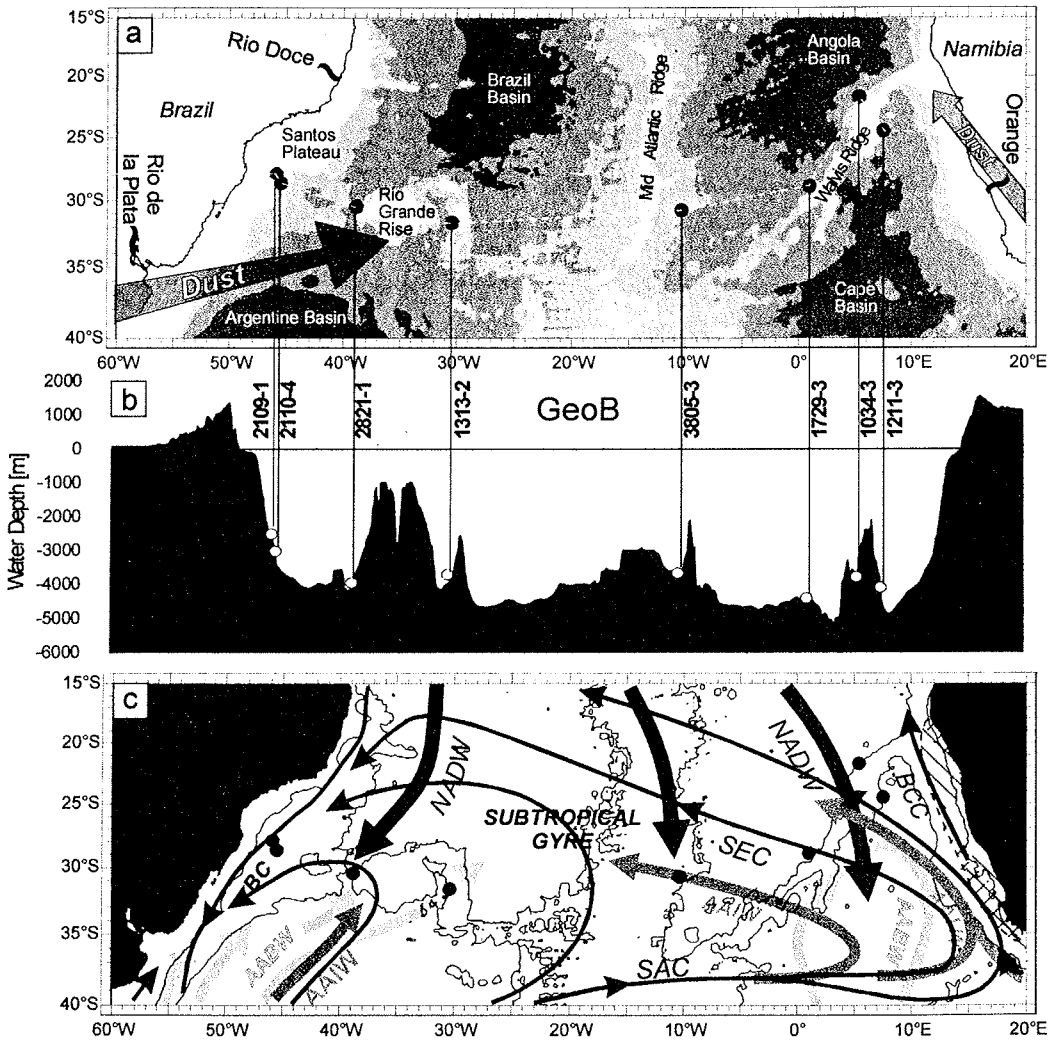

Fig. 1. (**a**) Bathymetry of the subtropical South Atlantic and locations of the eight core sites investigated (black dots). Rio de la Plata, Rio Doce, and Orange River are the major rivers to the subtropical South Atlantic. The main sources of dust are the Patagonian plain [*Clapperton*, 1993] and the arid regions of southern Africa [*Pye*, 1987]. Dust trajectory from southern Africa with the southeastern trades primarily follows the coast up to 20°S [*Prospero*, 1981]. The white line marks the course of the relief plot shown in (**b**). (**c**) Major Holocene current systems. Surface currents (black arrows): South Atlantic Current (SAC), Benguela Coastal Current (BCC), Brazil Current (BC). Deep water currents (light gray arrows): North Atlantic Deep Water (NADW), Antarctic Intermediate Water (AAIW), Antarctic Bottom Water (AABW). The high productive Benguela upwelling system. Modified after *Shannon and Nelson* [1996], *Talley* [1996], *Peterson and Stramma* [1991] and *Reid* [1996].

interglacial variability of the Rio Doce input on basis of kaolinite/chlorite ratios of a core collection including GeoB 2110-4 and 2821-1 of the present study.

Most cores consist of foraminiferal or nannofossil oozes deposited under oxic conditions. Their locations in water depths around the CCD should be most appropriate to resolve changes in deep water advection. Pore water analyses gave no indications of reductive diagenesis except for the continental slope sites GeoB 2109-1 and 2110-4 on the lower Santos Plateau. Specifically in core 2110-4 some concretions of iron oxides and hydroxides at about Termination I indicate a suboxic milieu. The Namibian continental slope was excluded from this study, because porewater

profiles [*Wefer et al.*, 1988] and magnetic analyses [*Hilgenfeldt*, 1999] indicate a strong diagenetic alteration of the sediments due to the enhanced deposition of organic matter from the high productive Benguela upwelling system.

3. Chronostratigraphy

Oxygen isotope stratigraphies based on SPECMAP correlations [*Imbrie et al.*, 1984] have been developed for 4 of the cores, GeoB 1034-3 and 1211-3 [*Bickert and Wefer*, 1996], 2109-1 [*Dürkoop*, 1998], and 2110-4 [*Gingele et al.*, 1999] (Figure 2). Cores GeoB 2821-1 and 1729-3 are part of the SUSAS (SUbtropical South Atlantic Susceptibility) stack [*von Dobeneck and Schmieder*, 1999; *Schmieder*, 1999] dated by orbital tuning of their magnetic susceptibility records. The susceptibility logs of cores GeoB 1313-2 and 3805-3 perfectly match this stack and were dated by graphical correlation.

Termination II is assumed at 128 ka [*Raymo*, 1997], the marine isotope substages 5.5 at 122 ka and 6.2 at 135 ka, respectively [*Imbrie et al.*, 1984; *Martinson et al.*, 1987]. To fully cover both substages, the age interval from 145 ka (stage 6.3) to 110 ka (stage 5.4) has been analyzed in all cores. To obtain representative data for substages 5.5 and 6.2 arithmetic means were calculated for all parameters over the time intervals 120-124 ka and 133-137 ka. Holocene data sets were derived from surface sediment samples for comparison.

4. Methods

4.1 Samples

Gravity cores GeoB 1729-3, 2109-1 and 2110-4 were subsampled at 2-3 cm, all other cores at 5 cm intervals with 6.2 cm^3 plastic cubes suitable for measurements of susceptibility and laboratory imparted remanent magnetizations. For hysteresis analysis sampling resolution was increased to 1-2 cm using miniature samples (< 50 mg) prepared as described by *von Dobeneck* [1996]. Additional samples were taken at core depths attributed to oxygen isotope substages 5.5 and 6.2 for thermal demagnetization experiments. Surface sediment samples have been retrieved with multicorer or boxcorer devices at all coring sites.

4.2 Rock magnetic parameters

Magnetic susceptibility κ, a largely grain size independent [*Heider et al.*, 1995] measure of magnetic mineral concentration, was determined with a Bartington Instruments MS2 spot sensor at 1 cm spacing on split core halves. Mass specific magnetic susceptibility χ referring to dry sediment density was measured on cube samples using a Geofyzika Kappabridge KLY-2. The frequency dependence of susceptibility $\kappa_{fd\%}$ [*Stephenson*, 1971; *Mullins and Tite*, 1973; *Maher*, 1988; *Dearing et al.*, 1996], determined with a Bartington single sample sensor, provides an estimate of relative amounts of ultrafine, superparamagnetic (SP) magnetite ($\leq$ 0.03 μm [*Dunlop and Bina*, 1977]).

Isothermal remanent magnetizations (M_{ir}), imparted in a 300 mT pulsed field, and anhysteretic remanences (M_{ar}) acquired in 300 mT alternating and 40 μT bias fields, were measured on a Molspin spinner magnetometer and a 2G Enterprises cryogenic magnetometer, respectively. As M_{ar} is characterized by a more pronounced grain size dependence than M_{ir} with focus on the single-domain (SD, magnetite: 0.03 μm < ∅ < 0.1 μm [*Dunlop*, 1973; *Butler and Banerjee*, 1975]) and pseudo-single-domain (PSD, magnetite: 0.1 μm < ∅ < ~5-10 μm [*Parry*, 1965]) fractions, the M_{ar}/M_{ir} ratio assesses fine

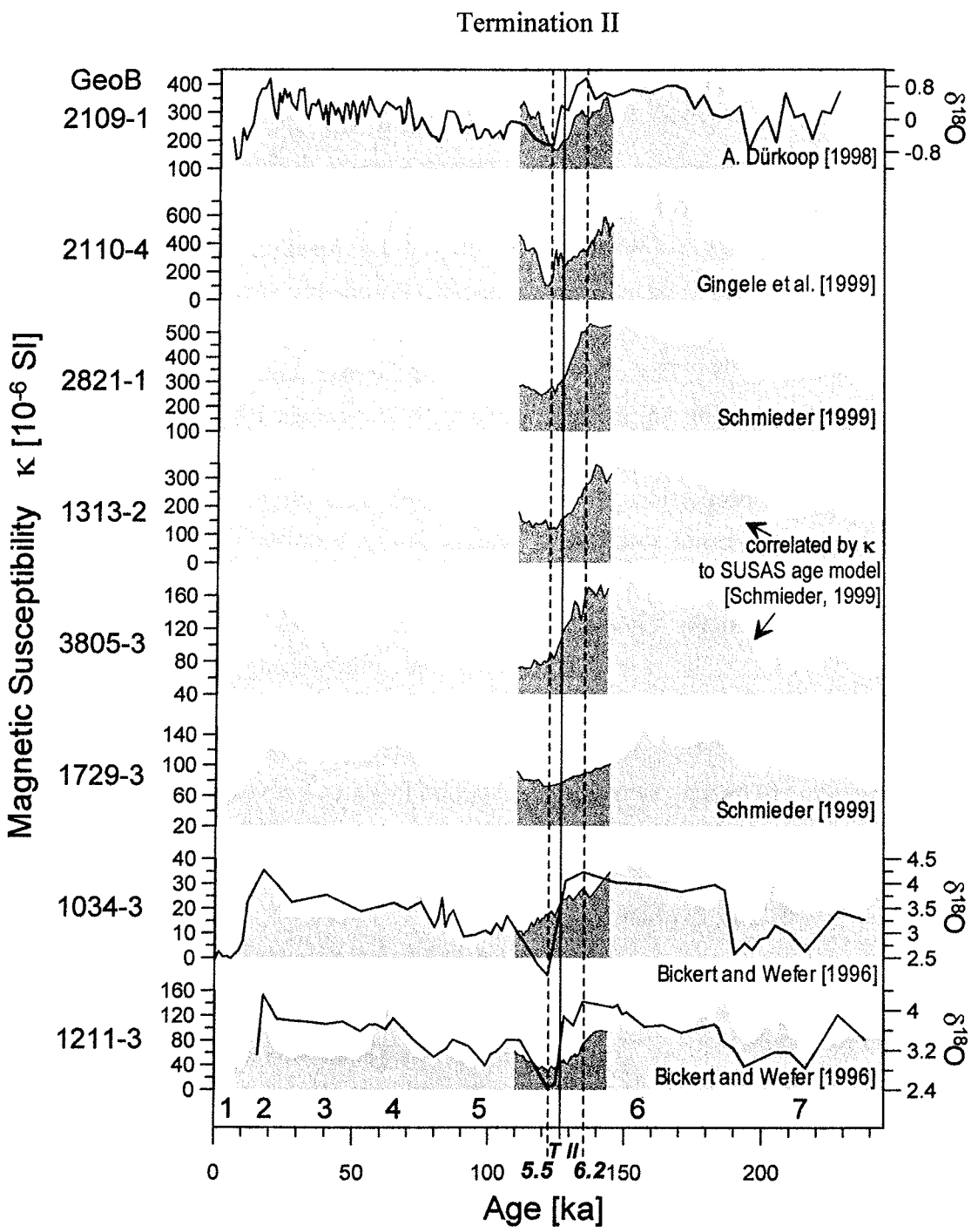

Fig. 2. Chronostratigraphy of the South Atlantic core transect. Gray shaded magnetic susceptibility records toned down within the investigated time interval. Stratigraphies are based on *d*18O for cores GeoB 1034-3, 1211-3 [*Bickert and Wefer*, 1996], 2109-1 [*Dürkoop*, 1998], and 2110-4 [*Gingele et al.*, 1999]. GeoB 1729-3 and 2821-1 are part of the SUSAS stack dated by orbital tuning of their susceptibility logs [*von Dobeneck and Schmieder*, 1999; *Schmieder*, 1999]. Susceptibilities of cores GeoB 1313-2 and 3805-3 were graphically correlated to the SUSAS age model. Termination II and oxygen isotope substages 5.5 and 6.2 are marked by continuous and broken lines, respectively.

particle variations of magnetite [*Maher*, 1988; *Heider et al.*, 1995]. Incremental triaxial alternating field (AF) demagnetizations of M_{ir} and M_{ar} primarily delimit the (micro-)coercivity spectrum of the respective remanence carrying ferri- and antiferromagnetic compounds. The median destructive fields necessary to randomize half of the initial isothermal or anhysteretic

remanence, $B_{1/2}(M_{ir})$ and $B_{1/2}(M_{ar})$, characterize their average magnetic stability.

The $S_{-0.3T}$ parameter [*Bloemendal et al.*, 1992] is defined as the ratio of high-coercive hematite to low-coercive magnetite fractions. With the experimental setting of a saturating field imparted at 1 T and a backfield of 0.3 T goethite does not contribute to $S_{-0.3T}$ [*Heller*, 1978]. The distinct grain size dependence of magnetite M_{ir} limits a quantitative interpretation of the $S_{-0.3T}$ parameter in terms of absolute mineral proportions. First-order estimates assume isothermal saturation remanences (M_{sir}) of 1 kAm^{-1} for hematite and of 50 kAm^{-1} for single-domain magnetite [*Thompson and Oldfield*, 1986].

Additional information about the magnetic mineralogy was obtained from thermal demagnetization treatment (14 heating steps from room temperature to 650 °C) of a three component M_{ir} (0-30 mT, 30-300 mT, and 300 mT-2.5 T) as described by *Lowrie* [1990] and *Lehman et al.* [1996].

4.3 Magnetic hysteresis studies

A Princeton MicroMag PMC M2900 alternating gradient magnetometer [*Flanders*, 1988] was used for hysteresis and backfield measurements. Maximum fields were restricted to 300 mT to delimit remanence and coercivity parameters of magnetite with the least influence of high coercive minerals. The non-ferromagnetic susceptibility was determined from 1 T loops.

Hysteresis and backfield data were further treated with the 'HYSTEAR' program by *von Dobeneck* [1996]. This approach-to-saturation analysis separates the total susceptibility signal χ_{tot}, the hysteresis loop gradient at B = 0, into its ferro- (χ_{fer}) and non-ferromagnetic fractions ($\chi_{nf} = \chi_{tot} - \chi_{fer}$). The processing also discriminates different remanent hysteresis components and splits them into spectral contributions of 30 mathematically defined particle classes with narrow, clearly defined coercivity ranges. The standard hysteresis parameters saturation magnetization M_s, saturation remanence M_{rs}, coercive field B_c, and coercivity of remanence B_{cr} compose the magnetite grain size indices M_{rs}/M_s and B_{cr}/B_c [*Day et al.*, 1977; *Dunlop and Özdemir*, 1997].

For selected samples the concentration of magnetically instable superparamagnetic (SP) particles was estimated by comparing room temperature and 5 K low temperature hysteresis. These measurements were performed on a Quantum Design Magnetic Properties Measurement System (MPMS) at the Institute of Applied Physics, University of Hamburg and the Max-Planck-Institut für Festkörperforschung in Stuttgart.

4.4 Accumulation rates

Magnetic accumulation rates reflect magnetic mineral influxes. The mass accumulation rate of magnetite AR_{Mag} is defined as

$$AR_{Mag} = SR \cdot \rho_{dry} \cdot C_{Mag}$$

with sedimentation rate SR, dry bulk density ρ_{dry}, and magnetite content C_{Mag} [*van Andel et al.*, 1975]. Magnetite susceptibility typically dominates the ferromagnetic signal (SD magnetite $\chi_{Mag} = 450 \cdot 10^{-6} m^3 kg^{-1} >> \chi_{Hem} = 6 \cdot 10^{-6} m^3 kg^{-1}$ hematite [*Thompson and Oldfield*, 1986]). To estimate C_{Mag} from magnetic susceptibility data, the contributions of para- and diamagnetic constituents to bulk susceptibility must be taken into account:

$$AR_{Mag} = SR \cdot \rho_{dry} \cdot \frac{\chi_{fer}}{\chi_{Mag}} = SR \cdot \rho_{dry} \cdot \frac{\chi - \chi_{nf}}{\chi_{Mag}}$$

with χ_{fer} the ferromagnetic and χ_{nf} the non-ferromagnetic susceptibility as derived from hysteresis measurements.

The hematite content C_{Hem} was assessed from the ratio of hard isothermal remanent magnetization $M_{hir} = 0.5 \cdot (M_{sir} + M_{-0.3T})$ primarily carried by antiferromagnetic minerals [*Stoner et al.*, 1996] to the saturation remanence of hematite $M_{rs,Hem} = 1$ kAm^{-1} [*Thompson and Oldfield*, 1986]. The mass accumulation of hematite AR_{Hem} is then derived from

$$AR_{Hem} = SR \cdot \rho_{dry} \cdot C_{Hem} = \frac{M_{hir}}{M_{rs,\,Hem}}$$

Note that M_{sir} was determined at 1 T, implying a slight underestimation of AR_{Hem}.

To infer variations that result in changes of the M_{ar}/M_{ir} grain size ratio, accumulation rates of anhysteretic and isothermal remanent magnetic moments μ_{ar} and μ_{ir} per unit area A and time t were calculated from

$$AR_{\mu_{ar(ir)}} = \frac{\mu_{ar(ir)}}{A \cdot t} = SR \cdot \rho_{dry} \frac{\mu_{ar(ir)}}{m} = SR \cdot M_{ar(ir)}$$

where m is the sediment mass.

The accumulation of paramagnetic compounds yields information both on primary terrigeneous influx and on secondary, diagenetically formed iron mineral phases. χ_{nf} combines para- and diamagnetic mineral components. Diamagnetism, a property of all matter, may be eliminated by an overall correction. In the study areas of the South Atlantic the sediment matrix is principally composed of $CaCO_3$. Its diamagnetic susceptibility ($\chi_{CaCO_3} = -0.5 \cdot 10^{-8}$ m^{3}kg^{-1}) therefore dominates the diamagnetic background, diamagnetism of other minerals are in the same range. The paramagnetic susceptibility $\chi_{para} = \chi_{nf} - \chi_{dia}$ yields a sedimentation rate of the induced paramagnetic moment per field B of

$$SR_{para} = \frac{\mu_{para}}{B \cdot A \cdot t} = \frac{\kappa_{para} \cdot V}{A \cdot t} = SR \cdot \rho_{dry,para} \cdot \chi_{para}$$

where V denotes the sediment volume. Since no information is available about composition and density of the paramagnetic fraction, an overall paramagnetic mass accumulation has been calculated based on dry mass density of the bulk sediment

$$AR_{para} = SR_{para} \cdot \rho_{dry}$$

5. Results and discussion

5.1 Magnetic mineralogy

Thermal demagnetization results of a three component M_{ir} (soft: 0-30 mT; medium: 30-300 mT; hard: 300 mT-2.5 T) together with respective M_{ir} acquisition curves are illustrated in Figure 3 for three representative samples. The data indicate that in all cores the controlling low coercive ferromagnetic remanence carrier is relatively fine grained magnetite (blocking temperature $T_B \leq 575$°C [*O'Reilly*, 1984]). Three types of thermal demagnetization behavior could be distinguished. Type A, characteristic for the southern Angola Basin cores GeoB 1034-3 and 1729-3 and the northern Cape Basin core 1211-3, shows a typical magnetite curve for the dominant 30–300 mT component. A kink at 250°C in the 0–30 mT curve suggests a ferromagnetic iron sulfide phase, possibly pyrrhotite ($T_B \approx 325$°C [*Clark*, 1984; *Dekkers*, 1988]) or greigite (disintegration temperature ≈200-350°C [*Snowball*, 1991]). In marine sediments, these minerals occur as intermediates in the pyritization process and are conserved at this metastable stage in case of H_2S paucity [*Roberts and Turner*, 1993]. Both minerals generally have a higher coercivity than

magnetite [*Dunlop and Özdemir*, 1997], they are not manifest in the 30–300 mT curve, however. Alternatively therefore, the thermal disintegration of maghemite, the low temperature oxidation product of magnetite and omnipresent in marine sediments, may cause the decay in the low coercivity curve. The 300–2500 mT remanence is at least partly carried by hematite ($T_B \approx 675$ °C [*O'Reilly*, 1984]), as indicated by a small remanence above 600 °C.

Type B is typical of the Rio Grande Rise (RGR) cores GeoB 1313-2 and 2821-1. Shapes of demagnetization curves are very similar for all three coercivity ranges. Their more pronounced decay at lower temperatures is attributed to a broader, on average coarser magnetite grain size distribution. As for all samples, the distinct susceptibility variations above about 400°C should primarily be due to metastable maghemite phases.

Type C, typical for cores GeoB 2109-1 and 2110-4 from the Santos Plateau, resembles Type A particularly in the 0-30 mT component. In this case, the steep decay at ~300 °C is also observed in the 30-300 mT curve, implying the presence of magnetic iron sulfides. High temperature cycling of M_{sir} on a Curie balance for samples of cores GeoB 1034-3 and 2110-4 (not shown) did not provide unequivocal evidence to support this interpretation, though. Considerable amounts of hematite are indicated by the slow decay of the 300-2500 mT remanence with a fraction remaining at 650°C.

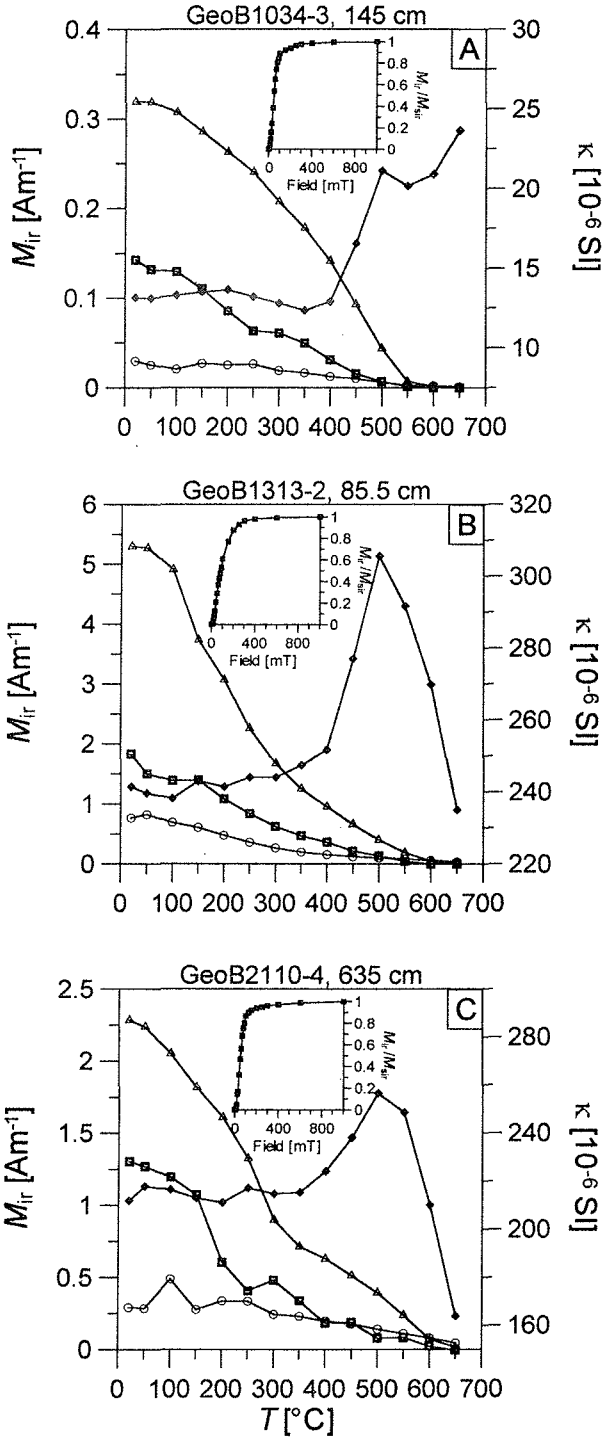

Fig. 3. Thermal demagnetization results of three component M_{ir} after [*Lowrie*, 1990] and [*Lehman et al.*, 1996]. Open squares: 0-30 mT, open triangles: 30-300 mT, open circles: 300 mT-2.5 T, filled diamonds: magnetic susceptibility after each heating step. Insert: M_{ir} acquisition to 1 T. Three regionally typical characteristics can be distinguished. Type A: cores GeoB 1034-3, 1211-3, and 1729-3 (southern Angola Basin and northern Cape Basin), Type B: cores GeoB 1313-2 and 2821-1 (Rio Grande Rise), Type C: cores GeoB 2109-1 and 2110-4 (Santos Plateau).

5.2 Regional trends and glacial/interglacial contrasts

Figure 4 illustrates both West/East and glacial/interglacial contrasts in various magnetic accumulation rates and rock magnetic properties for the transition from substage 6.2 to 5.5. For all

cores mass accumulation of magnetite, hematite, and paramagnetics are given together with isothermal and anhysteretic magnetic moment accumulation (Figure 4a-e). Holocene accumulation rates could not be determined, as age data and sedimentation rates of sufficient precision are not yet available for the surface layers.

The most prominent feature of the South Atlantic transect is the roughly logarithmic decrease in all accumulation rates from west to east, suggesting that all major sources of magnetite, hematite, as well as paramagnetic iron minerals are on the South American continent. Magnetite and hematite accumulation rates decline from about 4 $g \cdot m^{-2} kyr^{-1}$ and 5 $g\ m^{-2} kyr^{-1}$ in the lower Santos Plateau core GeoB 2110-4 to a minimum of about 0.03 $g\ m^{-2} kyr^{-1}$ for both these minerals in the southern Angola Basin (core GeoB 1034-3). The trend reversal towards the easternmost core GeoB 1211-3 implies some terrigeneous influx from the African continent into the northern Cape Basin, possibly eolian material from the Namib Dessert. The fact that the accumulation rates of the westernmost core GeoB 2109-1 are less than those in core 2110 hints at an additional, potentially AABW supplied southern magnetic particle source efficient up to 3000 m water depth on the Santos Plateau [*Hogg*, 1996].

In the western South Atlantic all accumulation rates decrease from glacial substage 6.2 to the interglacial substage 5.5, documenting an enhanced continental influx to the ocean during glacial periods. These contrasts systematically diminish towards the east and even reverse in the eastern Angola Basin (site 1034). On the Santos Plateau, the glacial accumulation enhancements in the deeper core GeoB 2110-4 largely surpass those at the shallower site 2109 indicating a strong glacial increase of AABW particle advection of southern origin, most likely of Rio de la Plata detritus.

Glacial/interglacial variations in hematite/magnetite ($S_{-0.3T}$) ratios (Figure 4f) are generally small. Slight shifts to increased hematite concentration during 5.5 at most sites should result from an increased NADW [e.g., *Broecker and Henderson*, 1998] advection of hematite-rich suspended matter from equatorial latitudes, where hematite/magnetite ratios are the highest of the entire Holocene South Atlantic [*Schmidt et al.*, 1999]. As a typical product of chemical weathering under warm semiarid to humid conditions high hematite concentrations characterize the Amazon and Congo detritus. On the other hand, hematite deposition in the equatorial Atlantic has been found typical for eolian dust from the Sahara and Sahel [*Balsam and Otto-Bliesner*, 1995] which is enhanced during glacials. Apparently this does not affect the study area. The notably high accumulation of hematite and especially paramagnetic minerals on the Santos Plateau reflects the considerable input of soils at continental proximity. As will be discussed below, a local diagenetic alteration should additionally contribute to this observation.

The M_{rs}/M_s ratio (Figure 4g), a measure of the average magnetite domain state and grain size, reveals a systematic magnetic particle fining from West to East, where all data are within the PSD/SD range. Since the theoretical value of $M_{rs}/M_s \geq 0.5$ [*Stoner and Wohlfarth*, 1948; *Joffe and Heuberger*, 1974] for ideal, non-interacting SD magnetite is not reached in natural sample collections [*Jackson*, 1990; *Gee and Kent*, 1995], $M_{rs}/M_s \approx 0.3$ should indicate a SD predominance. Fine grained magnetite in Holocene eastern South Atlantic sediments could be related to biomineralization in high productive upwelling areas [*Schmidt et al.*, 1999]. During the substages 6.2/5.5 period, increasing distance from the South

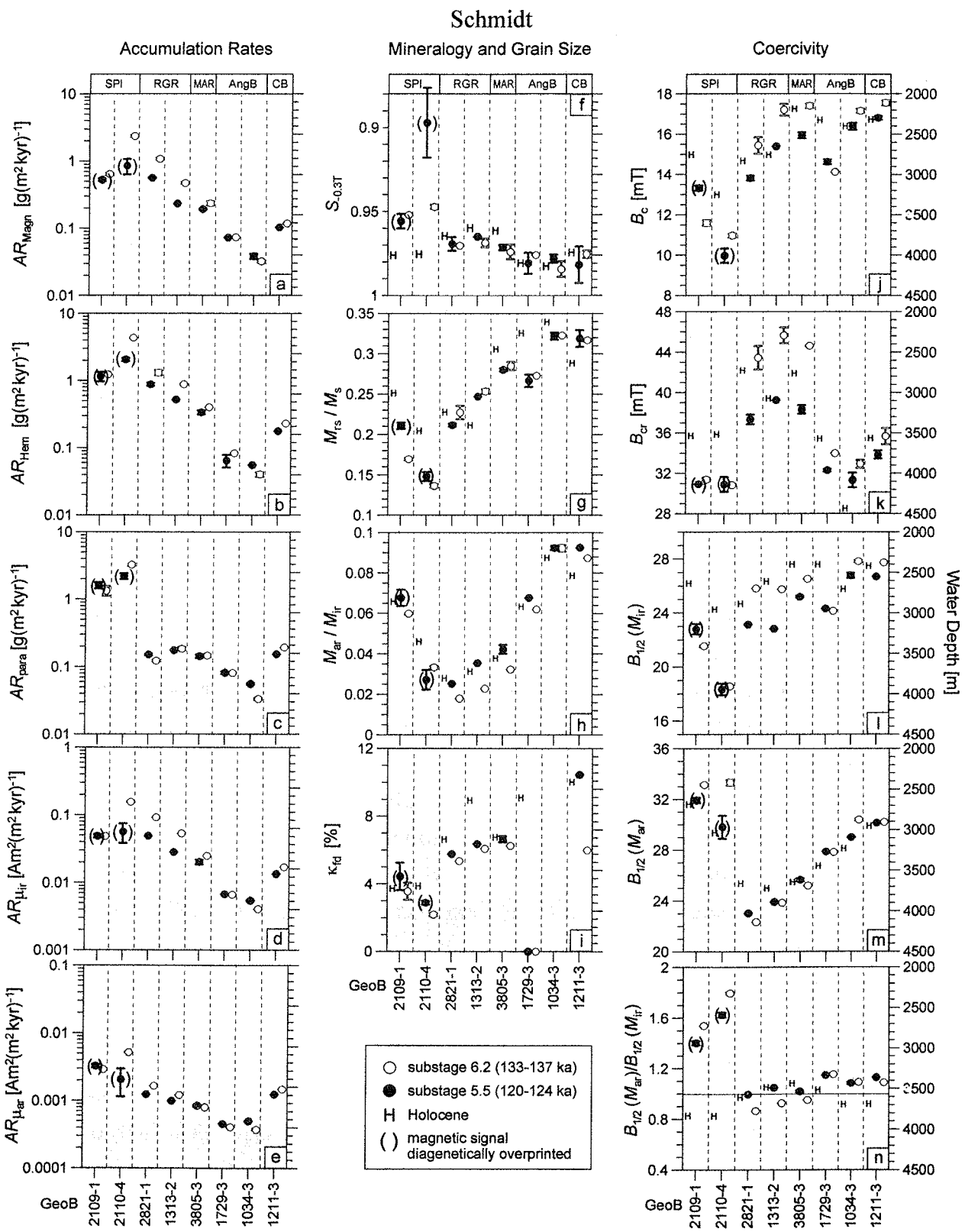

Fig. 4. Average magnetic accumulation rates and rock magnetic parameters with standard deviations for substage 5.5 (120-124 ka, black dots) and substage 6.2 (133-137 ka white dots) intervals. H represents Holocene rock magnetic parameters. The lack of exact sedimentation rates did not allow to quantify accumulation rates for the Holocene. For sites biased by diagenetic alteration data are bracketed. Mass accumulation rates are given for (**a**) magnetite, (**b**) hematite, and (**c**) paramagnetic compounds. Anhysteretic (**d**) and isothermal (**e**) magnetic moment accumulation rates delimit the potential of M_{ar} and M_{ir} acquisition, reflecting fine grained and bulk magnetite accumulation, respectively. (**f**) $S_{-0.3T}$ parameter represents relative concentrations of hematite and magnetite (**g**) M_{rs}/M_s ratio average magnetic grain-size, (**h**) M_{ar}/M_{ir} relative contents of fine grained, and (**i**) $k_{fd\%}$ ultrafine magnetite. (**j**) Bulk coercivity B_c, (**k**) coercivity of remanence B_{cr}, (**l**) stability of M_{ir} and (**m**) M_{ar}. (**h**) Modified Lowrie-Fuller test, comparing M_{ar} and M_{ir} stabilities. Geographic units are indicated in the top line (SPI Santos Plateau, RGR Rio Grande Rise, MAR mid-Atlantic Ridge, AngB Angola Basin, and CB Cape Basin). Core codes in the bottom line. Gray shades indicate water depth.

Termination II

American continent seems most important for the observed grain size distribution. Grain sizes are coarsest on the Santos Plateau particularly at site 2110, though 2109 is located closer to the coast. While a coarsening due to diagenetic dissolution of magnetite is thought to be the main cause, the previously mentioned AABW advection of Rio de la Plata detritus could also be significant as implied by the Holocene data. A coarsening of magnetic particles during substage 6.2 which would agree with the Vostok dust record and an enhanced continental aridity, dust mobilization and transport [*Petit et al.*, 1999] is evident only at site 2109, closest to South America. More distant locations show no discernible variability of the M_{rs}/M_s ratio during the glacial/interglacial transition, suggesting that the average grain size of particles transported over long distances remained largely unchanged. The content of more fine-grained magnetites, represented by the M_{ar}/M_{ir} ratio (Figure 4h), reflects a glacial coarsening along the whole transect with exception of site GeoB 1034 north of the Walvis Ridge. This is obviously not due to a decrease of M_{ar} magnetic moment accumulation, but to a relative rise of $AR_{\mu ir}$ during the glacial (Figures 4d and 4e). The W-E trend and, in most cores, also the glacial/ interglacial contrast is much less pronounced in M_{ar} than in M_{ir}. While the fine grained accumulation, e.g., of biogenic SD magnetite, remained mostly constant, variations in the coarser terrigeneous influx produced the observed changes. The reduced relative content of ultrafine SP magnetite in substage 6.2 (Figure 4i) corresponds to these results. Note that extremely low susceptibilities in core GeoB 1034-3 did not allow to quantify $\kappa_{fd\%}$.

The coercivity parameters B_c and B_{cr} (Figures 4j, k) are influenced by mineralogy, grain size, particle shape, and internal structure (stress). There is a conspicuous discrepancy between coercivity and grain size glacial/ interglacial variations in most cores. Only on the Santos Plateau B_c and grain size parameters show corresponding trends caused by an enhanced influx of low coercive coarse material during the glacial. At both sites GeoB 2109 and 2110 a diagenetic overprint is manifested by a grain size coarsening and reduction of coercivity during substage 5.5 (Figure 7). The modified Lowrie-Fuller-Test (Figure 4n) [*Xu and Dunlop*, 1995] reveals a high M_{ar} stability in contrast to a low M_{ir} coercivity becoming even more pronounced during the glacial. Similar observations have been made in Holocene deposits off the Rio de la Plata river mouth [*Schmidt et al.*, 1999]. The most plausible explanation would be a minor fraction of stable SD magnetite within a predominant coarse, terrigeneous magnetic assemblage. The SD content must be very minor as it is of no importance for the M_{ir} and average B_c coercivities, while it seems to exclusively carry the stable M_{ar}. Due to an elevated productivity in this coastal area the SD particles are presumably of biogenic origin. An alternative and likewise conceivable interpretation are SD areas within coarse, titanium-rich MD titanomagnetites, frequently occurring in basaltic rocks. Such SD areas result from local crystal stress for instance caused by low temperature oxidation of titanomagnetites [*Appel and Soffel*, 1985; *Appel*, 1987]. *Özdemir et al.* [1995] and *Özdemir and Dunlop* [1998] reported on SD-simulating closure domains in coarse MD particles under high surface stress.

Glacial/interglacial coercivity contrasts in the distal RGR and MAR cores GeoB 2821-1, 1313-2, and 3805-3 are inverse to respective grain size trends. The glacial sediments yield unusually high coercivities particularly accentuated in B_{cr}. B_{cr} for SD magnetite is ~33 mT [*Thompson and*

Oldfield, 1986] as reached in the eastern cores GeoB 1729-3, 1034-3 and 1211-3 ($B_{cr,max} \approx 36$ mT). Higher values have been observed only for synthetic crushed magnetite samples [*Day et al.*, 1977]. As grain size ratios indicate PSD particles, stress or extreme cation deficiency is the most likely cause for the elevated coercivities. In view of a slight glacial coarsening of grain sizes, the large glacial increase in magnetic stability should be assigned to an intensified, presumably eolian supply of such stressed material [*Hodych*, 1982]. $B_{½}(M_{ar})/B_{½}(M_{ir}) < 1$ during stage 6.2 (Figure 4n) reflect increasing M_{ir} (Figure 4l) and slightly reduced M_{ar} (Figure 4m) stability. This peculiar feature, illustrated for core GeoB 2821-1 in Figure 5, has already been observed for the Holocene situation in this area by *Schmidt et al.* [1999]. who proposed particles at the SD/SP boundary probably transported by southern intermediate water masses to carry the unstable M_{ar}

The glacial rise of M_{ar} as well as M_{ir} stabilities in core GeoB 1034-3 from the northern Walvis Ridge flank hints at an elevated production of SD bacterial magnetite induced by an enhanced productivity in the Benguela upwelling system during substage 6.2.

5.3 Coercivity spectra

The coercivity distribution in all cores has been further analyzed by modeling of hysteresis data using the HYSTEAR method [*von Dobeneck*, 1996]. In Figure 6 the micro-coercivity spectra are plotted as gray scales against age. There is one major peak in all cores marking the predominant coercivity class. Their median fields are in good agreement with previously discussed B_{cr} data. The decrease in intensity and coercivity from glacial to interglacial is primarily assigned to a rising glacial influx of higher coercive continental material related to strengthened wind systems during cold periods [e.g., *Broecker and Henderson*, 1998; *Petit*, 1999]. Alternative explanations like an apparent interglacial magnetite coarsening due to an enhancement of large scale deep water circulation [*Kellogg*, 1987; *Schmiedl and Mackensen*, 1997] impeding fine particles to settle or an increasing SD magnetite biomineralization coupled with a higher productivity during glacials [*Schmiedl and Mackensen*, 1997; *Broecker and Henderson*, 1998] are less plausible, because both should also influence the M_{ar}/M_{ir} ratios.

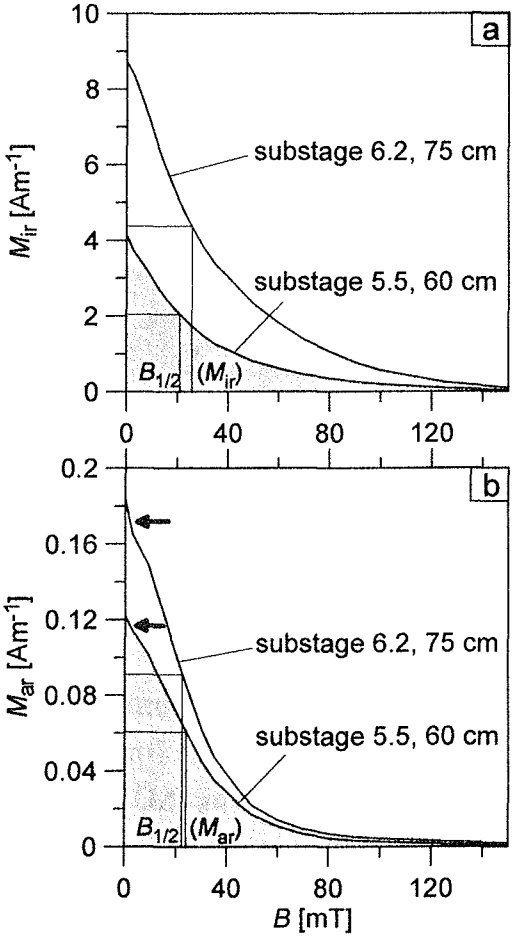

Fig. 5. Alternating field demagnetization of (**a**) M_{ir} and (**b**) M_{ar} for substage 5.5 and 6.2 samples from core GeoB 2821-1. Median destructive fields are marked. A glacial intensity increase in both, M_{ir} and M_{ar} correlates to a M_{ir} coercivity rise during the glacial. In contrast, M_{ar} coercivity slightly decreases due to an unstable component. This bend in the M_{ar} demagnetization curve demagnetized at very low fields (arrow) characterizes all central South Atlantic cores and is much more pronounced during glacial substage 6.2.

Termination II

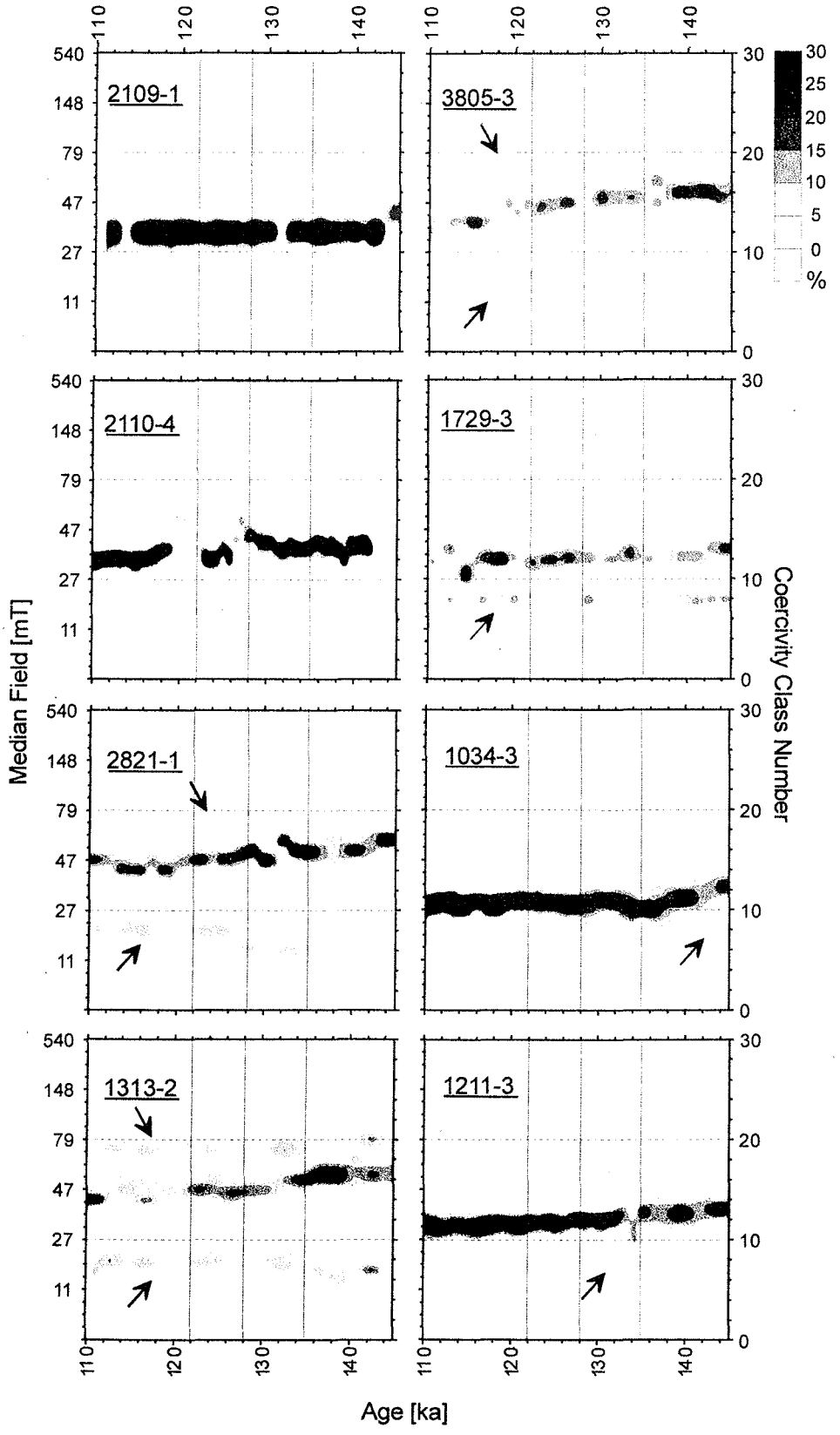

Fig. 6. Micro-coercivity spectra inferred from hysteresis measurements at room temperature to 300 mT maximum fields versus age. Gray levels denote % contribution of individual remanent hysteresis coercivity classes [*von Dobeneck*, 1996]. Arrows mark additional low and high coercivity bands interpreted as a SP/SD transitional mode.

A second peak at lower median fields ranging from 14 to 27 mT and contributing up to 15 % to the spectra is observed in cores GeoB 2821-1, 1313-2, 3805-3, 1729-3, and less developed and continuous also in 1211-3 and 2110-4. In cores GeoB 1313-2, 3805-3, and locally in 2821-1 it is accompanied by a third high coercive (~ 80 mT) peak. Theoretically, a magnetite grain size fraction near the SD/SP boundary could yield such a bimodal micro-coercivity spectrum with SP particles producing the low, fine SD particles the high coercive peak [*von Dobeneck*, pers. comm.]. Low temperature hysteresis measurements at 5 K for selected samples support this interpretation. *Schmidt et al.* [1999] assumed this fine material to be advected to the central and western South Atlantic during Holocene by southern source intermediate water masses. The low coercive peak is present in substage 6.2 but disappears towards the termination in core GeoB 1034-3 from the southern Angola Basin. A plausible explanation could be a fine particle transport with water masses like Circumpolar Deep Water (CPDW) or AAIW which cross the Walvis Ridge during glacials, but retreat southward in interglacials [*Reid*, 1989; *Petschick et al.*, 1996]. This fraction at the SD/SP boundary is likely to carry the previously discussed weak M_{ar} component, although the micro-coercivity spectra reflect no glacial/interglacial variability in its contribution to isothermal remanence.

5.4 Variability during the deglaciation

Detailed information about magnetic mineral accumulation and changes in magnetic properties during the substages 6.2 to 5.5 deglaciation is summarized in Figure 7. At most sites the decrease of accumulation rates clearly begins prior to the substage 6.2 main phase at ~140 ka. *Broecker and Henderson* [1998] reported similar findings in the dust record of the Vostok ice core. In the Santos Plateau cores GeoB 2109-1 and 2110-4 the data sets strongly suggest a reductive diagenetic dissolution of magnetite at around 130 ka (hatched in Figure 7) possibly representing a paleoredox boundary related to a higher C_{org} deposition. In core GeoB 2109-1 a peak in the paramagnetic moment accumulation is observed at this horizon which could result from of a precipitation Fe minerals (sulfide?). Moreover, a typical grain size coarsening (M_{rs}/M_s and M_{ar}/M_{ir}) [*Urbat et al.*, 1999; *Hilgenfeldt*, in press] occurs and the ultrafine fraction ($\kappa_{fd\%}$) diminishes drastically. In GeoB 2110-4 this coarsening is bound to sharp local peaks and even more accentuated in all rock magnetic parameters. This record lacks a peak in paramagnetic accumulation, however. In both cores no magnetite precipitation layer as described by *Urbat et al.* [1999] could be identified. A second less well developed horizon of magnetite dissolution seems to roughly coincide with substage 5.5.

Magnetic mass accumulation rates in cores GeoB 2109-1 and 2110-4 show a drastic increase directly following the diagenetically induced minimum durin stage 5.5. One potential terrestrial sediment source at the core the locations is the Rio Doce discharging a considerable particle load to the Santos Plateau during interglacials [*Gingele et al.*, 1999]. The exact timing of this enhanced fluvial influx is obscured by the diagenetic overprint.

In the eastern cores GeoB 1729-3, 1034-3, and 1211-3, subtle M_{rs}/M_s and B_c minima appear at the termination. These records should reflect a rising biogenesis of SD magnetite due to intensified productivity and upwelling during substage 6.2 ceasing at the termination, combined with decreasing dust influx causing a particle

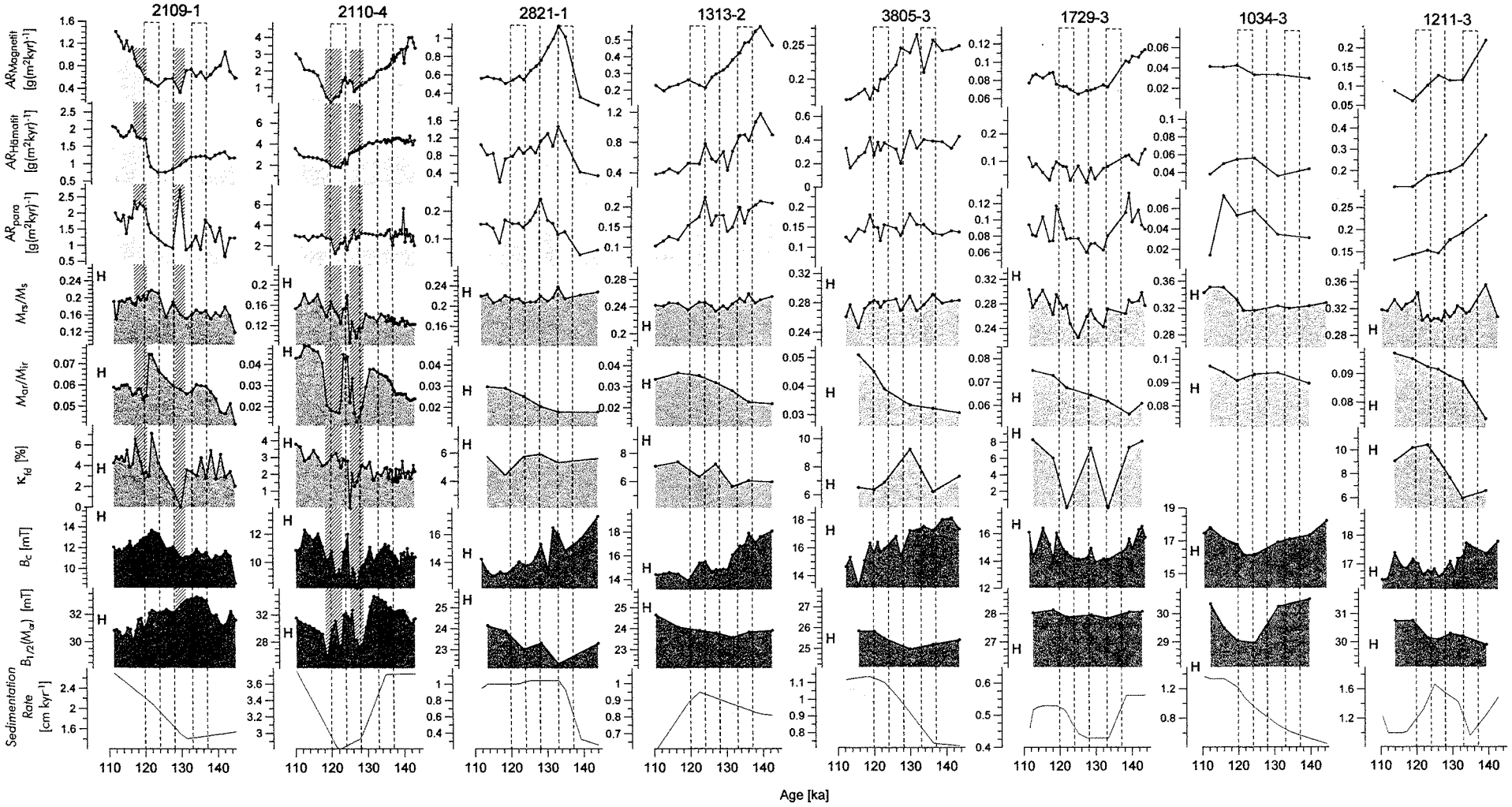

Fig. 7. Magnetic mineral accumulation and magnetic property variations during the deglaciation. Intervals of the previously discussed glacial and interglacial substages are shaded. Termination II is marked by a dashed line. Respective Holocene values are given to the left of each rock magnetic property curve and are mostly in the stage 5.5 range. Horizons of diagenetic dissolution of magnetite are marked by a hatched area. Susceptibility data for core GeoB 1034-3 were below the experimental resolution for $\kappa_{fd\%}$ determination.

fining towards substage 5.5. Apart from these peculiarities stage 5.5 strongly resembles the Holocene in most all parameters and cores. The higher M_{ar} stability in eastern cores implies a more intense bacterial biomineralization of SD magnetite and thus a higher substage 5.5 productivity than during Holocene.

6. Paleoceanographic implications and conclusions

Two major trends over the South Atlantic W-E transect, decreasing magnetic mineral accumulation and increasing particle fining clearly identify the South American continent as most important source of terrigeneous (magnetic) matter to the South Atlantic both during Holocene and throughout Termination II from substage 6.2 to 5.5. This particle supply can be subdivided on grounds of coercivity spectra into eolian inflow of volcanogenic dust from the Andes and Rio de la Plata fluvial discharge of material eroded from Jurassic flood basalt outcrops in the Paraná Basin.

The Andes, which were characterized by active and explosive volcanism during the entire Quaternary, and the Patagonian plains, which are the major depocenter of wind and (melt-) water transported detritus from the Andes, are the main sources of dust deposits in the South Atlantic [*Clapperton*, 1993]. Especially the Rio Grande Rise and mid-Atlantic Ridge cores GeoB 2821-1, 1313-2, and 3805-3 show clear evidence of eolian volcanogenic inflow in their magnetic characteristics such as uncommon high magnetic mineral contents and exceptionally elevated coercivities. During glacials, when the polar front and the westerlies moved northward, and aridity and dust mobilization intensified [*Petit et al.*, 1999], this influx of volcanogenic material dominated the magnetic mineral assemblage in the marine sedimentary deposits of the western and central South Atlantic at around 20 to 30°S.

On the Santos Plateau (cores GeoB 2110-4 and 2109-1) magnetic grain size parameters and overall coercivities indicate very coarse PSD to MD domain states. In remarkable contrast, the relatively small M_{ar} shows the highest coercivity of the whole transect interpreted to be carried either by a minor biogenic component or SD areas within coarse, presumably basaltic, Ti-rich titanomagnetites. Comparison of these data to Holocene rock magnetic characteristics from the entire South Atlantic [*Schmidt et al.*, 1999], identifies this attribute as typical for the deposits off the la Plata river mouth. Most of its feeders drain the Paraná Basin, where huge formations of Jurassic flood basalts crop out [*Clapperton*, 1993]. This suggests a northward transport of Rio de la Plata detritus by southern water masses to the Santos Plateau which intensified particularly during substage 6.2 [*Massé et al.*, 1994] with the northward retreat of NADW [*Diekmann et al.*, 1996; *Oppo et al.*, 1997], largely exceeding dust supply which predominated at more distant locations from the South American continent.

Eolian influx from Africa by stronger SE trades during the more arid glacial [*deMenocal et al.*, 1995] is only observed in core GeoB 1211-3 from the northern Cape Basin. It was apparently restricted to a quite narrow zone in continental proximity parallel to the coast. At the same time the South American source dust is transported by intensified and northwards shifted westerlies almost across the entire South Atlantic. A glacial enhancement of bioproductivity related to stronger upwelling in the eastern South Atlantic as described by *Schmiedl and Mackensen* [1997] and *Broecker and Henderson* [1998] is only seen in the southern Angola Basin.

The slight increase in the hematite/ magnetite ratio in the central South Atlantic cores

during substage 5.5 hints at an enhanced NADW particle advection from equatorial latitudes. A more humid interglacial climate on the South American continent [*Clapperton*, 1993] causing increased runoff and river discharge, combined with strengthened Brazil Current and NADW flow, obviously has caused a southward transport of Rio Doce fluvial load to the Santos Plateau as proposed by *Gingele et al.* [1999]. Magnetite dissolution horizons around substage 5.5 and directly at the termination mark peaks in productivity and organic matter deposition.

The low stability band in coercivity spectra is present throughout all distal cores but in the Angola Basin, where it shows up only during stage 6 and then disappears towards the termination. It can serve as a tracer for northward advection of ultrafine particles by Antarctic intermediate water masses restrained in their northward flow at the Walvis Ridge during interglacials.

The striking similarity of both warm stage records of this study suggests that, from the environmental magnetic point of view, the substage 5.5 subtropical South Atlantic was climatically very similar to the Holocene except for a slightly more intense productivity in the eastern parts.

8. Acknowledgments

Special thanks are to Sven Skwirblies from the Institute of Applied Physics, University of Hamburg and to Eva Bruecher from the Max-Planck-Institute Stuttgart, for low temperature hysteresis measurements, as well as to Jürgen Matzka for Curie balance measurements at the Ludwig-Maximilians-University, Munich. Fruitful discussions with Tilo von Dobeneck, Ulrich Bleil and Karl Fabian materially improved the manuscript and are gratefully acknowledged. This study was financially supported by the Deutsche Forschungsgemeinschaft (Sonderforschungsbereich 261 at Bremen University, contribution no. ###).

References

Appel, E., Stress anisotropy in Ti-rich titanomagnetites, *Physics of the Earth and Planetary Interiors*, 46, 233–240, 1987.

Appel, E. and Soffel, H.C., Domain state of Ti-rich titanomagnetites deduced from domain structure observations and susceptibility measurements, *Journal of Geophysics*, 56, 121–132, 1985.

Balsam, W.L. and Otto-Bliesner, B.L., Modern and last glacial maximum eolian sedimentation patterns in the Atlantic Ocean interpreted from sediment iron oxide content, *Paleoceanography*, 10, 493-507, 1995.

Bauch, H.A., Monitoring Termination II at high latitude: anomalies in the planktic foraminiferal record, *Marine Geology*, 131, 89-102, 1996.

Bickert, T. and Wefer, G., Late Quaternary deep water circulation in the South Atlantic: reconstruction from carbonate dissolution and benthic stable isotopes., In: G. Wefer, W.H. Berger, G. Siedler, and D.J. Webb (Editors), *The South Atlantic: present and past circulation*, Springer, Berlin, pp. 527-551, 1996.

Bleil, U. and cruise participants, Report and preliminary results of Meteor Cruise M 23/2, *Berichte, Fachbereich Geowissenschaften, Universität Bremen*, 133 pp., 1993.

Bleil, U. and cruise participants, Report and preliminary results of Meteor-Cruise M 29/2, *Berichte, Fachbereich Geowissenschaften, Universität Bremen*, 153 pp.,1994.

Bloemendal, J., King, J.W., Hall, F.R., and Doh, S.J., Rock magnetism of Late Neogene and Pleistocene deep-sea sediments: relationship to sediment source, diagenetic processes, and sediment lithology, *Journal of Geophysical Research*, 97, 4361–4375, 1992.

Broecker, W.S., Terminations, In: A. Berger et al., (Editors), J. Imbrie, J. Hays, G. Kukla and B. Saltzman (Editors), *Milankovitch and Climate: Understanding the Response to Orbital Forcing*, Reidel Publishing, Dordrecht pp. 687-698, 1984.

Broecker, W.S. and Henderson, G.M., The sequence of events surrounding Termination II and their implications for the cause of glacial-interglacial CO_2 changes, *Paleoceanography*, 13, 352-364, 1998.

Butler, R.F. and Banerjee, S.K., Theoretical single-domain grain size range in magnetite and titanomagnetite, *Journal of Geophysical Research*, 80, 4049–4058, 1975.

Clapperton, C., *Quaternary Geology and Geomorphology of South America*, Elsevier, Amsterdam, 779 pp., 1993.

Clark, D.A., Hysteresis properties of sized dispersed monoclinic pyrrhotite grains, *Geophysical Research Letters*, 11, 173–176, 1984.

Day, R., Fuller, M., and Schmidt, V.A., Hysteresis properties of titanomagnetites: grain-size and compo-

sitional dependence, *Physics of the Earth and Planetary Interiors*, 13, 260–266, 1977.

Dearing, J.A., Dann, R.J.L., Hay, K., Lees, J.A., Loveland, P.J., Maher, B.A., and O'Grady, K., Frequency dependent susceptibility measurements of environmental materials, *Geophysical Journal International*, 124, 228-240, 1996.

Dekkers, M.J., Magnetic properties of natural pyrrhotite Part I: behaviour of initial susceptibility and saturation-magnetization-related rock-magnetic parameters in a grain-size dependent framework, *Physics of the Earth and Planetary Interiors*, 52, 376–393, 1988.

deMenocal, P.B., Ruddiman, W.F., and Pokras, E.M., Plio-Pleistocene African climate, *Science*, 270, 53-59, 1995.

Diekmann, B., Petschick, R., Gingele, F.X., Fütterer, D., Abelmann, A., Brathauer, U., Gersonde, R., and Mackensen, A., Clay mineral fluctuations in late Quaternary sediments of the southeastern South Atlantic: implications for past changes of deep water advection, In: G. Wefer, W.H. Berger, G. Siedler, and D.J. Webb (Editors), *The South Atlantic: present and past circulation*, Springer, Berlin, pp. 621-644, 1996.

Dunlop, D.J., Superparamagnetic and single-domain threshold sizes in magnetite, *Journal of Geophysical Research*, 78, 1780–1793, 1973.

Dunlop, D.J. and Bina, M.-M., The coercive force spectrum of magnetite at high temperatures: evidence for thermal activation below the blocking temperature, *Geophysical Journal of the Royal Astronomical Society*, 51, 121–147, 1977.

Dunlop, D.J. and Özdemir, Ö., *Rock Magnetism: Fundamentals and Frontiers*, Cambridge Studies in Magnetism, Cambridge University Press, Cambridge, 573 pp., 1997.

Duplessy, J.-C. and Shackleton, N.J., Response of global deep-water circulation to Earth's climatic change 135,000-107,000 years ago, *Nature*, 316, 500-507, 1985.

Dürkoop, A., *Der Brasilstrom im Spätquartär: Rekonstruktion der oberflächennahen Hydrographie während der letzten 400.000 Jahre*, Ph.D. Thesis, Universität Bremen, 144 pp., 1998.

Flanders, P.J., An alternating-gradient magnetometer, *Journal of Applied Physics*, 63, 3940–3945, 1988.

Frederichs, T., Bleil, U., Däumler, K., von Dobeneck, T., and Schmidt, A., The magnetic view on the marine paleoenvironment: parameters, techniques, and potentials of rock magnetic studies as a key to paleoclimatic and paleoceanographic changes, In: G. Fischer and W. Wefer (Editors), *Use of Proxies in Paleoceanography: Examples from the South Atlantic*, Springer, Berlin, pp. 575-599, 1999.

Gee, J. and Kent, D.V., Magnetic hysteresis in young mid-ocean ridge basalts: dominant cubic anisotropy?, *Geophysical Research Letters*, 22, 551–554, 1995.

Gingele, F.X., Schmieder, F., von Dobeneck, T., Petschick, R., and Rühlemann, C., Terrigeneous flux in the Rio Grande Rise area during the past 1500 ka: evidence of deep-water advection or rapid response to continental rainfall patterns?, *Paleoceanography*, 14, 84-95, 1999.

Heider, F., Zitzelsberger, A., and Fabian, K., Magnetic susceptibility and remanent coercive force in grown magnetite crystals from 0.1 mm to 6 mm, *Physics of the Earth and Planetary Interiors*, 93, 239-256, 1995.

Heller, F., Rock magnetic studies of Upper Jurassic limestones from southern Germany, *Journal of Geophysics*, 44, 525-543, 1978.

Hilgenfeldt, K., Diagenetic dissolution of biogenic magnetite in surface sediments of the Benguela upwelling system, *Geologische Rundschau*, in press, 1999.

Hodych, J.P., Magnetostrictive control of coercive force in multidomain magnetite, *Nature*, 298, 542–544, 1982.

Hogg, N.G., Circulation in the deep Brazil Basin, In: G. Wefer, W.H. Berger, G. Siedler, and D.J. Webb (Editors), *The South Atlantic: Present and Past Circulation*, Springer, Berlin, pp. 251-260, 1996.

Imbrie, J., Hays, J.D., Martinson, D.G., McIntyre, A., Mix, A.C., Morley, J.J., Pisias, N. G., Prell, W.L., and Shackleton, N.J., The orbital theory of Pleistocene climate: support from a revised chronology of the marine $\delta^{18}O$ record, In: A. Berger, J. Imbrie, J. Hays, G. Kukla and B. Saltzman (Editors), *Milankovitch and Climate: Understanding the Response to Orbital Forcing*, Reidel Publishing, Dordrecht, pp. 269–305, 1984.

Jackson, M.J., Diagenetic sources of stable remanence in remagnetized Paleozoic cratonic carbonates: a rock magnetic study, *Journal of Geophysical Research*, 95, 2753–2761, 1990.

Joffe, I. and Heuberger, R., Hysteresis properties of distributions of cubic single-domain ferromagnetic particles, *Philosophical Magazine*, 29, 1051–1059, 1974.

Johnson, D.A., Regional oceanographic setting in the southwestern Atlantic, In: P.F. Barker, R.L. Carlson et al. (Editors), *Initial Reports of the Deep Sea Drilling Project*, 72, U.S. Govt. Printing Office, Washington, D.C., pp. 15-35, 1983.

Kellogg, T.B., Plaeoclimatology and paleo-oceanography of the Norwegian and Greenland seas, *Geological Society of America*, Memoir, 145, 77-110, 1980.

Kellogg, T.B., Glacial-interglacial changes in global deep water circulation, *Paleoceanography*, 2, 259-271, 1987.

King, J.W. and Channell, J.E.T., Sedimentary magnetism, environmental magnetism, and magnetostratigraphy, *Reviews of Geophysics*, 29 Suppl., 358–370, 1991.

Ledbetter, M.T., Bottom-current speed in the Vema Channel recorded by particle size of sediment fine-fraction, *Marine Geology*, 58, 137-149, 1984.

Ledbetter, M.T., A Late Pleistocene time-series of bottom-current speed in the Vema Channel., *Palaeogeography, Palaeoclimatology, Palaeoecology*, 53, 97-105, 1986.

Lehman, B., Sagnotti, L., Winkler, A., and Lo Cascio, C., Magnetic mineralogy changes in the Pleistocene marine sequence of Montalto di Castro (central Italy) and influences on the magnetic anisotropy,

Geophysical Journal International, 127, 529-541, 1996.

Lowrie, W., Identification of ferromagnetic minerals in a rock by coercivity and unblocking temperature properties, *Geophysical Research Letters*, 17, 159–162, 1990.

Lund, S.P. and Karlin, R., Introduction to the special section on physical and biogeochemical processes responsible for the magnetization of sediments., *Journal of Geophysical Research*, 95, 4353-4354, 1990.

Maher, B.A., Magnetic properties of some synthetic submicron magnetites, *Geophysical Journal*, 94, 83–96, 1988.

Martinson, D.G., Pisias, N.G., Hays, J.D., Imbrie,J., Moore, T.C. Jr., and Shackleton, N.J., Age dating and the orbital theory of the Ice Ages of a high-resolution 0 to 300,000-year chronostratigraphy, *Quaternary Research*, 27, 1-29, 1987.

Massé, L., Faugères, J.-C., Bernat, M., Pujos, A., and Mézerais, M.-L., A 600,000-year record of Antarctic Bottom Water activity inferred from sediment textures and structures in a sediment core from the southern Brazil Basin, *Paleoceanography*, 9, 1017-1026, 1994.

Mullins, C.E. and Tite, M.S., Magnetic viscosity, quadrature susceptibility, and frequency dependence of susceptibility in single-domain assemblies of magnetite and maghemite, *Journal of Geophysical Research*, 78, 804–809, 1973.

Oldfield, F., Environmental magnetism: a personal perspective, *Quaternary Science Reviews*, 10, 73–85, 1991.

Oppo, D.W., Horowitz, M., and Lehman, S.J., Marine core evidence for reduced deep water production during Termination II followed by a relatively stable substage 5e (Eemian), *Paleoceanography*, 12, 51-63, 1997.

O'Reilly, W., *Rock and Mineral Magnetism*, Blackie, Glasgow, 220 pp., 1984.

Özdemir, Ö. and Dunlop, D.J., Single-domain-like behavior in a 3-mm natural single crystal of magnetite, *Journal of Geophysical Research*, 103, 2549-2562, 1998.

Özdemir, Ö., Xu, S., and Dunlop, D.J., Closure domains in magnetite, *Journal of Geophysical Research*, 100, 2193–2209, 1995.

Parry, L.G., Magnetic properties of dispersed magnetite powders, *Philosophical Magazine*, 11, 303–312, 1965.

Pätzold, J. and cruise participants, Report and preliminary results of the Meteor Cruise M 15/2, *Berichte, Fachbereich Geowissenschaften, Universität Bremen*, 46 pp., 1993.

Peterson, R.G. and Stramma, L., Upper-level circulation in the South Atlantic Ocean, *Progress in Oceanography*, 26, 1-73, 1991.

Petit, J.R., Jouzel, J., Raynaud, D., Barkov, N.I., Barnola, J.-M., Basile, I., Bender, M., Chappellaz, J., Davis, M., Delaygue, G., Delmotte, M., Kotlyakov, V.M., Legrand, M., Lipenkov, V.Y., Lorius, C., Pépin, L., Ritz, C., Saltzman, E., and Stievenard, M., Climate and atmospheric history of the past 420,000 years from the Vostok ice core, Antarctica, *Nature*, 399, 429 - 436, 1999.

Petschick, R., Kuhn, G., and Gingele, F., Clay mineral distribution in surface sediments of the South Atlantic: sources, transport and relation to oceanography, *Marine Geology*, 130, 203-229, 1996.

Raymo, M.E., The timing of major climate terminations, *Paleoceanography*, 12, 577-585, 1997.

Reid, J.L., On the total geostrophic circulation of the South Atlantic Ocean: flow patterns, tracers and transports, *Progress in Oceanography*, 23, 149-244, 1989.

Roberts, A.P. and Turner, G.M., Diagenetic formation of ferrimagnetic iron sulphide minerals in rapidly deposited marine sediments, South Island, New Zealand, *Earth and Planetary Science Letters*, 115, 257–273, 1993.

Schmidt, A.M., von Dobeneck, T., and Bleil, U., Magnetic characterization of Holocene sedimentation in the South Atlantic, *Paleoceanography*, 14, 465-481, 1999.

Schmieder, F., *Magnetic Cyclostratigraphy of South Atlantic Sediments*, Ph.D. Thesis, Universität Bremen, Bremen, 82 pp., 1999.

Schmiedl, G. and Mackensen, A., Late Quaternary paleoproductivity and deep water circulation in the eastern South Atlantic Ocean: evidence from benthic foraminifera, *Palaeogeography, Palaeoclimatology, Palaeoecology*, 130, 43-80, 1997.

Schulz, H.D. and cruise participants, Report and preliminary results of the Meteor-Cruise M 20/2, *Berichte, Fachbereich Geowissenschaften, Universität Bremen*, 173 pp., 1992.

Snowball, I.F., Magnetic hysteresis propeties of greigite (Fe_3S_4) and a new occurrence in Holocene sediments from Swedish Lappland, *Physics of the Earth and Planetary Interiors*, 68, 32–40, 1991.

Stephenson, A., Single domain grain distributions I. A method for the determination of single domain grain distributions, *Physics of the Earth and Planetary Interiors*, 4, 353–360, 1971.

Stoner, E.C. and Wohlfarth, E.P., A mechanism of magnetic hysteresis in heterogeneous alloys, *Philosophical Transactions of the Royal Society of London*, 240, 599–602, 1948.

Stoner, J.S., Channel, J.E.T., and Hillaire-Marcel, C., The magnetic signature of rapidly deposited detrital layers from the deep Labrador Sea: relationship to North Atlantic Heinrich layers, *Paleoceanography*, 11, 309-325, 1996.

Talley, L.D., Antarctic Intermediate Water in the South Atlantic, In: G. Wefer, W.H. Berger, G. Siedler, and D.J. Webb (Editors), *The South Atlantic: Present and Past Circulation*, Springer, Berlin, pp. 219-238, 1996.

Thompson, R., Bloemendal, J., Dearing, J.A., Oldfield, F., Rummery, T.A., Stober, J.C., and Turner, G.M., Environmental applications of magnetic measurements, *Science*, 207, 481–486, 1980.

Thompson, R. and Oldfield, F., *Environmental Magnetism*, Allen and Unwin, London, 227 pp., 1986.

Urbat, M., Dekkers, M.J., and Vriend, S.P., The isolation of diagenetic

groups in marine sediments using fuzzy c-means cluster analysis, In: D.H. Tarling and P. Turner (Editors), *Paleomagnetism and Diagenesis in Sediments*, Special Publications, Geological Society, London, pp. 85-93, 1999.

van Andel, T.H., Heath, G.R. and Moore, T.C., Cenozoic history and paleoceanography of the central equatorial Pacific Ocean, *Geological Society of America, Memoir*, 143, 143, 1975.

Verosub, K.L. and Roberts, A.P., Environmental magnetism: past, present, and future, *Journal of Geophysical Research*, 100, 2175–2192, 1995.

von Dobeneck, T., A systematic analysis of natural magnetic mineral assemblages based on modeling hysteresis loops with coercivity-related hyperbolic basis functions, *Geophysical Journal International*, 124, 675-694, 1996.

von Dobeneck, T. and Schmieder, F., Using rock magnetic proxy records for orbital tuning and extended time series analysis into the super and sub-Milankovitch bands, In: G. Fischer and G. Wefer (Editors), *Use of Proxies in Paleoceanography: Examples from the South Atlantic*, Springer, Berlin, pp. 601-633, 1999.

Wefer, G. and cruise participants, Report and preliminary results of the Meteor-Cruise M 6/6, *Berichte, Fachbereich Geowissenschaften, Universität Bremen*, 97 pp., 1988.

Wefer, G. and cruise participants, Report and preliminary results of the Meteor-Cruise M 12/1, *Berichte, Fachbereich Geowissenschaften, Universität Bremen*, 66 pp., 1990.

Wefer, G. and cruise participants, Report and preliminary results of the Meteor-Cruise M 34/3, *Berichte, Fachbereich Geowissenschaften, Universität Bremen*, 168 pp., 1996.

Witworth, T.I. and Nowlin, W.D.J., Water masses and currents of the Southern Ocean at the Greenwich meridian., *Journal of Geophysical Research*, 92, 6462-6476, 1987.

Xu, S. and Dunlop, D., Toward a better understanding of the Lowrie-Fuller test, *Journal of Geophysical Research*, 100, 22533-22542, 1995.

CHAPTER 7. Summary and perspectives

The objective of this thesis is the identification of linkages between terrigeneous and biogeneous magnetic particle fluxes to the South Atlantic sedimentary environment and their climatic and oceanographic controls during Holocene and the penultimate major deglaciation, Termination II. For this approach, environmental magnetic and statistical analyses were successfully performed in three interconnected studies, each represented by an individual publication.

The environmental magnetic results characterize the magnetic mineral inventories of the sediments by their concentration, mineralogy, magnetic grain-size, and coercivity. These primary data are related to the climatic conditions in the source areas, means and pathways of transport, and the depositional environment.

Concentration dependent magnetic parameters like susceptibility primarily reflect calcareous and/or siliceous major sediment component variability controlled by production and dissolution. Susceptibilities related to "magnetic" and "nonmagnetic" iron mineral fractions are elevated in most continental margin areas documenting terrigeneous sedimentation of ferrimagnetic, antiferromagnetic, and paramagnetic minerals.

Hematite is ubiquitous and the dominant magnetic mineral in the western South Atlantic. Hematite/magnetite mixing ratios > 4:1 prevail in a tropical belt at ~ 5°N combining eolian Saharan and fluvial Amazonian hematite. At continental margins, high hematite contents correspond to an enhanced terrigeneous supply.

Magnetite grain-sizes systematically coarsen from east to west. In highly productive eastern areas the abundance of magnetofossils and a fine-grained particle discharge by the Congo River account for predominant SD/PSD properties. The supply of South American rivers is in a coarser grain-size range.

Multivariate probabilistic cluster analyses of concentration independent rock magnetic properties allowed to classify Holocene sedimentary deposits in the entire South Atlantic, revealing transitions and overlaps of sedimentation patterns. The classes represent deposits of Holocene terrigeneous particle supply like the North African dust fans and the discharge of major South American and African rivers as well as the enhanced biomineralization of magnetite in high productive areas like the Benguela and equatorial upwelling systems.

The Holocene magnetic sediment classification served as actualistic basis for the investigation of paleoclimatic and paleoceanographic changes during Termination II, the rapid climate transition between oxygen isotope substages 6.2 and 5.5 at around 130 ka. Eight gravity cores from a West-East transect across the South Atlantic at about 30°S were rock magnetically analyzed in an age interval between 145 and 110 ka. Stepwise thermal demagnetization of a three component remanence indicated that the prevailing magnetic minerals in this area are magnetite and hematite.

Two major trends over the South Atlantic WE transect, decreasing magnetic mineral accumulation and increasing particle fining clearly identify the South American continent as most important origin of lithogenic magnetic particles to the South Atlantic during Holocene and also throughout Termination II. In this region, the main sources of dust are the Patagonian plain and the arid regions of southern Africa. Patagonian dust is transported far eastwards, while the dust trajectory from southern Africa essentially follows the coast. The distinct magnetic properties

of the mainly volcanogenic material deposited in the Patagonian plain allow a clear distinction from the fluvial supply by the Rio de la Plata river which primarily drains the Paraná Basin, where vast formations of flood basalts crop out. During the glacial, when the polar front and the westerlies moved northward, combined enhanced aridity and dust mobilization [*Petit et al.*, 1999], intensify the eolian inflow and rise the volcanogenic content in the marine sedimentary deposits. Elevated eolian influx from Africa by stronger SE trades during the glacial is only observed in the northern Cape Basin. It was apparently restricted to a quite narrow zone in continental proximity.

Magnetite dissolution horizons around substage 5.5 and directly at Termination II mark peaks in productivity and organic matter deposition at the mid South American continental margin.

This thesis answered a number of questions about the interconnection between rock magnetic sediment characteristics and paleoclimatic and paleoceanographic controls in the South Atlantic. Nevertheless, it also raised severals new ones:

- The investigated area is confined by northern and southern open ocean boundaries. The material transport from the Antarctic and North Atlantic Oceans is not clear. An expansion of the Holocene sediment characterization beyond these limits should yield more detailed information on these fluxes.
- The investigation of Termination II primarily delimited glacial/interglacial contrasts, but due to the low sedimentation rates could not resolve higher-frequency variations during the deglaciation. It would therefore be interesting to extend the time-slice analysis to areas with higher sedimentation rates.
- The occurrence of the sharpen bounded diagenetically altered layers around Termination II and stage 5.5 on the Santos Plateau could not unequivocally be explained. Further information about the discharge of the Rio Doce might reveal the underlying mechanism.

Danksagung

Die vorliegende Arbeit wurde im Rahmen des Sonderforschungsbereiches 261 am Fachbereich Geowissenschaften der Universität Bremen angefertigt.

Herrn Professor Dr. Ulrich Bleil möchte für die Vergabe und Betreuung der Dissertation, seine konstruktive Kritik und stete Diskussionsbereitschaft danken.

Die Zusammenarbeit mit Dr. Tilo von Dobeneck war inspirierend und nährte meine Begeisterung für die Wissenschaft. Ich habe immer seine ausführlichen Erläuterungen verschiedenster Themen des Lebens genossen. Tilo zu meinen Kollegen zu zählen war eine Bereicherung.

Ich möchte auch herzlich Dr. Thomas Frederichs für die nette Zusammenarbeit danken. Ratschläge aus seiner praktischen Erfahrung haben mir so manches mal die experimentelle Arbeit erleichtert.

Die Arbeit in der Gruppe "Marine Geophysik" hat mir immer Freude bereitet, was nicht zuletzt ein Verdienst meiner netten Kollegen, Dr. Karl Fabian, Jens Funk, Katharina Hilgenfeldt und Dr. Frank Schmieder, der Techniker Liane Brück, Christian Hilgenfeldt und Heike Piero und unseres ehemaligen Kollegen Dr. Harald Petermann ist.

Besonders bedanke ich mich auch bei unseren Studentinnen Anke Dreyzehner und Christine Franke, die sehr engagiert im Labor mitgeholfen haben. Ohne ihre Hilfe hätte ich die große Anzahl von Proben und Messungen wohl nicht bewältigen können.

Dr. Laurence Vidal stellte mir freundlicherweise zum Teil unveröffentlichte Daten zur Verfügung.

Die Besatzung der FS METEOR auf den Fahrtabschnitten M23/1, M34/3, M29/2, M29/3 und M38/2, sowie die Mitarbeiter des gesamten "Fachbereich 5" schafften immer eine angenehme Arbeitsatmosphäre. Ich möchte auch Gisela Boelen und Carmen Murken danken, die mit großer Geduld die Interessen der Doktoranden vertreten.

Nicht zuletzt bedanke ich mich bei Dirk, der mir immer neue Energie für die Arbeit an meiner Dissertation gegeben hat.

References

Appel, E., Stress anisotropy in Ti-rich titanomagnetites, *Physics of the Earth and Planetary Interiors*, 46, 233–240, 1987.

Bacher, J., *Clusteranalyse: anwendungsorientierte Einführung*, Oldenbourg Verlag, München, 424 pp., 1994.

Banerjee, S.K., Hunt, C.P., and Liu, X.-M., Separation of local signals from the regional paleomonsoon record of the Chinese loess plateau: a rock-magnetic approach, *Geophysical Research Letters*, 20, 843–846, 1993.

Banerjee, S.K., King, J.W., and Marvin, J.A., A rapid method for magnetic granulometry with applications to environmental studies, *Geophysical Research Letters*, 8, 333–336, 1981.

Berger, W.H. and Wefer, G., Central themes of South Atlantic circulation, In: G. Wefer, W.H. Berger, G. Siedler and D.J. Webb (Editors), *The South Atlantic: Present and Past Circulation*, Springer Verlag, New York, pp. 1-11, 1996.

Bezdek, J.C., *Fuzzy mathematics in pattern classification*, Ph.D. Thesis, Cornell University, Ithaca, N.Y., 1973.

Bezdek, J.C., *Pattern recognition with fuzzy objective function algorithms*, Plenum Press, New York, 1981.

Bezdek, J.C. and Dunn, J.C., Optimal fuzzy partitions: a heuristic for estimating the parameters in a mixture of normal distributions, *IEEE, Trans. Comp.*, C-24, 835-838, 1975.

Bleil, U. and Petersen, N., Magnetic properties, In: G. Angenheister (Editor), *Landolt-Börnstein Numerical Data and Functional Relationships in Science and Technology*, Springer-Verlag, New York, pp. 308–432, 1982.

Bloemendal, J., King, J.W., Hall, F.R. and Doh, S.-J., Rock magnetism of Late Neogene and Pleistocene deep-sea sediments: relationship to sediment source, diagenetic processes, and sediment lithology, *Journal of Geophysical Research*, 97, 4361–4375, 1992.

Brunhes, B., Recherches sur la direction d'aimantation des roches volcaniques, *Journal de Physique*, 5, 705–724, 1906.

Butler, R.F. and Banerjee, S.K., Theoretical single-domain grain size range in magnetite and titanomagnetite, *Journal of Geophysical Research*, 80, 4049–4058, 1975.

Clark, D.A., Hysteresis properties of sized dispersed monoclinic pyrrhotite grains, *Geophysical Research Letters*, 11, 173–176, 1984.

David, P., Sur la stabilité de la direction d'aimantation dans quelques roches volcaniques, *Comptes rendus hebdomadaires des séances de l'Académie des Sciences (Paris), Série B*, 138, 41–42, 1904.

Davis, J.C., *Statistics and Data Analysis in Geology*, John Wiley & Sons, New York, 646 pp., 1986.

Day, R., Fuller, M. and Schmidt, V.A., Hysteresis properties of titanomagnetites: grain-size and compositional dependence, *Physics of the Earth and Planetary Interiors*, 13, 260–266, 1977.

Dekkers, M.J., Magnetic properties of natural pyrrhotite Part I: behaviour of initial susceptibility and saturation-magnetization-related rock-magnetic parameters in a grain-size dependent framework, *Physics of the Earth and Planetary Interiors*, 52, 376–393, 1988a.

Dekkers, M.J., *Some rock magnetic parameters for natural goethite, pyrrhotite, and fine-grained hematite*, Ph. D. Thesis, University of Utrecht, 1988b.

Dekkers, M.J., Magnetic properties of natural pyrrhotite. II. High- and low-temperature behavior of J_{rs} and TRM as a function of grain size, *Physics of the Earth and Planetary Interiors*, 57, 266–283, 1989.

DeMenocal, P.B., Laine, E.P., Ciesielski, P.F., A magnetic signature of bottom current erosion, *Physics of the Earth and Planetary Interiors*, 51, 326-348, 1988.

Doh, S.J., King, J.W., and Leinen, M., A rock-magnetic study of giant piston core LL44-GPC3 from the central North Pacific and its paleoceanographic implications, *Paleoceanography*, 3, 89-111, 1988.

Dunlop, D.J., Superparamagnetic and single-domain threshold sizes in magnetite, *Journal of Geophysical Research*, 78, 1780–1793, 1973.

Dunlop, D.J., Developments in rock magnetism, *Reports on Progress in Physics*, 53, 707–792, 1990.

Dunlop, D.J. and Özdemir, Ö., *Rock Magnetism: Fundamentals and Frontiers*, Cambridge Studies in Magnetism, Cambridge University Press, Cambridge, 573 pp., 1997.

Fassbinder, J.W.E., Stanjek, H. and Vali, H., Occurence of magnetic bacteria in soil, *Nature*, 343, 161–163, 1990.

Frederichs, T., Regional and temporal variations of rock magnetic parameters in Arctic marine sediments, *Reports on polar research*, 164, 212 pp., 1995a.

Frederichs, T., *Regionale und altersabhängige Variation gesteinsmagnetischer Parameter in marinen Sedimenten der Arktis*, Dissertation Bremen, 1995b.

Frederichs, T., Bleil, U., Däumler, K., von Dobeneck, T. and Schmidt, A., The magnetic view on the marine paleoinvironment: parameters, techniques, and potentials of rock magnetic studies as a key to paleoclimatic and paleoceanographic changes, In: G. Fischer and W. Wefer (Editors), *Use of Proxies in Paleoceanography*, Springer, New York, pp. 575-599, 1999.

Gauss, C.F., Allgemeine Theorie des Erd-magnetismus, Leipzig, *reprinted in C.F. Gauss, Werke*, Königliche Gesellschaft der Wissen-schaften, 1877, Göttingen, 121-193, 1839.

Gilbert, W., *De magnete*, reprinted by Dover, 1600, New York, 1958.

Glaccum, R.A. and Prospero, J.M., Saharan aerosols over the tropical north Atlantic - Mineralogy, *Marine Geology*, 37, 295-321, 1980.

Gordon, A.L., Inter-ocean exchange of thermo-cline water, *Journal of Geophysical Research*, 91, 5037-5046, 1986.

Hedley, I.G., The weak ferromagnetism of goethite (α-FeOOH), *Zeitschrift für Geo-physik*, 37, 409-420, 1971.

Heider, F., Zitzelsberger, A., and Fabian, K., Magnetic susceptibility and remanent coercive force in grown magnetite crystals from 0.1 mm to 6 mm, *Physics of the Earth and Planetary Interiors*, 93, 239-256, 1995.

Heller, F., Rock magnetic studies of upper Jurassic limestones from southern Germany, Journal of Geophysical Research, 44, 525-543, 1978.

Heller, F. and Liu, T.-S., Magnetism of Chinese loess deposits, *Geophysical Journal of the Royal Astronomical Society*, 77, 125–141, 1984.

Hodych, J.P., Magnetostrictive control of coer-cive force in multidomain magnetite, *Nature*, 298, 542–544, 1982.

Hoffmann, V., Greigite (Fe_3S_4): magnetic properties and first domain observations, *Physics of the Earth and Planetary Interiors*,

70, 288–301, 1992.

Karlin, R., Magnetic mineral diagenesis in suboxic sediments at Bettis site W-N, NE Pacific Ocean, *Journal of Geophysical Research B: Solid Earth*, 95, 4421–4436, 1990.

Karlin, R. and Levi, S., Diagenesis of magnetic minerals in recent hemipelagic sediments, *Nature*, 303, 327–330, 1983.

Kellogg, T.B., Plaeoclimatology and paleooceanography of the Norwegian and Greenland seas, *Geological Society of America*, Memorial, 145, 77-110, 1980.

King, J.W., Banerjee, S.K., Marvin, J.A., and Özdemir, Ö., A comparison of different magnetic methods for determining the relative grain size of magnetite in natural materials: some results from lake sediments, *Earth and Planetary Science Letters*, 59, 404–419, 1982.

King, J.W. and Channell, J.E.T., Sedimentary magnetism, environmental magnetism, and magnetostratigraphy, *Reviews of Geophysics*, 29 Suppl., 358–370, 1991.

Kobayashi, K. and Nomura, M., Ferromagnetic minerals in the sediment cores collected from the Pacific Basin, *Journal of Geophysics*, 40, 501–512, 1974.

Koenigsberger, J.G., Natural residual magnetism of eruptive rocks, *Terrestrial Magnetism and Atmospheric Electricity*, 43, 119-130, 1938.

Landau, L.D. and Lifshitz, E.M., On the theory of the dispersion of magnetic permeability in ferromagnetic bodies, *Physikalische Zeitschrift der Sowjetunion*, 8, 153–167, 1935.

Leslie, B.W., Lund, S.P. and Hammond, D.E., Rock magnetic evidence for the dissolution and authigenic growth of magnetic minerals within anoxic marine sediments of the California continental borderland, *Journal of Geophysical Research*, 95, 4437–4452, 1990a.

Leslie, B.W., Hammond, D.E., Berelson, W.M. and Lund, S.P., Diagenesis in anoxic sediments from the California continental borderland and its influence on iron, sulfur, and magnetite behavior, *Journal of Geophysical Research*, 95, 4453–4470, 1990b.

Liebermann, R.C. and Banerjee, S.K., Magnetoelastic interactions in hematite: implications for geophysics, *Journal of Geophysical Research*, 76, 2735-2756, 1971.

Lillefors, H.W., On the Komolgorov-Smirnov test for normality with mean and variance unknown, *Journal of the American Statistical Association*, 62, 399-402, 1967.

Lisitzin, A.P., *Oceanic sedimentation: Lithology and Geochemistry*, American Geophysical Union, Washington D.C., 1996.

Liu, X.-M., Shaw, J., Liu, T.-S., Heller, F. and Baoyin, Y., Magnetic mineralogy of Chinese loess and its significance, *Geophysical Journal International*, 108, 301–308, 1992.

Lowrie, W., Channell, J.E.T., and Heller, F., On the credibility of remanent magnetization measurements, *Geophysical Journal of the Royal Astronomical Society*, 60, 493-496, 1980.

Lowrie, W. and Heller, F., Magnetic properties of marine limestones, *Reviews of Geophysics and Space Physics*, 20, 171–192, 1982.

Lund, S.P., Gorsline, D.S. and Henyey, T.L., Rock magnetic characteristics of surficial marine sediments from the California continental borderland, *Earth and Planetary Science Letters*, 109, 93–108, 1992.

Lund, S.P. and Karlin, R., Introduction to the special section on physical and biogeochemical processes responsible for the magnetization of sediments, *Journal of Geophysical Research*, 95, 4353-4354, 1990.

Maher, B.A., Magnetic properties of some

synthetic submicron magnetites, *Geophysical Journal*, 94, 83–96, 1988.

Maher, B.A. and Thompson, R., Mineral magnetic record of the Chinese loess and paleosols, *Geology*, 19, 3–6, 1991.

Mann, S., Sparks, N.H.C., Frankel, R.B., Bazylinski, D.A. and Jannasch, H.W., Biomineralization of ferrimagnetic greigite (Fe_3S_4) and iron pyrite (FeS_2) in a magnetotactic bacterium, *Nature*, 343, 258–261, 1990.

Matuyama, M., On the direction of magnetisation of basalt in Japan, Tyosen and Manchuria, *Proc. Imper. Acad. Japan*, 5, 203-205, 1929.

Milliman, J.D. and Meade, R.H., World-wide delivery of river sediment to the oceans, *Journal of Geology*, 91, 1-21, 1983.

Moskowitz, B.M., Frankel, R.B., Flanders, P.J., Blakemore, R.P., and Schwartz, B.B., Magnetic properties of magnetotactic bacteria, *Journal of Magnetism and Magnetic Materials*, 73, 273–288, 1988.

Nagata, T., The natural remanent magnetism of volcanic rocks and its relation to geomagnetic phenomena, *Bulletin of the Earthquake Research Institute, University of Tokyo*, 21, 1943.

Néel, L., Propriétés d'un ferromagnètique cubique en grain fins, *Comptes Rendus Sommaire des Seances de l'Acadedie des Sciences Paris*, 224, 1488-1490, 1948.

Oldfield, F., Environmental magnetism: a personal perspective, *Quaternary Science Reviews*, 10, 73–85, 1991a.

Oldfield, F., Sediment magnetism: soil erosion, bushfires or bacteria?, *Geology*, 19, 1153–1156, 1991b.

Oldfield, F., Toward the discrimination of fine-grained ferrimagnets by magnetic measurements in lake and near-shore marine sediments, *Journal of Geophysical Research*, 99, 9045-9050, 1994.

O'Reilly, W., *Rock and Mineral Magnetism*, Blackie, Glasgow, 220 pp., 1984.

Özdemir, Ö. and Banerjee, S.K., High temperature stability of maghemite (γ-Fe_2O_3), *Geophysical Research Letters*, 11, 161–164, 1984.

Özdemir, Ö., Xu, S., and Dunlop, D.J., Closure domains in magnetite, *Journal of Geophysical Research*, 100, 2193–2209, 1995.

Özdemir, Ö. and Dunlop, D.J., Thermoremanence and Néel temperature of goethite, *Geophysical Research Letters*, 23, 921-924, 1996.

Parry, L.G., Magnetic properties of dispersed magnetite powders, *Philosophical Magazine*, 11, 303–312, 1965.

Peregrinus, P., *Epistola de Magnete, 1269, see Smith, P.J., Petrus Peregrinus Epistola-The beginning of experimental studies of magnetism in Europe*, Atlas (News Supplement of Earth Science Reviews), 6, 1970.

Petermann, H. and Bleil, U., Detection of live magnetotactic bacteria in South Atlantic deep-sea sediments, *Earth and Planetary Science Letters*, 117, 223-228, 1993.

Petersen, N., von Dobeneck, T. and Vali, H., Fossil bacterial magnetite in deep-sea sediments from the South Atlantic Ocean, *Nature*, 320, 611–615, 1986.

Petersen, N., Weiss, D. and Vali, H., Magnetotactic bacteria in lake sediments, In: F. Lowes (Editor), *Geomagnetism and Paleomagnetism*, Kluwer Academic Publishers, Dordrecht, pp. 231–241, 1989.

Peterson, R.G. and Stramma, L., Upper-level circulation in the South Atlantic Ocean, *Progress in Oceanography*, 26, 1-73, 1991.

Petit, J.R. et al., Climate and atmospheric history of the past 420,000 years from the Vostok ice core, Antarctica, *Nature*, 399, 429 - 436, 1999.

Pye, K., *Aeolian Dust and Dust Deposits*, Academic Press, London, 334 pp, 1987.

Reid, J.L., On the circulation of the South Atlantic Ocean, In: W.H.Berger, G. Wefer, G. Siedler, D.J. Webb (Editors), *The South Atlantic: Present and Past Circulation*, Springer-Verlag, Berlin, 13-44, 1996.

Roberts, A.P., Magnetic properties of sedimentary greigite (Fe_3S_4), *Earth and Planetary Science Letters*, 134, 227-236, 1995.

Roberts, A.P. and Turner, G.M., Diagenetic formation of ferrimagnetic iron sulphide minerals in rapidly deposited marine sediments, South Island, New Zealand, *Earth and Planetary Science Letters*, 115, 257–273, 1993.

Robinson, S.G., The late Pleistocene palaeoclimatic record of North Atlantic deep-sea sediments revealed by mineral-magnetic measurements, *Physics of the Earth and Planetary Interiors*, 42, 22-47, 1986.

Rochette, P. and Fillion, G., Field and temperature behavior of remanence in synthetic goethite: paleomagnetic implications, *Geophysical Research Letters*, 16, 851-854, 1989.

Schmidt, A.M., von Dobeneck, T. and Bleil, U., Magnetic characterization of Holocene sedimentation in the South Atlantic, *Paleoceanography*, 14, 465-481, 1999.

Schmieder, F., *Magnetic Cyclostratigraphy of South Atlantic Sediments*, Ph.D. Thesis, Universität Bremen, Bremen, 82 pp., 1999.

Schneider, R.R., Müller, P.J., Ruhland, G., Meinecke, G., Schmidt, H., and Wefer, G., Late Quaternary surface temperatures and productivity in the east- equatorial South Atlantic: response to changes in trade/ monsoon wind forcing and surface water advection, In: W.H. Berger, G. Wefer, G. Siedler, D.J. Webb (Editors), *The South Atlantic: Present and Past Circulation*, Springer-Verlag, Berlin, pp. 527-551, 1996.

Shannon, L.V. and Nelson, G., The Benguela: Large scale features and processes and system variability, In: W.H. Berger, G. Wefer, G. Siedler, and D.J. Webb (Editors), *The South Atlantic: Present and Past Circulation*, Springer-Verlag, New York, 163-210, 1996.

Skinner, B.J., Erd, R.C., and Grimaldi, F.S., Greigite, the thio-spinel of iron; a new mineral, *American Mineralogist*, 49, 543–553, 1964.

Snowball, I.F., Magnetic hysteresis propeties of greigite (Fe_3S_4) and a new occurrence in Holocene sediments from Swedish Lappland, *Physics of the Earth and Planetary Interiors*, 68, 32–40, 1991.

Snowball, I.F., Bacterial magnetite and the magnetic properties of sediments in a Swedish lake, *Earth and Planetary Science Letters*, 126, 129–142, 1994.

Stober, J.C. and Thompson, R., Magnetic remanence acquisition in Finnish lake sediments, *Geophysical Journal of the Royal Astronomical Society*, 57, 727–739, 1979.

Stoner, J.S., Channel, J.E.T., and Hillaire-Marcel, C., The magnetic signature of rapidly deposited detrital layers from the deep Labrador Sea: relationship to North Atlantic Heinrich layers, *Paleoceanography*, 11, 309-325, 1996.

Talley, L.D., Antarctic Intermediate Water in the South Atlantic, In: W.H. Berger, G. Wefer, G. Siedler, and D.J. Webb (Editors), *The South Atlantic: Present and Past Circulation*, Springer-Verlag, New York, 219-238, 1996.

Tarduno, J.A., Temporal trends of magnetic dissolution in the pelagic realm: gauging paleoproductivity?, *Earth and Planetary Science Letters*, 123, 39–48, 1994.

Tarduno, J.A., Superparamagnetism and reduction diagenesis in pelagic sediments: enhance-

ment or depletion?, *Geophysical Research Letters*, 22, 1337–1340, 1995.

Tarduno, J.A. and Wilkison, S.L., Non-steady state magnetic mineral reduction, chemical lock-in, and delayed remanence acquisition in pelagic sediments, *Earth and Planetary Science Letters*, 144, 315-326, 1996.

Thellier, E., Sur l'aimantation des terres cuites et ses applications géophysiques, *Annales de l'Institut de Physique du Globe, Université de Paris et Bureau Central de Magnètisme Terrestre*, 16, 157–302, 1938.

Thompson, R., Bloemendalk J, Dearing, J.A., Oldfield, F., and Rummery, T.A., Environmental applications of magnetic measurements, *Science*, 207, 481–486, 1980.

Thompson, R. and Oldfield, F., *Environmental Magnetism*, Allen and Unwin, London, 227 pp, 1986.

Urbat, M., Dekkers, M.J., and Vriend, S.P., The isolation of diagenetic groups in marine sediments using fuzzy c-means cluster analysis, In: D.H. Tarling and P. Turner (Editors), *Paleomagnetism and Diagenesis in Sediments*, Special Publications, Geological Society, London, pp. 85-93, 1999.

Vali, H. and Kirschvink, J.L., Observations of magnetosome organization, surface structure, and iron biomineralization of undescribed magnetic bacteria: evolutionary speculations, In: R.B. Frankel and R.P. Blakemore (Editors), *Iron Biominerals*, Plenum Press, New York, pp. 97–115, 1991.

Verosub, K.L. and Roberts, A.P., Environmental magnetism: past, present, and future, *Journal of Geophysical Research*, 100, 2175–2192, 1995.

von Dobeneck, T., *Neue Ansätze zur Messung und Interpretation der magnetischen Hysterese von Tiefsee-sedimenten*, Verlag Marie L. Leidorf, Buch am Erlbach, 190 pp., 1993.

von Dobeneck, T., A systematic analysis of natural magnetic mineral assemblages based on modeling hysteresis loops with coercivity-related hyperbolic basis functions, *Geophysical Journal International*, 124, 675-694, 1996.

von Dobeneck, T. and Schmieder, F., Using rock magnetic proxy records for orbital tuning and extended time series analysis into the super and sub-Milankovitch bands, In: G. Fischer and G. Wefer (Editors), *Proxies in Paleoceanography*, Springer Verlag, New York, 601-633, 1999.

Wasilewski, P.J., Magnetic hysteresis in natural materials, *Earth and Planetary Science Letters*, 20, 67–72, 1973.

Weiss, P., L'hypothèse du champ moleculaire et la propriété ferromagnétique, *Journal de Physique*, 6, 661-690, 1907.

Zadeh, L.A., Fuzzy sets, *Inf. Control.*, 8, 338-353, 1965.